RADIATION RESPONSE AND RELIABILITY OF HIGH SPEED AlGaN/GaN HEMTS

By

Jin Chen

Dissertation

Submitted to the Faculty of the

Graduate school of Vanderbilt University

in partial fulfillment of the requirements

for the degree of

DOCTOR OF PHILOSOPHY

in

Electrical Engineering

August, 2016

Nashville, Tennessee

Approved by:

Professor Daniel M. Fleetwood
Professor Ronald D. Schrimpf
Professor Sokrates T. Pantelides
Professor Robert A. Weller
Professor En Xia Zhang

Acknowledgements

I'm so grateful to thank those people who not only helped me a lot in this work, but also gave me pleasant experience here far away from home.

I would like to first and foremost thank my advisor, Dr. Daniel M. Fleetwood, for his guidance and continuous support in my scientific research, and his confidence in my ability. Without his encouragement, the long-term experiments with little progress would be much more painful. I also thank Dr. Ron D. Schrimpf for teaching me device physics and for all the intellectual discussions we had every week. I am not a careful person and his incisive understanding of devices always helped to avoid neglecting key points when performing the experiments. I thank Dr. Sokrates T. Pantelides and his group, for being extremely helpful throughout my work. Without their calculations and analysis, this work cannot be completed. I thank Dr. Robert Weller for giving me interesting lectures on Monte Carlo simulation and electromagnetic theories, which are extremely helpful in this work. I am extremely grateful for Enxia. She is always helping in labs, listening and encouraging when I have difficulties. Her positive attitude not only encourages my research work but also makes the life much warmer in Nashville.

I am grateful to all my sponsors for supporting this project. I thank the Defense Threat Reduction Agency for financially supporting this work through grant No. HDTRA1-11-1-0023. Also I thank our collaborators at the University of California, Santa Barbara, for providing us with the AlGaN/GaN HEMTs used in this work. I thank Dr. Anthony B. Hmelo of the Vanderbilt Institute of Nanoscale Science and Engineering (VINSE)

and Mike McCurdy for their experimental support.

I thank Dr. Yevgeniy Puzyrev who performed the DFT calculation for the defects in this work. He is always excited with any observations I found in experiments and without his help, much of my work cannot explained well. I also thank Dr. Xiao Shen, who explained the defects and mechanism clearly and precisely. He is always there to help and answer my questions even it is time to go home.

I thank Cher and Tania, who helped me learn to use the noise system in the lab. I am grateful to all my friends in Vanderbilt University, especially fellows in the RER group, who made the lab and office warm and pleasant.

At last, I would like to thank my family for their unconditional love and support. They are always good listeners to whatever I want to say, mostly my babblings and complaints. I thank Yi Dong, my boyfriend, for his love and always taking care of me.

TABLE OF CONTENTS

PAGE

LIST OF FIGURES

PAGE

LIST OF TABLES

Page

ABSTRACT

In recent years, GaN-based high-electron-mobility-transistors (HEMT) have demonstrated excellent high power and high frequency performance compared with counterparts based on other materials. Although AlGaN/GaN HEMTs are of great interest owing to the large band gap of GaN (3.4 eV), high breakdown field (~3.1 MV/cm), high saturation electron velocity (~2.5 × 10^7 cm/s) and the presence of a high-mobility two-dimensional electron gas (2DEG) at the hetero-interface, the reliability of devices can be limited by a number of factors, impeding the way to commercialization. GaN HEMTs have demonstrated very good radiation tolerance. In this work, the radiation response and reliability issues of AlGaN/GaN HEMTs grown using molecular beam epitaxy (MBE) are studied. Devices subjected to 1.8 MeV proton irradiation and/or voltage stress are characterized via DC and RF measurements. Low frequency 1/*f* noise measurements are employed to help understand the defects that affect the reliability and radiation response of AlGaN/GaN HEMTs, and density functional theory (DFT) calculation is used to identify possible defect candidates. The temperature-dependent noise spectra show changes in defect distributions. Hydrogenated O_N defects, Fe complexes and V_{Ga}-V_N-H_x divacancies are some of the dominating defects limiting the device radiation response and reliability. The results of combined high field and radiation effects provide better insight into device response in practical space applications.

Chapter I

Introduction

Overview of GaN HEMTs

In recent years, GaN-based high-electron-mobility-transistors (HEMT) have demonstrated excellent high power and high frequency performance compared with counterparts based on other materials. Although AlGaN/GaN HEMTs are of great interest owing to the large band gap of GaN (3.4 eV), high breakdown field (~3.1 MV/cm), high saturation electron velocity (~2.5 × 10^7 cm/s) and the presence of a high-mobility two-dimensional electron gas (2DEG) at the hetero-interface, the reliability of devices can be limited by a number of factors, impeding the way to commercialization [1]. In this work, the radiation response and reliability of AlGaN/GaN HEMTs grown using molecular beam epitaxy (MBE) are studied. Devices are characterized electrically and/or subjected to 1.8 MeV proton irradiation and/or voltage stress at different temperatures. 1/*f* noise measurements are employed to help understand the defects that affect the reliability and radiation response of AlGaN/GaN HEMTs. Small-signal characterization is also performed before and after irradiation/stress. To provide better insight to practical space applications, combined high field and radiation effects are investigated systematically.

People are making progress on GaN devices all over the world. Table 1.1 lists the material properties of GaN compared to other competing materials [2][3]. The first GaN HEMT was introduced in 1993 [4]. Based on wide bandgap material, GaN HEMTs have attracted lots of interest and are very promising for high frequency,

high power applications.

Due to a large breakdown electric field of 2 MV/cm [5], GaN devices can be easily applied in commercial systems without stepping down the operating voltage, which reduces the cost of voltage conversion. Thanks to the strong chemical bonds in the semiconductor crystal, GaN HEMTs and other GaN-based devices are also desirable for operations under high temperature and radiation exposure (Fig. 1-1).

Table 1.1. The materials properties of GaN compared to competing materials (after [3]).

Material	μ **(cm^2/Vs)**	ε	***Eg*** **(eV)**	***Tmax*** **(℃)**
Si	1300	11.4	1.1	300
GaAs	5000	13.1	1.4	300
SiC	260	9.7	2.9	600
GaN	1500	9.5	3.4	700

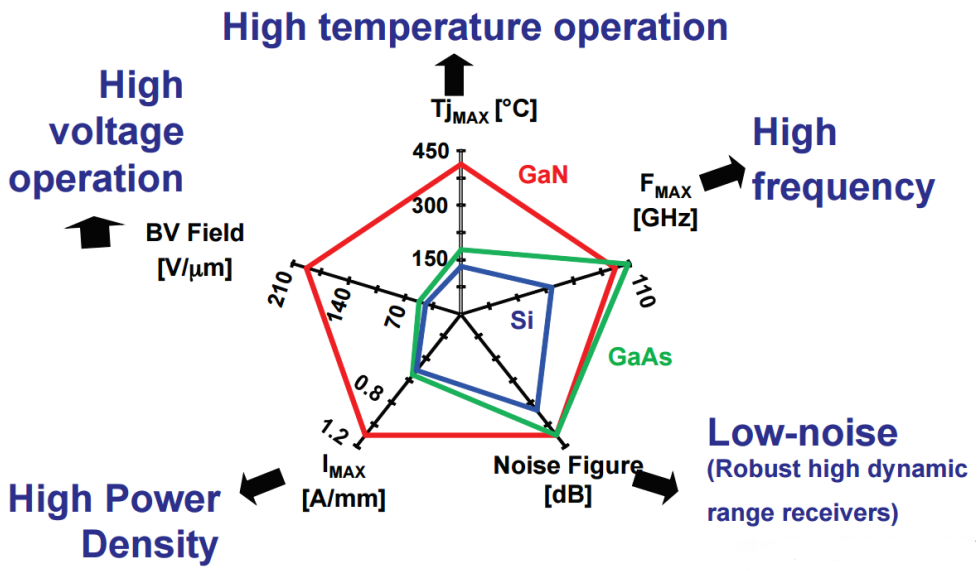

Fig. 1-1 GaN HEMTs performances compared with Si and GaAs (after [6]).

The heterojunction under the gate and the two-dimensional electron gas (2DEG) play very important roles in the operation of HEMTs. A high 2DEG sheet density is essential in HEMT design. In traditional GaAs- and InP-based HEMTs, the barrier layer is n-doped and the donors are the sources of the 2DEG electrons. In GaN HEMTs, spontaneous and piezoelectric polarization contribute to a large interface sheet charge at the heterojunction. Both AlGaN and GaN have strong spontaneous polarization, with larger polarization in AlGaN than in GaN [7]. Since the lattice constant of bulk AlGaN is smaller than that of GaN, the AlGaN layer is under tensile strain, which brings in another polarization component, known as piezoelectric polarization. Due to the effects of polarization, a 2DEG with high sheet density can be achieved at the AlGaN/GaN heterojunction without intentional doping, which is a unique feature of GaN HEMTs [3][8].

Molecular Beam Epitaxy Growth of GaN Devices

One of the most powerful techniques for growing GaN-based HEMT epi-structures is molecular beam

epitaxy (MBE). High-quality growth via plasma-assisted MBE (PAMBE), ammonia-based MBE (NH_3-MBE) and metal-organic chemical vapor deposition (MOCVD) provide advantages of low on-resistance and high output power, ensuring great high-power high-frequency performance [8]. MOCVD growth is more attractive for industry, due to its higher growth rate. The growth rate of III-N MBE is around 0.5 ~ 1 μm/h, relatively lower than that under MOCVD growth [9]. The advantage of MBE growth is that it offers heterostructure growth with precise definition of interfaces, low point defect concentration, and very low carbon and hydrogen impurity concentrations. Based on the nitrogen sources used for growth, the GaN MBE research has divided into two camps, i.e., using a nitrogen plasma source or an ammonia source. Each technique has its own advantages and shortcomings.

PAMBE generally involves precisely controlled, low-temperature Ga-rich growth, though high-temperature N-rich PAMBE growth has also been developed. [10] At lower temperatures (550 ℃ to 800 ℃), the PAMBE technique can achieve atomically flat surfaces under Ga-rich growth conditions. However, it usually needs to grow on high quality GaN templates by MOCVD to achieve the best results. Two main issues of Ga-rich PAMBE are the need for precise temperature control at the boundary of the Ga-droplet regime and the high density of leakage pathways, which are supposedly formed through highly conductive Ga-decorated threading dislocations (TDs). These two main issues can be circumvented by growing GaN slightly N-rich at high-T, beyond the GaN decomposition temperature (~750 ℃). Though the leakage current of high-temperature N-rich PAMBE is far less than Ga-rich PAMBE, the relatively poor 2DEG characteristics may be the result of interface roughness scattering and compensating defects associated with high TDD [11].

Much like PAMBE, growth by NH_3-MBE is performed under an environment with very low carbon and hydrogen content. In NH_3-MBE, active nitrogen is introduced to the growth surface through NH_3, which is then

thermally cracked and incorporated. The NH_3-MBE technique grows at higher temperatures compared with PAMBE techniques, i.e., 800 ℃ to 900 ℃, and readily obtains high electron mobility GaN layers on sapphire and SiC substrates. The NH_3-MBE growth technique is developed to achieve a method combining a low-impurity, ultrahigh vacuum environment with the higher growth rates of MOCVD. The growth rate of NH_3-MBE is greater than Ga-rich PAMBE, which is higher than 500 nm/h. Due to a larger wider growth window (Ga/N = 0.001), tight temperature control is not that important in NH_3-MBE growth.[13]

Reliability Issues of GaN HEMTs

In addition to the device performance, reliability is the highest priority issue to be addressed for mass production. GaN HEMTs are currently popular candidates for power microwave amplifiers, which are typically operated at very high drain-source voltages. Various degradation mechanisms of GaN HEMTs have been reported in previous research [1]. For high power and high voltage applications, hot electron-induced degradation in peak transconductance and saturation current is an issue when devices are operated under high electric fields. The semi-ON bias condition is typically the worst case for hot-carrier stress [1][14]-[17]. At high bias levels, devices are subjected to electrical stress, leading to electron trapping at interface traps, in the AlGaN barrier layer, and/or in the GaN buffer layer. The applied high voltage stress can degrade the electrical characteristics such as the saturation drain current I_{Dsat}, the maximum transconductance g_m, and the threshold voltage V_{TH} [2][15][16]. Current collapse has been observed in almost all AlGaN/GaN systems [18][19]. Due to the low thermal conductivity of the substrate, self-heating effects can lead to negative output conductance under high current conditions. Long-term reliability is studied by many groups, especially under high temperatures (>

150 ℃). The experiments were performed under different test conditions, such as voltage, current and temperature. The value of MTTF (mean time to failure) is on the order of 1×10^6 to 10^7 hours, with a calculated activation energy of ~ 2 eV [20]-[23]. Electrical stress also leads to degradation of RF performance. By small-signal S parameter measurement, degradations in current gain and unity gain frequency f_T are observed.

Radiation Effects on GaN HEMTs

A variety of effects in the characteristics of GaN HEMTs system can occur after radiation exposure including shifts in pinch-off voltage, mobility degradation and increase in junction leakage and noise. Due to the higher surface state density in GaN, and usually the absence of a gate or parasitic dielectric layer, ionization effects are less important compared to silicon-based MOS devices [24]-[31]. Moreover, the insertion of buffer or capping layers isolate surface trapping from the active region of the devices. Therefore, most research shows that displacement damage is more dominant than ionization effects in AlGaN/GaN HEMTs.

The threshold energy for a specific material can be determined by measuring the energy dependence of displacement damage. It has been found that the minimal and average energies of defect formation are much higher than average recoil energies [32][33], which suggests that the degradation after irradiation is hard to explain only by the displacement of atoms from a perfect lattice. Previous proton irradiation studies at different energies [34]-[42] suggest that GaN-based devices are extremely radiation hardened and proton energy has a strong effect on the amount of damage created in the 2DEG of the HEMT because of differences in nonionizing energy loss. 1.8 MeV protons are commonly used to assess displacement damage in GaN HEMTs, due to much larger non-ionizing energy loss than higher energy protons.[31][45] In this work, the radiation response of GaN HEMTs is evaluated with 1.8 MeV protons.

Overview of Dissertation

This dissertation will focus on the defects that result in degradation during proton irradiation and during electrical stressing of AlGaN/GaN HEMTs. We employ DC and AC measurements to parameterize the device degradation, and perform low-frequency 1/*f* noise measurements to help identify crystallographic defects.

Chapter II provides the background of this dissertation, including proton-induced damage, reliability issues of GaN HEMTs and the theory of low frequency 1/*f* noise. The device information and measurement techniques are also introduced in Chapter II. Commercial parts from *Qorvo* are also tested and compared with devices fabricated at the University of California Santa Barbara (UCSB).

In Chapter III, the responses of devices to proton irradiation with all pins grounded are characterized systematically. To obtain deeper understanding of defect formation during the irradiation, low frequency noise measurement results are discussed in Chapter IV.

After long-term hot electron stress, threshold voltage shifts show opposite polarities for Ga-rich and ammonia-rich devices, suggesting different dominating defects. The high field effects of both devices are investigated and compared with commercial parts in Chapter V.

The combined radiation and high field effects are discussed in Chapter VI. Three different biases (OFF, GND and semi-ON) are applied during the irradiation. Semi-ON stress before/during irradiation greatly enhances the degradation, which provides insight to space applications.

The last chapter provides a summary and conclusions of this work.

Chapter II

Background

Introduction

In this dissertation, proton irradiation and hot carriers introduce defects in GaN HEMTs, therefore degrading the device performance. In this chapter, previous work on radiation effects, particularly displacement damage and failure mechanisms of GaN HEMTs, are discussed in order to provide context for this work. Low frequency 1/*f* noise, as a diagnostic tool, is also introduced in this chapter. The last part of this chapter introduces the device structure and the measurement setup of this work.

Displacement damage on GaN HEMTs

The radiation hardness of GaN-based devices exposed to energetic particles that produce displacement damage is about one order of magnitude higher than for competitors like AlGaAs/GaAs HEMTs, as a consequence of higher binding energy in GaN. A higher binding energy translates to a reduced introduction rate of primary radiation defects. The energetic particles in space causing permanent damage in electronics include protons, electrons and heavy charged particles. A variety of effects in the characteristics of GaN HEMTs system can occur after radiation exposure:

(1) Shift in pinch-off voltage

(2) Increase in junction leakage

(3) Mobility degradation

(4) Increase in noise

Several different physical processes are involved when these energetic particles interact with semiconductor devices. The first process is ionization, when charged particles interact with target materials and create electron-hole pairs. The second process is displacement damage when an incident particle transfers enough energy to move the target atom from its normal lattice position to another position, creating a vacancy in the lattice.

The ionization process results in the generation of defects, with the defect creation rates depending on sample quality and doping level [24]-[26]. Significant degradation of AlGaN/GaN HEMTs was observed only after a γ-ray (^{60}Co) dose of many tens or even hundreds of Mrad(Si) [27][28]. Devices show a negative shift in threshold voltage, which is dominated by an increase in trap density. Other experiments [29], [30] and [31] with similar results suggest that damage due to particle irradiation is of much more concern in GaN-based devices, which are more sensitive to displacement damage than ionization effects.

The minimal energies to remove a Ga or N atom from a perfect lattice are measured as 18 eV for Ga and 22 eV for N, with the average displacement energies much higher, 45 eV for Ga and 109 eV for N [32][46]. The average thresholds are much higher than the average recoil energies (less than 20 eV [33]), which suggests that the degradation after irradiation is hard to explain only by the displacement of atoms from a perfect lattice. Various processing technologies employ different surface and layer growth, which leads to different degradation responses to both proton irradiation and electrical stress. These as-processed defects dominate the radiation response and reliability issues of GaN HEMTs, as discussed in detail in the following chapters.

Proton damage and annealing effects in GaN/AlGaN HEMTs were initially investigated by Cai. *et al*. [47]. The dc current and transconductance decreased from 260 to 100 mA/mm and from 80 to 26 mS/mm, respectively, after devices were irradiated to a 1.8 MeV proton fluence of 10^{14} p/cm^2. The room temperature annealing was not significant until the temperature was raised to over 600 ℃ (Fig. 2-1), suggesting lattice strain may play a role in annealing at very high temperature.

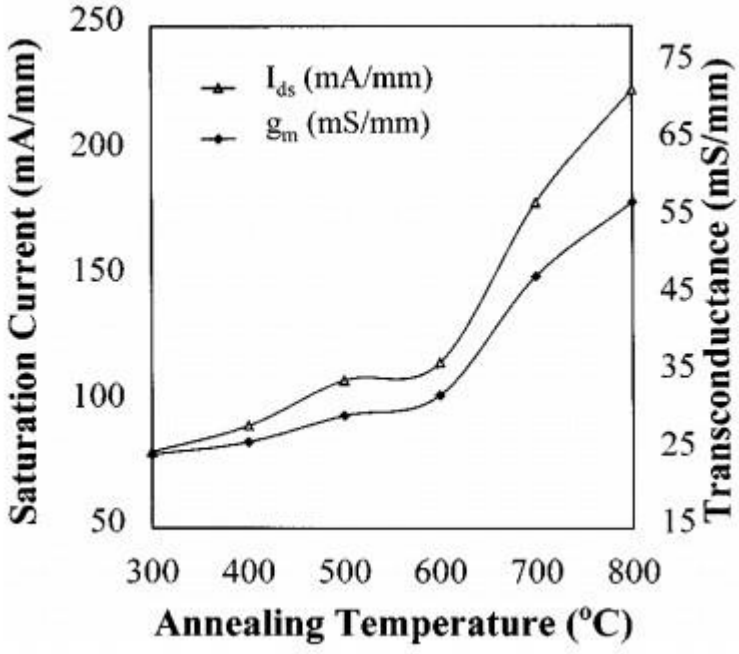

Fig. 2-1 Transconductance and saturation current of the HEMT vs. annealing temperature at V_{ds} = 10 V, and V_g = 0.5 V. Before irradiation, g_{m0} = 80 mS/mm, I_{ds0} = 260 mA/mm. (after [47]).

Similar proton irradiation studies at different energies ([34]-[40]) suggest that GaN-based devices are extremely radiation hardened and proton energy has a strong effect on the amount of damage created in the 2DEG of the HEMT because of differences in nonionizing energy loss [41][42].

To understand the effects of radiation species in space environments, Sonia *et al.* [43] irradiated devices with 2 MeV protons, carbon, oxygen, iron, and krypton ions with fluences ranging from

1×10^{9}/cm^2 to 1×10^{13}/cm^2. Hu *et al.* [31] evaluated the energy dependence of proton-induced degradation at 1.8, 15, 40, and 105 MeV. Maximum transconductance and saturation current reductions were obtained at 1.8 MeV energy and fluences of 10^{12}/cm^2, due to much larger non ionizing energy loss.

Roy *et al*. studied the 1.8-MeV proton radiation response of GaN HEMTs fabricated under Ga-rich, N-rich and NH_3-rich conditions. Positive shifts in pinch-off voltage were obtained in all three kinds of devices and N vacancies were suggested to be responsible for an increase in $1/f$ noise after irradiation [38][44]. N vacancies and divacancies can be generated during the irradiation. At the operating bias condition, these acceptor-like traps were negatively charged, leading to the positive shift in V_{th}. Fig. 2-2 shows the formation energy of N vacancies a function of the position of the Fermi Level in the band gap of AlGaN, while under operating bias conditions, the Fermi level is 1.2 eV below E_C. The slopes indicate different charge states, and the change in slopes, one of which is pointed out in the figure, identifies a potential trapping level at a particular energy.

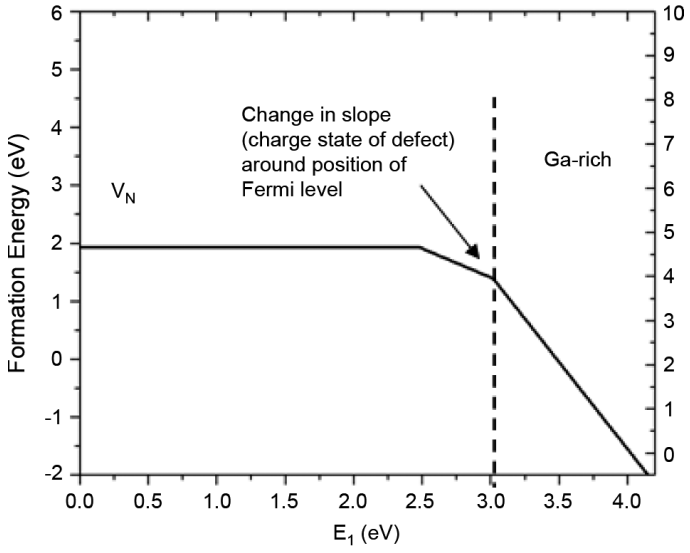

Fig. 2-2. Formation energy of N vacancies as a function of the position of the Fermi level in the band gap of AlGaN. (after [38])

Proton Irradiation Setup in this dissertation:

AlGaN/GaN HEMTs were irradiated with 1.8 MeV protons to a maximum fluence of 1×10^{14} cm^{-2} using the Vanderbilt Pelletron facility. The proton irradiation effects are firstly investigated with all terminals grounded during irradiation (Chapter III). In Chapter VI, as combined high-field and radiation effects are considered, the devices are irradiated at three different biases (GND, OFF and semi-ON), which will be introduced in detail in Chapter VI. The proton energy is chosen for large non-ionizing effective loss (NIEL), and 1×10^{14} cm^{-2} is a very high particle fluence [48], compared to realistic space environments. The irradiation is performed at room temperature. DC, RF and *1/f* noise measurements are taken before and after exposure. The damage to the devices is stable, as little annealing was observed at room-temperature.

Reliability Study on GaN HEMTs

Due to its high breakdown voltage, GaN HEMTs can operate in conditions that are not readily realizable with other device technologies. Since 2004, commercial GaN HEMTs have started to appear on the market, targeting the low-frequency, high efficiency end of the market. With the development of GaN HEMTs, achieving a high level of reliability and stability with high-performance operation becomes one of the greatest challenges [49], which requires a better understanding of failure mechanisms of GaN HEMTs.

Temperature-activated degradation:

Due to their wide band-gap and chemical stability, high-temperature applications are one of the

distinctive advantage of GaN HEMTs. The reliability and performance under high-temperature conditions have been studied often [50]. GaN HEMTs appear to provide stable device performance at room temperature (with junction temperatures up to ~150-200 ℃) [51]. Standard metallizations (Ti/Al/Pt/Au ohmic contacts and Pt/Au Schottky contacts) were investigated by Chou *et al*. [52]. The stability of 0.25-μm AlGaN/GaN HEMTs was evaluated for devices subjected to step-stress for 48 hours up to 400 ℃ junction temperature. Though the HEMTs degrade significantly above 300 ℃, the morphology of the metal contacts still provides good stability, pointing to material defects as the main limiting factor for high-temperature reliability. Thermal stabilities of other metallizations [53]-[58] also indicate that "gate sinking," which is one of the major failure mechanisms of GaAs MESFETs and HEMTs, appears not to be problem for GaN HEMTs. The long-term reliability of AlGaN/GaN HEMTs is less likely to be limited by temperature-activated wear-out than by the electrical degradation phenomena.

Reverse-bias (OFF-state) degradation:

GaN and AlGaN are both strongly piezoelectric materials. Large electric fields between the gate and drain can modify the strain configuration in the layer structure. For OFF-state accelerated tests with negligible channel currents, the existence of a failure mechanism accelerated by the electric field only has been reported, resulting in trap generation and charge trapping. Reductions in I_{DSS}, g_m and increase in the drain resistance and in the gate leakage current were found by Joh and del Alamo [16][59], who demonstrated that the electric field in the gate-drain region would increase the strain in the AlGaN/GaN heterojunction, which is also identified as the "inverse piezoelectric effect."

Simin *et al.* [18] reported that the gate field increases the tensile strain under the gate and

decreases it on the gate sides, thereby lowering the piezoelectric charge and increasing the parasitic resistance. It was also found via micro-Raman spectroscopy [60] that very large strain exists in the gate-drain surface area and the strain increases with drain-gate bias. In other work [16][17], it was reported that defects may form through relaxation of this inverse piezoelectric strain. The critical gate-drain voltage that triggers this effect is around V_{GD} ~ 20 to 30 V for the tested devices, showing a permanent increase in gate leakage current.

The negative influences from inverse piezoelectric effects and pre-existing strain provide motivations for research on InAlN barrier layers, for potential future device applications. In [61] it was shown that InAlN/GaN HEMTs can achieve high breakdown voltage, low leakage current and high temperature operation.

Other mechanisms can also affect the reliability of GaN devices under OFF state bias. As the field increases, the vertical breakdown of the AlGaN layer can cause a leakage path between the gate and GaN buffer layer. Moreover, the electrons injected from the gate due to trap-assisted tunneling can achieve very high energies, therefore damaging the semiconductor surface and interfaces and inducing traps [62].

Hot electron degradation:

Degradation due to hot electrons is one of the most significant failure mechanisms of GaN HEMTs, which are typically operated at very high drain voltages. Hot electrons can generate traps, leading to degradation including current collapse and gate-lag; they may also be trapped on the device surface, in the AlGaN or in the buffer, giving rise to reversible degradation of I_{DSS} and g_m [63]-[74]. In order to evaluate hot carrier effects in GaN HEMTs, electroluminescence (EL) microscopy and

spectroscopy are introduced as a powerful failure analysis tool [1][75]-[77]. EL intensity is a good indicator of the hot electron concentration in GaN HEMTs. Fig 2-3 shows EL micrographs for two conditions: (a) ON state and (b) close to pinch-off. The false colors in Fig 2-3(a) show that the emission is evenly distributed along the channel, and in Fig 2-3(b) the preferential emission sites are observed due to the contribution to EL of electrons injected from the gate into the channel.

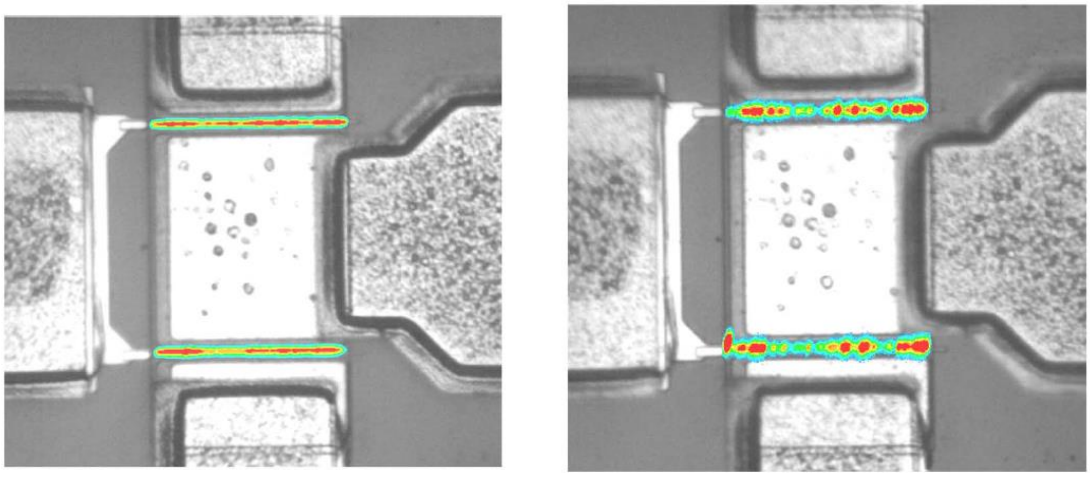

(a) (b)

Fig. 2-3 (a) EL micrograph under ON state. (b) EL micrograph close to pinch-off. (After [1]).

The EL intensity is plotted as a function of gate bias in Fig 2-4. The parabolic response shows three bias regimes. On the left side, where gate bias is very close or smaller than pinch-off, negligible current with high electric field is observed, suggesting low hot-electron density. In the middle part, medium current with medium electric field is observed. The peak of the bell-shaped curve suggests fairly high hot electron density at that regime, which is the so-called “semi-ON” region. On the right side, when the device is fully ON, high current and lower electric field is observed, while achieving low hot electron density. To better assess hot electron induced degradation with a fixed V_{DS}, it is of great significance to set the gate bias in the semi-ON region, which is often found to be the bias condition for which the most degradation occurs.

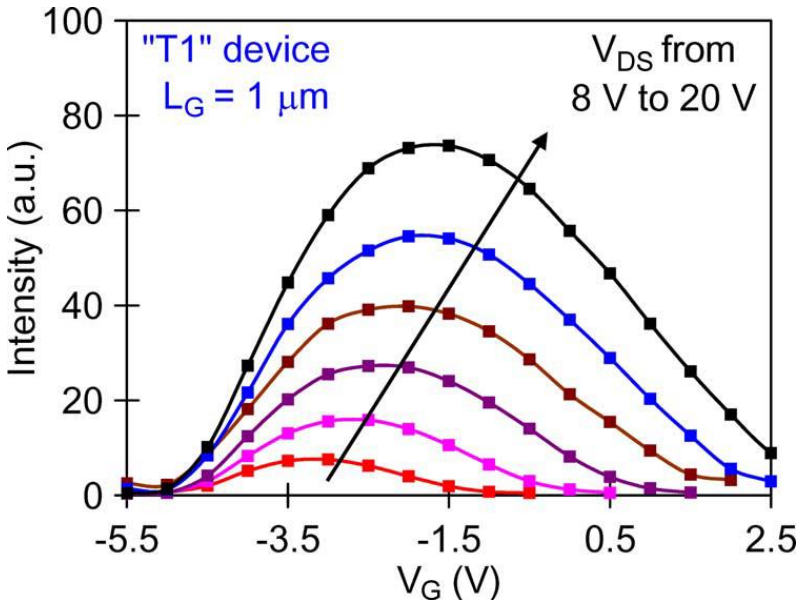

Fig. 2-4 EL intensity as a function of gate bias at various of drain voltages. (After [1]).

Low Frequency 1/f Noise

Many physical systems exhibit spontaneous fluctuations (noise), which contain a large amount of information about a system and its interaction with the surrounding environment. When a constant bias is applied to a semiconductor device, the current will show fluctuations, and the spectral density varies over a large range of frequencies. Two sources of current-induced noise are frequently observed. At high frequencies, the noise is white, and results from a combination of shot noise and Johnson noise. However, at sufficiently low frequencies, the noise is proportional to $1/f^{\alpha}$ (with typical value of α close to 1). This noise is known as *1/f* noise, pink noise, or flicker noise.

There are a variety of mechanisms that have been considered to be responsible for noise in the intrinsic HEMT, e.g., carrier velocity fluctuation, gate leakage, and traps [78][79]. The velocity fluctuation corresponds to the thermal noise and the gate leakage noise is associated with electron

injection into the channel over the gate Schottky barrier, which is frequency independent. Here we consider the effects causing by trapping of electrons in interface traps (located at the AlGaN/GaN interface), which leads to a 1/*f* dependence [85]-[87]. The excess drain-voltage noise power spectral density S_V is proportional to $f^{-\alpha}$, with α value close to unity [38][81][82].

Dutta and Horn [84] have shown that noise magnitude of metal films typically has a strong temperature dependence. They also demonstrated that the temperature dependence of the *1/f* noise is often due to a thermally activated random process with a distribution of activation energies, which varies with temperature.

Low frequency 1/*f* noise measurement setup:

In this work, low frequency *1/f* noise is measured for AlGaN/GaN HEMTs, before and after radiation/stress. The excess noise measurements were performed when the devices were biased in the linear regime, supplied by a HP 4140B constant voltage supply. A resistor is connected to the drain terminal for protecting and adjusting the drain bias. The gate voltage is adjusted so that the noise originates from the gated portion of the channel. The drain voltage noise is then amplified using a low-noise amplifier SR 560 and the power spectral density was calculated by a SR 760 spectrum analyzer, across a frequency span from 3 Hz to 390 Hz.

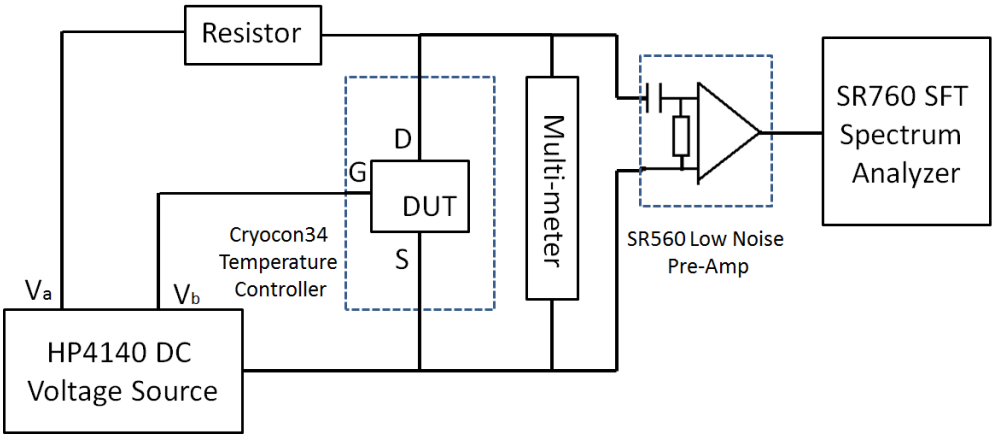

Fig. 2-5 Low frequency 1/*f* noise measurement setup. (after [83])

Device Information

AlGaN/GaN HEMTs were fabricated on AlGaN/GaN heterostructure layers grown by molecular beam epitaxy (MBE) on 4H-SiC substrates at the University of California, Santa Barbara. Commercial parts with similar structure from *Qorvo Inc.* are also investigated and compared with the university-fabricated devices.

A schematic cross-section of a GaN HEMT is shown in Fig 2.6(a), and the top view of the device is shown in Fig 2.6(b). Devices are mounted in a high-speed package for RF and low frequency noise measurements (after [85], shown in Fig 2.6(c)). The MBE growth of the AlGaN/GaN heterostructures was performed under Ga-rich and NH_3-rich conditions. PAMBE growth traditionally occurs at lower temperatures in a Ga-rich environment. NH_3-rich growth traditionally occurs at higher temperatures in excess NH_3 which pyrolizes on the growth surface [86] [87]. For each process type, the devices under test are 150 µm wide. The gate length of the samples is 0.7 µm; L_{GD} = 1 µm and L_{GS} = 0.5 µm. The 2DEG lies below the AlGaN layer and a buffer layer of AlN separates the GaN and the SiC substrate.

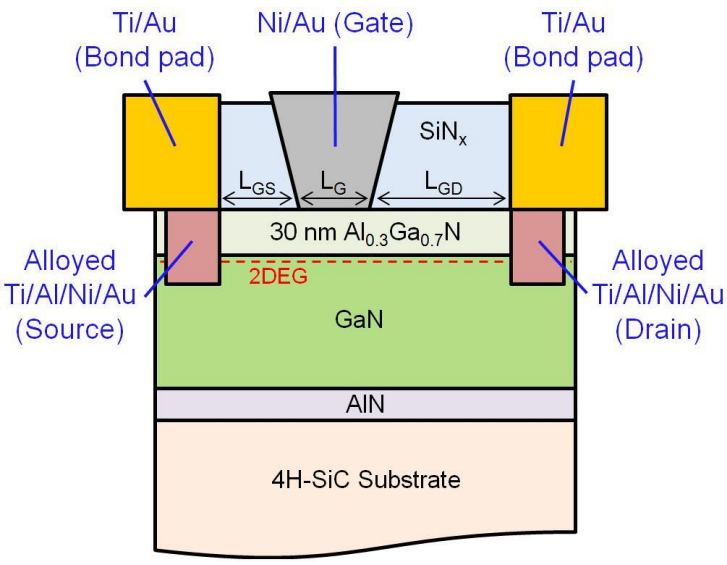

(a)

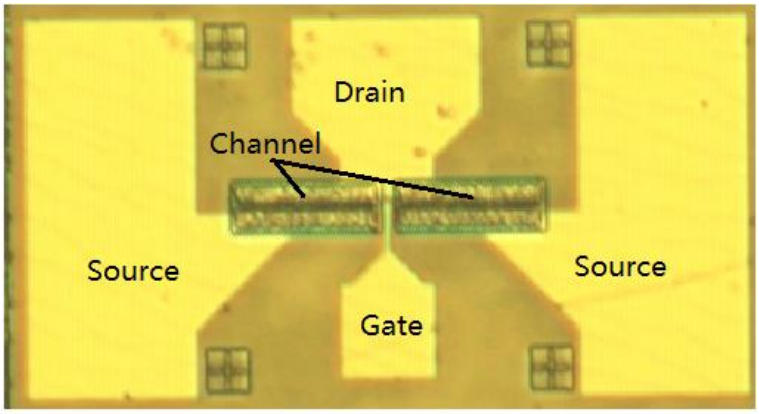

(b)

(c)

Fig. 2-6 (a)Schematic cross-section of an AlGaN/GaN HEMT. (after [91]) (b) Topview of DUT. (c) High-speed package (after [85]).

Experiment Setup and Measurement Techniques

DC Measurement Example:

The DC characteristics are measured with HP 4156B and Agilent B1505 parameter analyzers. Fig. 2.7 shows the DC characteristics for a typical Ga-rich GaN/GaN HEMTs. In Fig. 2-7(a), I_d-V_d curves of AlGaN/GaN HEMTs are shown. V_{gs} starts from V_{th}, with V_{gs} steps = 1 V. V_{ds} is swept from 0 to 10 V. The saturation current is around 120 mA at V_g-V_{th} = 4 V, corresponding to a current density of 800 mA/mm. Fig. 2-7(b) shows the I_d-V_g characteristics, with a pinch-off voltage of -3.41 V here. For other HEMTs in this thesis, it varies from -3 to -5 V. The gate length is 0.7 μm, corresponding to a gate leakage current density of ~2 mA/mm around pinch-off (Fig. 2-7(b)). Qorvo parts show an original threshold voltage around -3 V and a drain current 4-5 times larger.

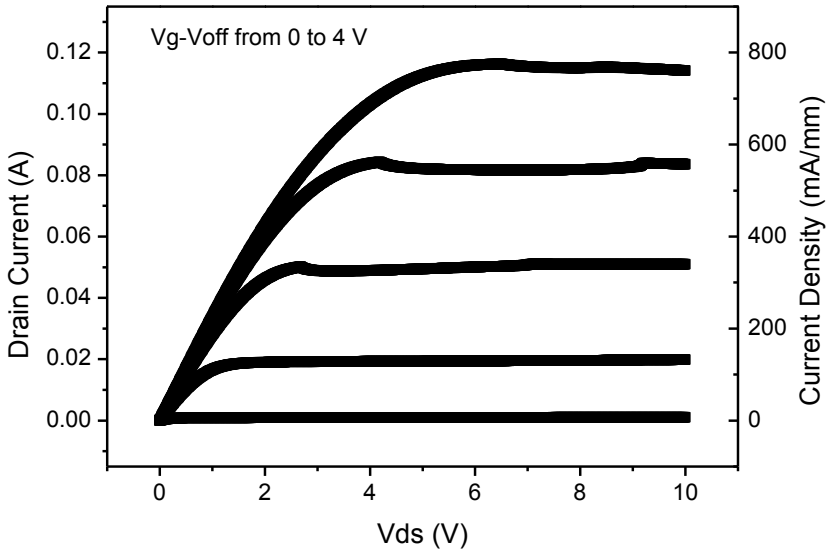

(a)

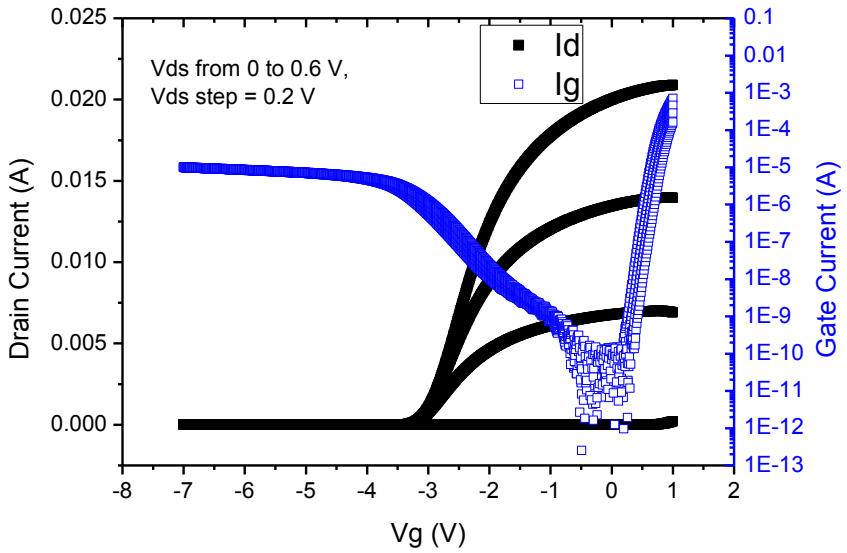

(b)

Fig. 2-7 DC characteristics: (a) Id-Vd, (b) Id-Vg (left) and Ig-Vg (right) of GaN/AlGaN HEMTs.

RF Measurement Example:

The RF performance was characterized from 100 MHz to 20 GHz in a high speed package [85] (Fig. 2.6 (c)), using an Agilent N5245A network analyzer. Calibration was performed before testing, followed by a two-step de-embedding procedure under short and open circuits for all the data analysis [87]. Open and short patterns were used to subtract the effects of parasitic pad capacitances and inductances from the measured S-parameters [85], [89].

Measurement/bias conditions may change due to different research interests and device properties (*e.g*. Sensitive and fragile parts cannot be measured under high V_d bias). The detailed measurement condition for each section will be introduced separately in more details.

Chapter III

Radiation-induced Degradation on GaN HEMTs

Introduction

In space environments, energetic particles incident on semiconductor devices lose their energy to ionizing and nonionizing processes as they travel through the devices. The energy loss causes the production of electron-hole pairs (ionization) and displaced atoms (displacement damage).

Most previous studies of radiation effects of GaN HEMTs suggest significant radiation tolerance and ionizing damage is less important compared to displacement damage. Due to higher surface state density, much higher total dose levels are required to affect the interface-trap density. Moreover, in many AlGaN/GaN HEMTs, there is no oxide or other insulators at the gate or anywhere else in the structure. Therefore, little TID degradation would be expected [48]. In this chapter, the radiation-induced degradation is focused on 1.8 MeV proton irradiation with all pins grounded.

Experiment Design & Setup

The radiation effects on DC and RF performance of GaN HEMTs are studied in this section. The fluence of 1.8 MeV proton steps from 1×10^{12} to 1×10^{14} protons/cm^2. All pins are grounded during the irradiation, and DC/RF measurements are taken soon after the proton beam is turned off. Multiple times of measurements are taken for average, without finding significant changes between run to run.

DC sweep is measured at drain bias from 0 to 1V with step of 0.2 V. The peak transconductance is the maximum first derivative (slope) point of the I_d-V_g curves; the threshold voltage reported below is the gate-voltage axis intercept of the linear extrapolation of the I_d-V_g curve at that point The peak transconductance is then normalized to the value before irradiation, to cancel the sizing variations from part to part.

RF measurements are taken at semi-ON condition, with drain bias at 5V and gate bias close to pinch-off. Frequency ranges from 10 MHz to 20 GHz, with sampling points of 400, minimum signal level -15 dB. The system is calibrated at the same temperature and connections as irradiated beforehand. AC signals from gate and drain terminals are connected to the two channels on the PNA (parameter network analyzer) via high-quality bias-tees (while DC signals connected to parameter analyzer). Source terminals are grounded.

Temperature is not controlled intentionally, assuming room temperature of 300K is applied according to lab environment.

At least 5 devices with similar trends are studied and analyzed. The figure in this sections show the device that performs closest to average.

DC Measurement after Proton Irradiation

Previous proton irradiation studies ([34]-[40]) suggest that GaN-based devices are extremely radiation hardened and proton energy has a strong effect on the amount of damage created in the 2DEG of the HEMT. In this work, both Ga-rich PAMBE and ammonia MBE AlGaN/GaN HEMTs were subjected to 1.8 MeV proton irradiation and the DC, RF characteristics before and after radiation

exposure were measured to show the proton-induced degradation.

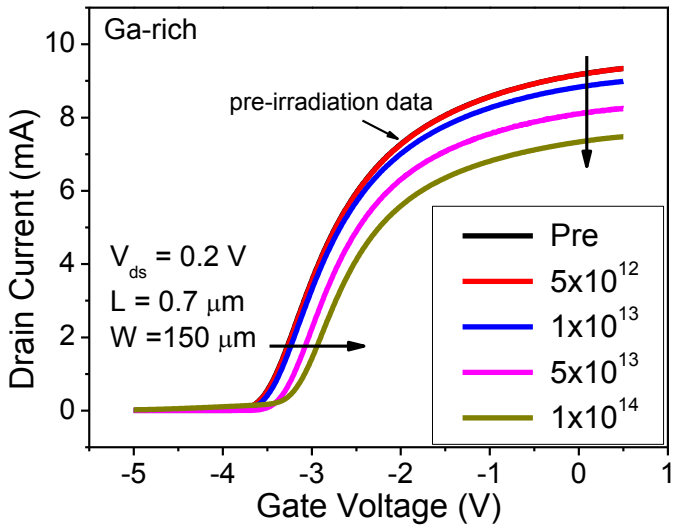

(a)

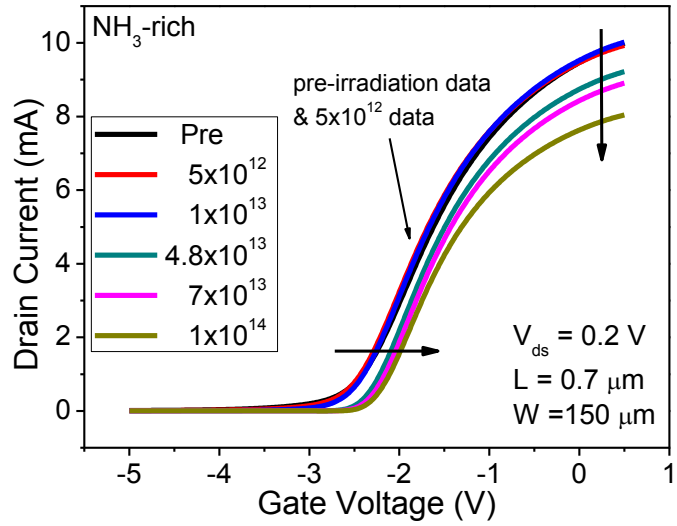

(b)

Fig. 3-1 I_D-V_G curves for (a) Ga-rich and (b) N-rich devices, before and after proton irradiation. Fluences are quoted in protons/cm^2. (after [91])

Fig. 3-1 shows the I_D-V_G characteristics of AlGaN/GaN HEMTs grown under (a) Ga-rich and (b) ammonia-rich conditions, before and after irradiation. A positive shift in pinch-off voltage $V_{pinch\text{-}off}$ with increasing fluence is shown for each device type in Fig. 3-2, indicating the creation of acceptor-like

traps by proton bombardment. These have been attributed in previous work to an increase in N vacancy-related defects [38]. After a fluence of 1×10^{14} cm^{-2}, the pinch-off voltage shift is 0.27 ± 0.03 V for both device types. The on-state current decreases after irradiation in Fig. 3-1, suggesting that proton irradiation creates deep acceptor traps.

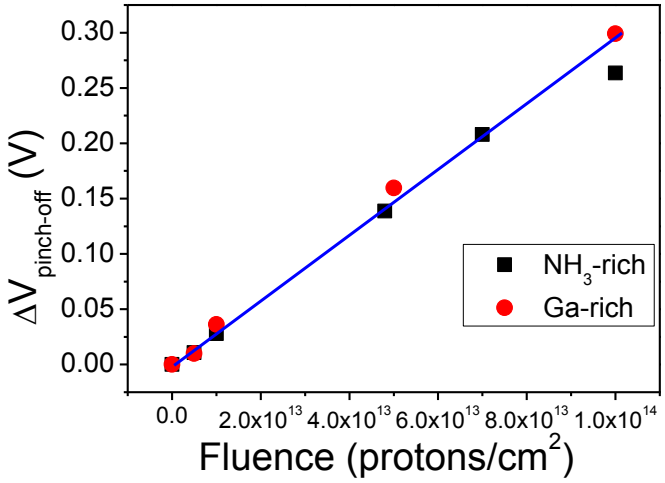

Fig. 3-2 Changes in pinch-off voltage as a function of proton fluence for Ga-rich and ammonia-rich AlGaN/GaN HEMTs. (after [91])

Fig. 3-3 shows the peak transconductance of the Ga-rich and NH_3-rich devices as a function of proton fluence. The peak transconductance of the Ga-rich HEMTs drops by an average of ~12%, while that of NH_3-rich devices drops by only ~2%. This result is somewhat surprising, since approximately similar shifts in $V_{pinch\text{-}off}$ are observed in Fig. 3-2 for the two device types, and there is clearly a decrease in on-current for each of the device types in Fig. 3-1.

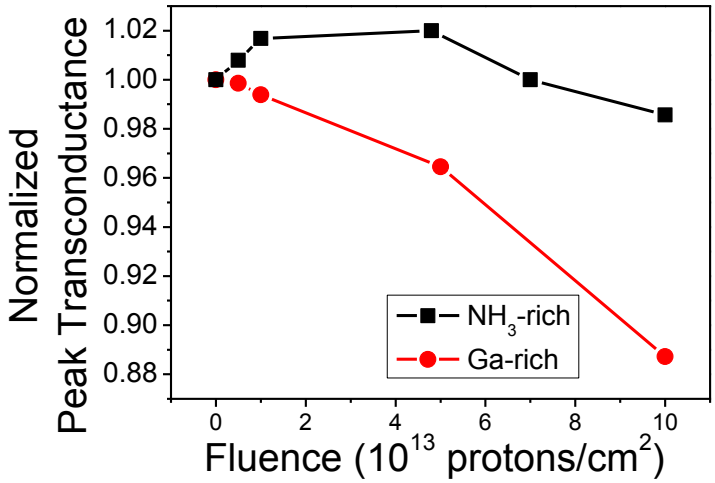

Fig. 3-3 Changes in normalized peak transconductance as a function of proton fluence. (after [91])

We examine the full transconductance curves as a function of V_G - $V_{pinch\text{-}off}$ in Fig. 3-4. For the Ga-rich devices, there is a decrease in transconductance with proton irradiation at all values of V_G - $V_{pinch\text{-}off}$, but for the NH_3 rich devices, the transconductance increases for V_G - $V_{pinch\text{-}off}$ < 0.5 V, but decreases at higher values of V_G - $V_{pinch\text{-}off}$. Because the transconductance degradation is related to defect scattering, and because the occupancy of charged defect sites can vary significantly with applied gate voltage [44], [92]-[84], these results suggest that, despite the similarities in $V_{pinch\text{-}off}$ shifts in Fig. 3-1, there are different defect densities and energy distributions in irradiated Ga-rich and NH_3-rich devices. This conclusion is reinforced by detailed studies of the low frequency noise below.

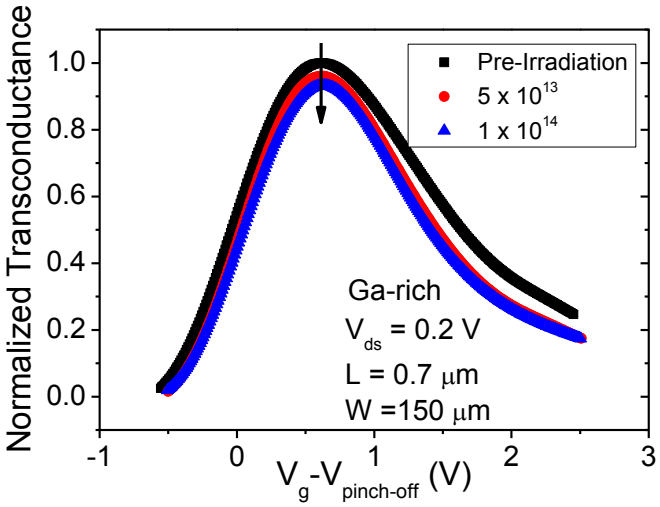

(a)

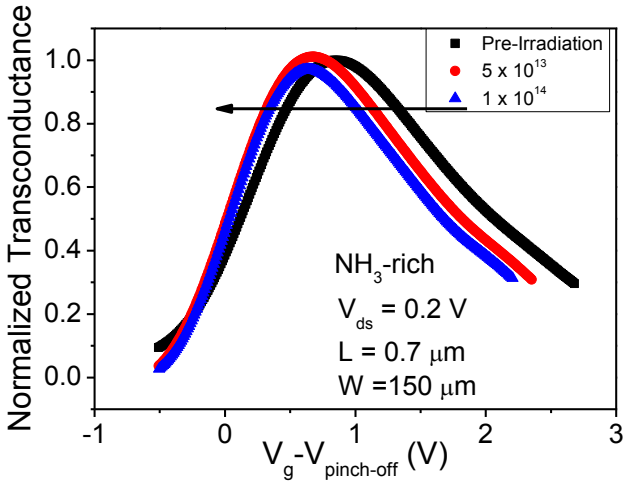

(b)

Fig. 3-4 Changes in normalized peak transconductance as a function of V_G - $V_{pinch\text{-}off}$, for (a) Ga-rich and (b) ammonia-rich devices. (after [117])

Fig. 3-5 shows the I_G-V_G characteristics for both types of devices, before and after irradiation. Little change in forward gate current is observed after a proton fluence of 1×10^{14} cm^{-2}, indicating that the Schottky barrier height of the gate contact does not degrade much during the irradiation. The reverse gate leakage decreases with increasing fluence for both device types. Thus, gate leakage does not play a significant role in the degradation of these devices with proton irradiation.

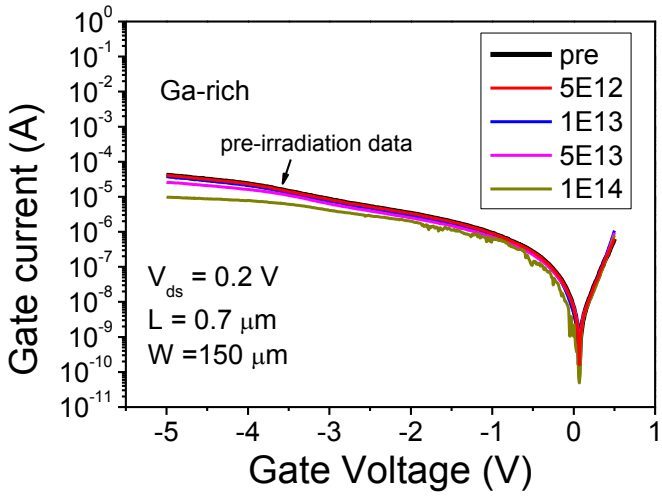

(a)

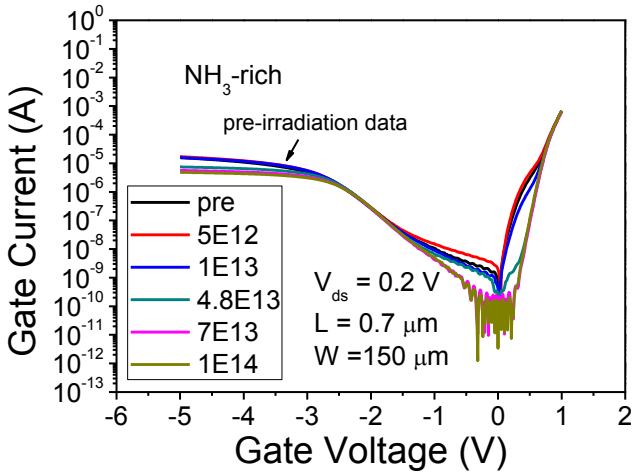

(b)

Fig. 3-5 I_G-V_G curves for (a) Ga-rich and (b) N-rich devices, before and after irradiation. (after [91])

Small Signal Responses

Small-signal scattering parameters (S-parameters) were measured for devices in high speed packages [85][88][89] before and after irradiation. The levels of S parameters show strong toggle with bias conditions, both gate and drain biases. Positive S_{21} value are observed at semi-ON condition, and the maximum of S_{21} increase with drain bias significantly at moderate ranges (<25V). After irradiation,

changes are observed on each S parameters, as shown in Fig. 3-6. For better observation, in the following measurement, drain bias is set to 5 V and gate bias is chosen to reach the maximum S_{21} value before irradiation.

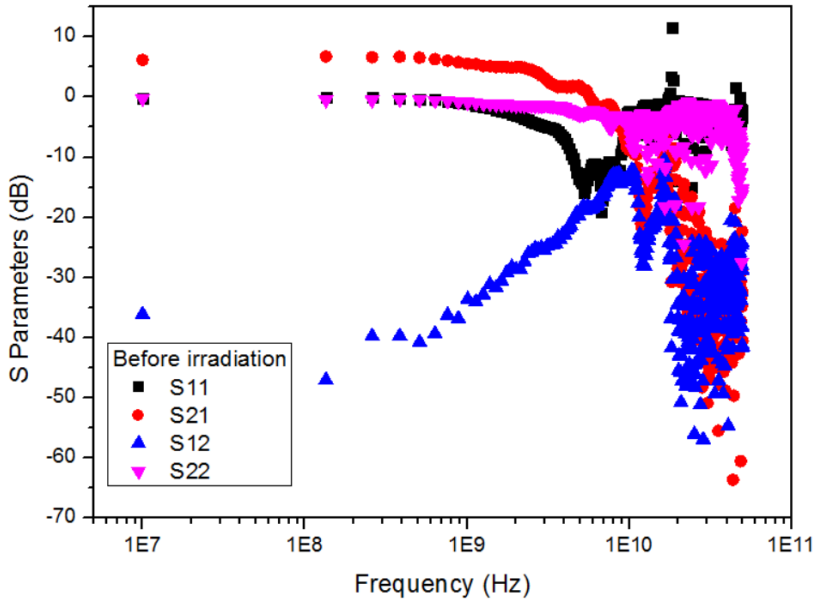

(a)

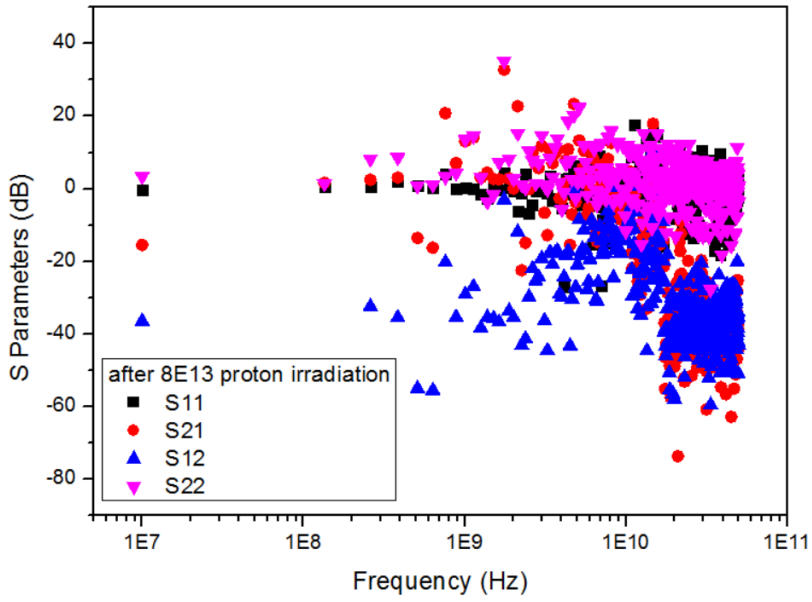

(b)

Fig. 3-6 S parameters measurement (a) before and (b) after irradiation on NH_3-rich devices.

Of particular interest, $|S_{21}|^2$ represents the forward power gain of the transistor, so any significant change in S_{21} is a convenient measure of RF performance degradation. The small-signal current gain ($|h_{21}|$) is calculated from the measured S-parameters via [94]:

$$h_{21} = \frac{2S_{12}}{(1-S_{11})(1+S_{22})+S_{12}S_{21}}$$

After irradiation, the values of $|S_{21}|$ measured at V_d = 5 V and V_g = 0 V decrease for both device types, as shown in Fig. 3-7. The value of $|S_{21}|$ of Ga-rich devices decreases by 0.7 dB, which indicates that the output voltage drops by 7.8% after irradiation, thus reducing the power gain $|S_{21}|^2$ by 15%. The reduction in $|S_{21}|$ is 0.8 dB, corresponding to an ~8.8% reduction in output voltage, and ~17% reduction in output power. The percentage reduction in $|S_{21}|$ for the Ga-rich devices matches the degradation in DC g_m well, but the reduction in $|S_{21}|$ for the NH_3-rich devices is much larger than the DC g_m degradation (<2%). The proton irradiation also influences the frequency limit of operation, especially for the NH_3-rich devices, as we will discuss below. Note that, up to ~ 3 GHz, NH_3-rich devices show superior RF performance before and after irradiation. Above ~3 GHz, the Ga-rich devices exhibit superior performance (Fig. 3-7).

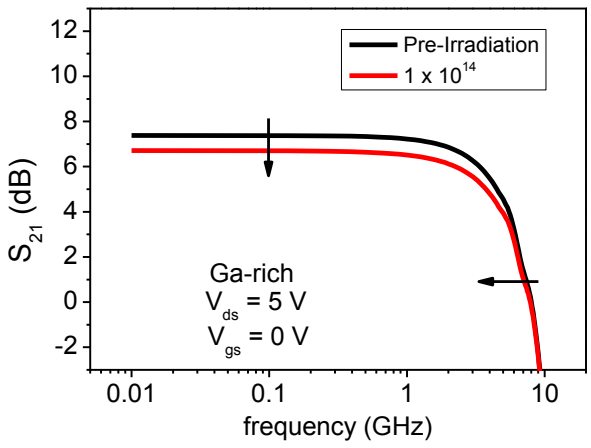

(a)

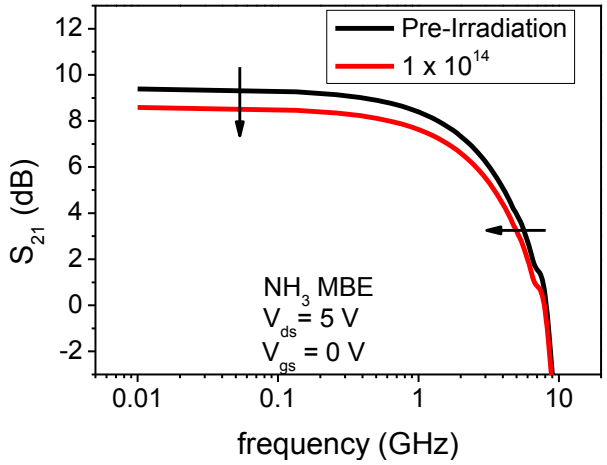

(b)

Fig. 3-7 Changes in S_{21} as a function of frequency for (a) Ga-rich and (b) NH_3-rich devices. (after [117])

Fig. 3-8 plots $|h_{21}|$ as a function of proton fluence and gate bias. For Ga-rich devices (Fig. 3-8(a)) at all fluence levels, $|h_{21}|$ does not shift significantly, after correcting for the changes in the pinch-off voltage, consistent with the DC g_m *vs.* V_G - $V_{pinch\text{-}off}$ response shown in Fig. 3-3(a). The average value of $|h_{21}|$ over the full voltage range drops by 1 dB (decrease of ~ 11% in output signal) at 10^{14} protons/cm^2. The degradation in $|h_{21}|$ is a little bit larger than the corresponding decreases in DC parameters in Figs. 3-3(a) and 3-4(a). In Fig. 6(b), the $|h_{21}|$ curve for NH_3-rich devices is translated negatively, as referred to the pinch-off voltage, matching the behavior of DC transconductance in Fig. 3-4(b) well. However, the average loss of $|h_{21}|$ is around 2 dB (decrease of ~ 21% in output signal) at a fluence of 10^{14} protons/cm^2. The maximum loss reaches 3.5 dB (decrease of ~ 34% in output signal), which is much larger than the degradation in DC performance for these devices.

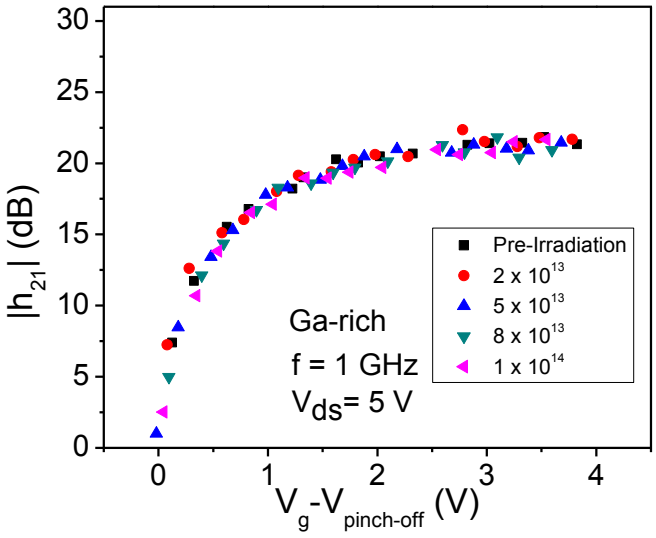

(a)

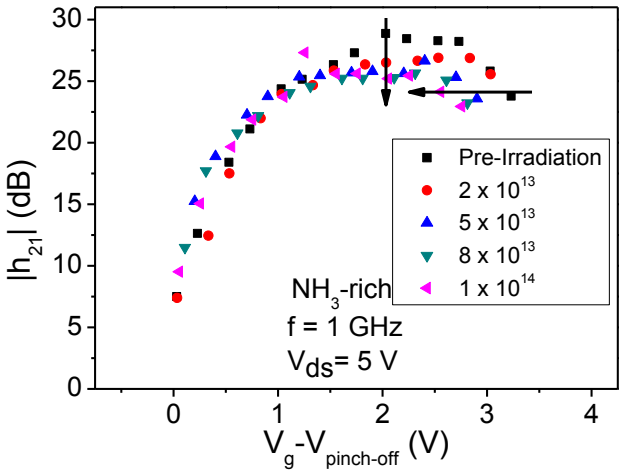

(b)

Fig. 3-8 Small-signal current gain before and after proton irradiation, measured at V_d = 5 V and f =1 GHz. (after [117])

The cutoff frequency f_T is the point where the current gain $|h_{21}|$ drops to unity. The maximum oscillation frequency f_{max} is extracted from Mason's unilateral gain [94]. Both f_T and f_{max} depend strongly on bias voltage and current, so we have characterized these parameters as a function of $V_G - V_{pinch-off}$, as shown in Figs. 3-9 and 3-10. The peak f_T values are ~ 12 GHz and ~ 11 GHz, for the Ga-rich and NH_3-rich devices, respectively, before proton irradiation. After irradiation, the peak

cutoff frequency decreases by 8% for Ga-rich devices and 9% for NH_3-rich devices (Fig. 3-9). The peak f_{max} is around 10 GHz for both types of devices, and decreases by 8% for Ga-rich devices and 10% for NH_3-rich devices after proton irradiation, as shown in Figs. 3-10(a) and (b), respectively.

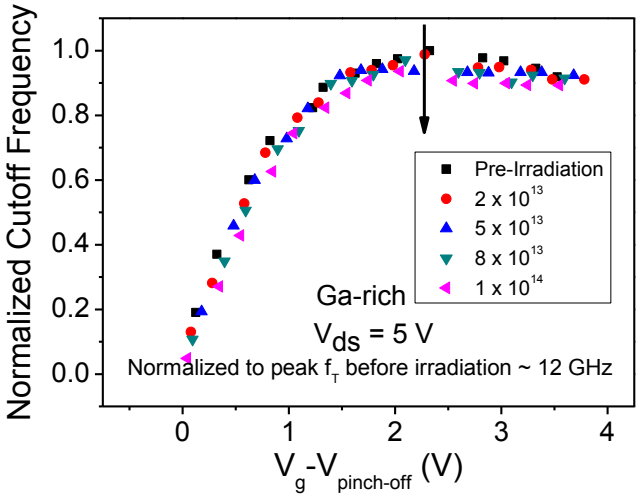

(a)

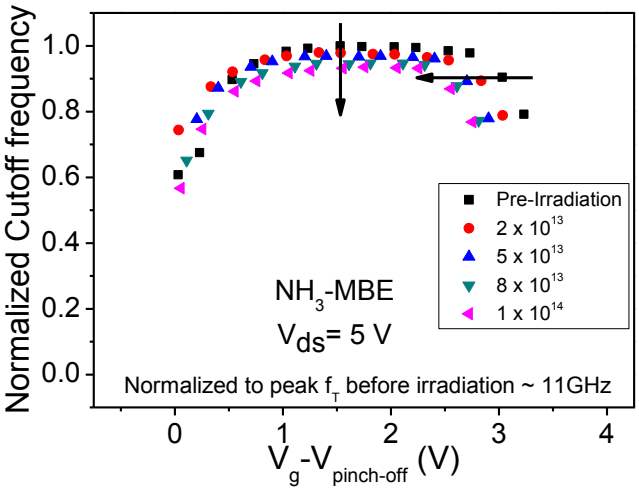

(b)

Fig. 3-9 Cutoff frequency f_T before and after proton irradiation, measured at V_d = 5 V. (after [117])

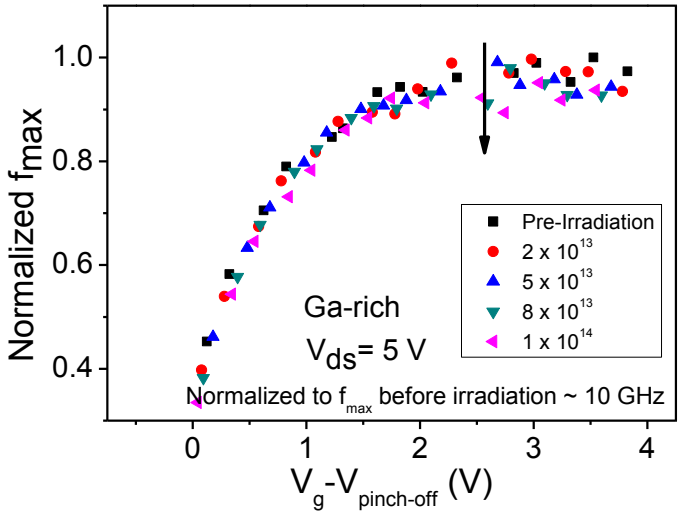

(a)

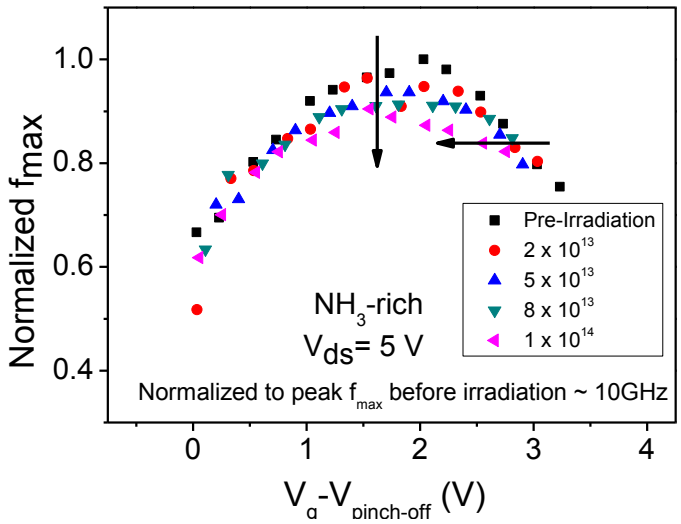

(b)

Fig. 3-10 Maximum oscillation frequency (f_{max}) of AlGaN/GaN HEMTs as a function of gate bias before and after proton irradiation, measured at V_d = 5 V. (after [117])

The frequency limit for the devices under study is approximately 10 GHz, as observed from small signal measurements. The small signal gains degrade after high-fluence proton irradiation. The degradation values measured via DC and small signal AC measurements are summarized in Table 3-1.

Table 3-1. DC and AC degradation for Ga-rich and NH_3-rich devices after proton

irradiation to 10^{14}/cm^2. $|S_{21}|$, $|S_{21}|^2$, and H_{21} are measured at f = 1 GHz, V_{ds} = 5 V. Frequency limits are measured at V_{ds} = 5 V. (after [117])

	Ga-rich	NH_3-rich
peak g_m	7.5%	3.5%
$\|S_{21}\|$	7.8%	8.8%
$\|S_{21}\|^2$(power gain)	15%	17%
H_{21} (current gain)	11%	21%
average f_T	8%	9%
average f_{max}	8%	10%

Because the non-ionizing energy loss of 1.8-MeV protons is much higher than that of the higher-energy protons that typically result in the degradation in space systems [43][95][96], the equivalent displacement damage doses in this study are quite high compared with most realistic space environments. Thus, both types of devices would exhibit excellent radiation tolerance in nearly any realistic space environment. For operation at frequencies from DC up to ~ 3 GHz, the NH_3-rich devices show clearly superior performance to the Ga-rich devices. However, at higher frequencies, the Ga-rich devices can provide superior performance. The RF performance of each type of device degrades more than the DC performance, especially for the NH_3-rich devices.

The greater RF degradation results from fast bulk and surface traps under the gate and in the gate/drain access region that can lead to gate lag, increased channel resistance, and increased device capacitance in AlGaN/GaN HEMTs [19], [97], [98]. The NH_3-rich devices, which naturally contain more hydrogen-related defects with low energy levels (≤ 0.3 eV) [38],[86],[99], show more RF degradation than the Ga-rich devices with fewer hydrogen-related defects. Thus, it is likely that the fast

traps in these devices are associated with the dehydrogenation of a defect-hydrogen complex [38],[44],[91], which is a common degradation mode in AlGaN/GaN HEMTs. However, future study is required to determine the microstructure of the particular defects that lead to the observed degradation in these particular devices.

The cutoff frequency f_T and f_{max} can be also be related to g_m, but these parameters are also quite sensitive to changes in the resistance and capacitance of the device, as described via [99]:

$$f_T = \frac{g_m}{2\pi(C_{gd} + C_{gs})}$$

and

$$f_{\max} \approx \frac{f_T}{2\sqrt{(R_i + R_s + R_g)/R_{ds} + (2\pi f_T) R_g C_{gd}}}$$

Here C_{gd} and C_{gs} are the gate-drain and gate-source capacitances, and R_i, R_s, R_g and R_{ds} are the resistances that correspond to input, source, gate, and drain-source, respectively. Because many of these parameters change significantly with irradiation, it is challenging to deconvolve the separate effects of individual parameters. Moreover, the changes in resistance and capacitance can lead to a significant impedance mismatch in an operating or testing circuit [89],[100]. However, device performance changes only modestly during high-fluence proton irradiation, so from a practical standpoint, these devices should continue to function with only slight degradation in any realistic space radiation environment.

Conclusion

In this chapter, proton-induced radiation effects in Ga-rich and NH_3-rich MBE-grown

AlGaN/GaN HEMTs are investigated via DC and RF measurements. After proton irradiation, acceptor-like traps are created, causing a positive shift in pinch-off voltage and changes in DC transconductance over the full range of gate biases applied. Critical device RF parameters such as current gain, f_T, and f_{max}, degrade more than DC g_m or carrier mobility. Fast bulk and surface traps contribute more significantly to RF parametric degradation than DC parametric degradation as a result of gate lag, increased channel resistance, and increased device capacitance. The resulting changes in resistance and capacitance cause impedance mismatches that increase the measured degradation of HEMT RF response in circuit applications. The NH_3-rich devices degrade more at RF frequencies than the Ga-rich devices, but show generally superior performance before and after irradiation up to ~ 3 GHz. At higher frequencies of operation, the Ga-rich devices offer superior RF performance.

The difference in RF responses between Ga-rich PAMBE and ammonia MBE devices is due to variations in fabrication process. The as-processed defects inside the devices can affect the radiation responses and reliability performance. By employing low frequency $1/f$ noise measurements, a deeper understanding of defects limiting device performances can be achieved, which will be discussed in the next chapter.

Chapter IV

Proton-induced defects Identification via Low Frequency *1/f* Noise Measurement

Introduction

Low frequency *1/f* noise can provide helpful information about the nature of the defects that limit the reliability of semiconductor devices. Temperature-dependent noise measurements were performed to provide helpful information on defect energy distributions. As the threshold voltage changes with temperature, the gate voltage is adjusted for a fixed increment from pinch-off voltage so that the electric fields remain approximately constant in the device. The drain-source bias is maintained at 0.15 V.

Experiment Design & Setup

Low frequency *1/f* noise is applied for a diagnose tool of radiation effects. After irradiated to target fluence levels with all pins ground, which is the same as described in Section III, DC measurements are taken on site. The device will be taken out of the Pelletron chamber and sent to the cryostat immediately. DC measurements will be taken again with all connections finished for noise measurement to check consistency. No significant changes are supposed to observe. The noise measurement is performed from 85 K to 445 K. Liquid nitrogen is used for cooling the system and

vacuum is required. Shielding and grounding need to be checked carefully as vacuum and grounding issues may introduce fluctuation to the results. The cryostat will assume reaching the target temperature with error range of +/- 0.3 degree. At each measurement, the noise signal is amplified by 200 times, sampled 4500 times and the floor is set to 1×10^{-17} (V^2/Hz). Background noise is subtracted.

For temperature-dependent noise measurement, the noise is measured from 85 K to 445 K continuously (~8 hours), and during the cooling-down, consistency check will be performed at a few temperatures. No significant changes are observed due to potential annealing. Once noise measurement finish, the DUT will be sent back to the Pelletron chamber again for higher fluences if needed.

Noise Spectrum of AlGaN/GaN HEMTs

Fig. 4-1 plots the excess drain-voltage noise power spectral density S_{Vd} (corrected for background noise) for Ga-rich HEMTs at constant $V_g - V_{pinch\text{-}off}$ = 2 V and V_d = 0.15 V as a function of frequency and temperature before and after exposure to a proton fluence of 1×10^{14} cm^{-2}. The bias voltages are chosen to ensure the noise originates from the gated portion of the channel, with an approximately constant channel resistance [38],[92]. The noise varies approximately inversely with frequency in Fig. 4-1. The frequency exponent γ at room temperature is 1.08 ± 0.03 for the devices of Fig. 4-1, which is typical of values observed in previous studies of AlGaN/GaN HEMTs [38],[92],[101],[82].

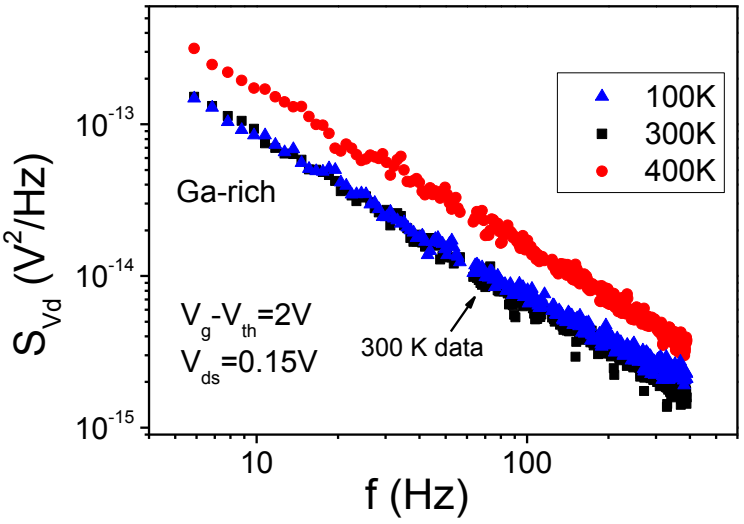

(a)

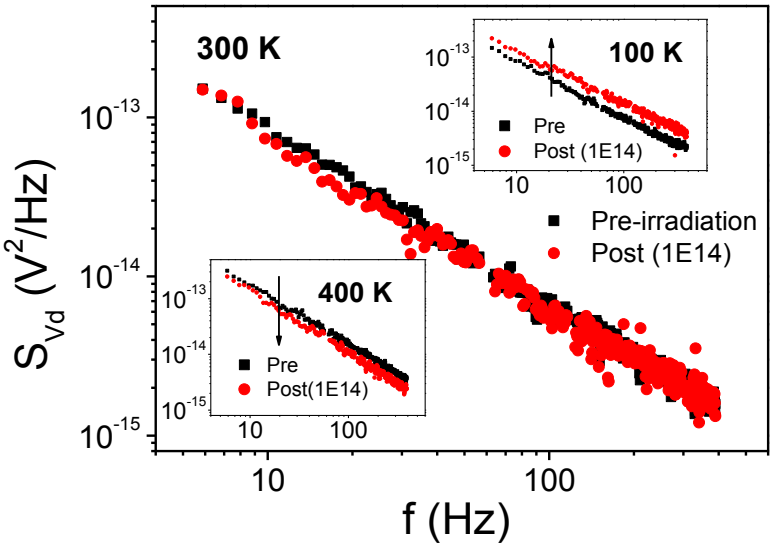

(b)

Fig. 4-1 Excess voltage noise power spectral density S_v as a function of frequency for Ga-rich HEMTs, at 100 K, 300 K and 400 K, (a) before and (b) after irradiation. $V_g - V_{pinch\text{-}off}$ = 2 V, and V_d = 0.15 V. (after [91])

In Fig. 4-1(a) the noise magnitudes are similar at 100 K and 300 K before irradiation, and increase at a measurement temperature of 400 K. Fig. 4-1(b) shows that the noise magnitude after proton irradiation increases at a measurement temperature of 100 K; stays approximately the same at a

measurement temperature of 300 K, and decreases at a measurement temperature of 400 K. At different temperatures, the noise levels increase or decrease after irradiation. Hence, it is of interest to evaluate the temperature dependence of the noise in more detail, especially since it is possible to relate changes in the temperature dependence of the noise of many types of semiconductor devices to changes in their underlying defect densities and energy distributions [87],[92],[84].

Temperature Dependence of Noise

The low frequency noise is measured over the temperature range from 85 K to 450 K. These temperatures correspond to an energy window from 0.20 eV to 1.05 eV. Devices were biased with constant V_d = 0.15 V and $V_g - V_{pinch\text{-}off}$ = 2 V as a function of temperature. The low frequency noise behavior can be quantitatively described by the Dutta-Horn model if the noise is due to random processes with thermally activated characteristics times [92],[84]. Assuming no new defects are generated or annealed during the measurement, the frequency and temperature dependence of the noise are related via:

$$\gamma(\omega,T)=1-\frac{1}{\ln(\omega\tau_0)}\left(\frac{\partial \ln S_V(\omega,T)}{\partial \ln T}-1\right).$$

Over the entire range of temperatures, for both Ga-rich and ammonia-rich devices, before and after proton irradiation, the experimental γ values fits the Dutta-Horn model well, as shown in Fig. 4-2. This suggests that the 1/*f* noise follows the Dutta-Horn model accurately [84],[101], which permits the association of features in the temperature dependence of the noise with changes in the defect-energy distribution $D(E_0)$. Here E_0 is the energy barrier between two metastable charge states of a defect, calculated via

$$E_0 = -kT \ln(\omega\tau_0)$$

Here k is the Boltzmann constant, T is the absolute temperature, $\omega = 2\pi f$, and τ_0 is the characteristic time for carrier-defect scattering. A typical value of τ_0 for defects in GaN is $\sim 3\times10^{-14}$ s [92]. The defect-energy distribution $D(E_0)$ is related to the temperature dependence of the noise magnitude in Fig. 4-3 via

$$D(E_0) \propto \frac{\omega}{kT} S_V(\omega, T).$$

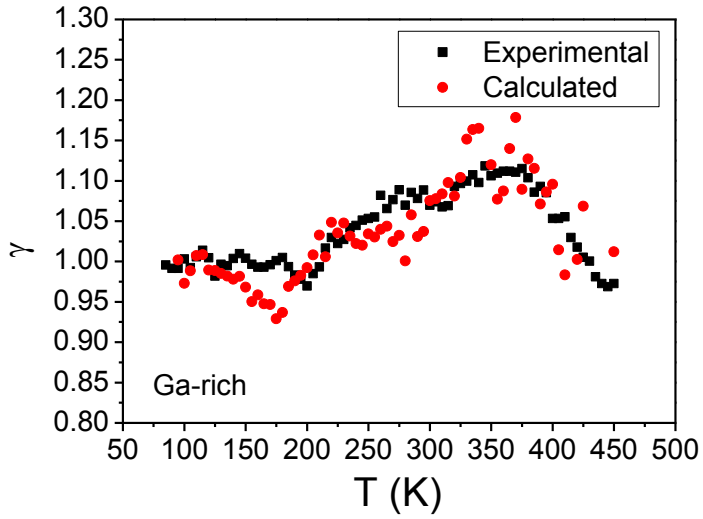

(a)

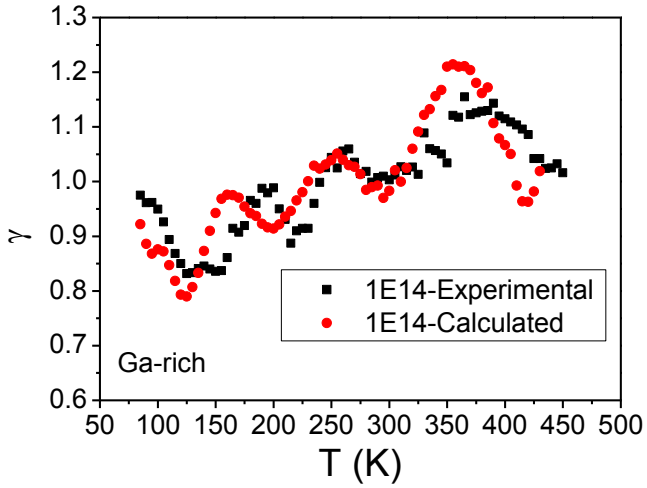

(b)

Fig. 4-2 Experimental and calculated frequency exponent of noise power spectral density as a function of temperature from 85 K to 450 K (a) before irradiation, (b) after a fluence of 1×10^{14} cm^{-2}. (after [91])

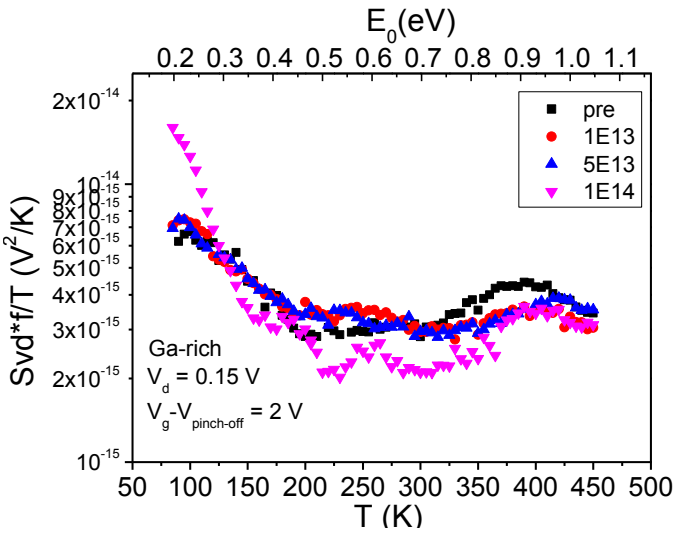

(a)

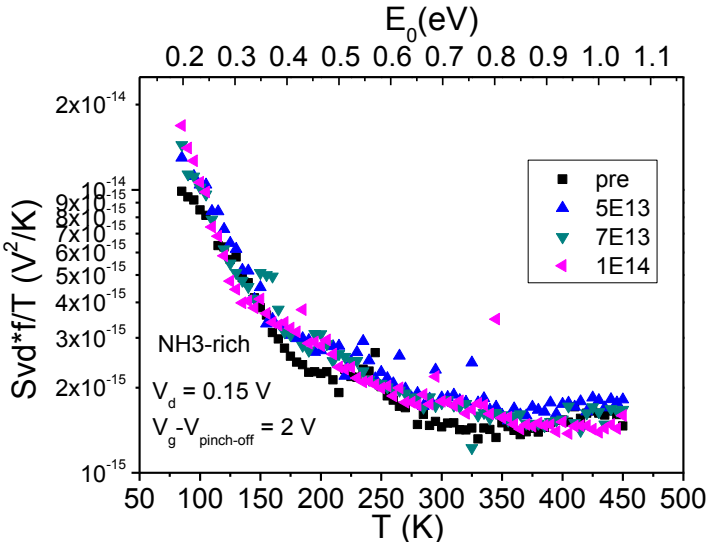

(b)

Fig. 4-3 Temperature-dependent noise measurements from 85 K to 450 K, before and after irradiation. Here $V_g - V_{pinch\text{-}off}$ = 2 V, V_d = 0.15 V for (a) Ga-rich and (b) ammonia-rich HEMTs for f = 10 Hz. The energy scale on the upper x-axis is derived from the Dutta-Horn model of low-frequency noise. The statistical uncertainty in the noise measurements is approximately equal to the symbol size. Noise measurements were reproducible from run to run and from day to day on these devices. (after [91])

For Ga-rich HEMTs in Fig. 4-3 (a), before irradiation, peaks are observed in the noise magnitude at ~90 K and ~400 K, with activation energies of ~ 0.2 eV and ~ 0.9 eV, respectively. The magnitude of the low-temperature peak increases with irradiation, while the high temperature peak decreases by a similar amount. In addition, a noise peak at ~ 0.5 eV is observed after proton irradiation. After a fluence of 1×10^{14} protons/cm^2, this new peak decreases, and the 0.2 eV peak increases significantly. The 0.9 eV peak does not vary much with fluence. The changes in peaks show that the defect distribution in the Ga-rich devices changes substantially after proton irradiation.

The NH_3-rich HEMTs in Fig. 4-3(b) do not show changes in noise spectra as large as the Ga-rich devices. This is consistent with the smaller degradation in peak transconductance of the NH_3-rich devices after proton irradiation (Fig. 3-3), as well as previous noise results obtained at room temperature [38].

Defect Identification

We performed density functional calculations to investigate the atomic-scale mechanisms of the defect evolution for the Ga-rich devices in Fig. 4-3(a). We used a plane-wave basis and the formulation of density functional theory implemented in the VASP (Vienna ab-initio pseudo-potential) package [102]. The exchange-correlation potential was used in the form of the Perdew-Burke-Ernzerhof generalized gradient approximation [103]. Electron-core interactions were treated in the projector augmented wave method [104][105]. The supercell we employed for the calculations contained 64 N, 45 Ga, and 19 Al atoms. The Brillouin zone was sampled with a 2 × 2 × 2 k-point grid (K is the wave number). All the atoms were relaxed until the self-consistent forces reached 0.05 eV/Å. For calculation

of the energy barriers, the nudged elastic band method [106] was used to find the saddle points.

Using similar computational methods, it was shown in [92] that the low temperature peak (~ 0.2 eV) often observed in AlGaN/GaN noise is most likely due to an oxygen DX center; i.e., O_N. We have found through extensive calculation, which included search among all possible geometric configurations of O and H atoms, that the 0.9 eV and 0.55 eV peaks observed in Fig. 4-3(a) are most likely associated with hydrogenated substitutional oxygen, i.e., O_N-H defects, which are depicted schematically in Fig. 4-4. The calculations show that the energy barriers for the reconfiguration of the O_N-H defect complexes are 1.0 and 0.5 eV for configurations I and II in Fig. 4-4(a), respectively. These barriers reflect the energy that is required for a hydrogen atom to move near a substitutional oxygen atom. If H is initially in configuration I, then energy of ~ 1 eV is required to move into configuration II. H in configuration II captures the electron. This process is equivalent to a 0/-1 charge state transition. However, if a negatively charged O_N-H defect is in configuration II, then after releasing an electron, only 0.5 eV is necessary to switch to configuration I.

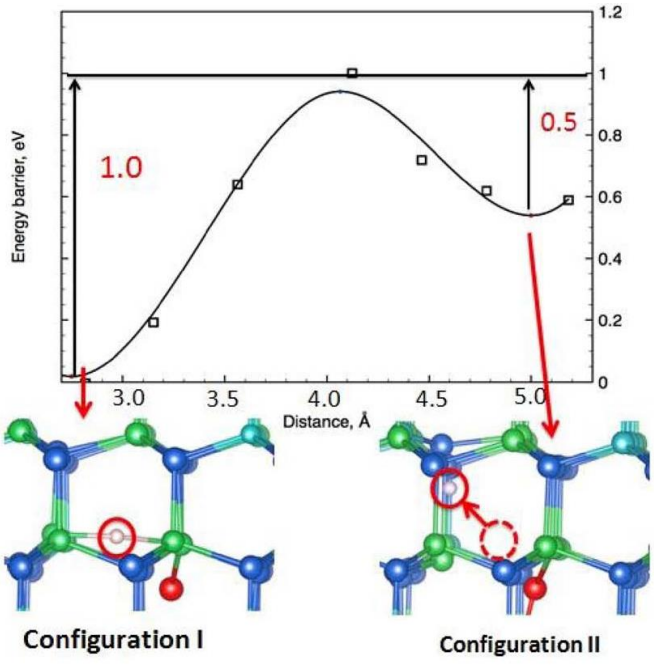

(a)

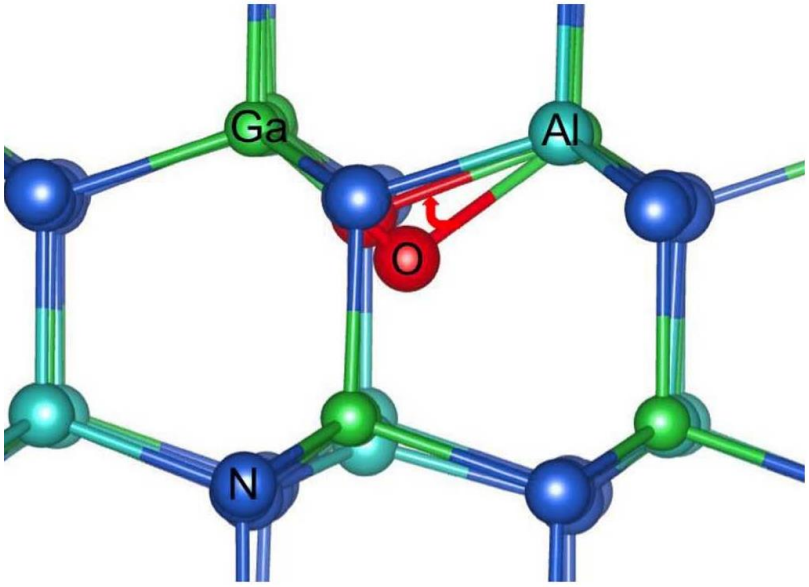

(b)

Fig. 4-4 Energy barriers as a function of O–N distance and defect configurations (I) and (II) of O –H (after [91])

During proton irradiation, a H atom can be removed from the O_N-H. This occurs most easily via interaction of transporting holes with the O_N-H, a process that is similar to what occurs in irradiated Si/SiO_2 structures when a transporting H is near an O-H complex [107]. This reaction occurs with a low energy barrier, as illustrated in Fig. 4-4(a). These calculations demonstrate that the decreases in the 0.9 eV defect peak and the increases in the 0.2 eV defect peak can be related to hydrogen removal from the O_N-H complex (Fig. 4-4(a)). The resulting reactions reduce the O_N-H density and increase the O_N defect density, as shown in Fig. 4-4(b). The small peak near 0.55 eV in Fig. 4-3(a) is likely associated with a reverse transition from intermediate configuration of the O_N-H complex, which is configuration II in Fig. 4-4(a). At larger fluences, the reductions in the 0.9 eV and 0.55 eV peaks are much smaller than the increase in the 0.2 eV peak, strongly suggesting that new low-energy defects are generated at the highest fluences. These newly created defects most likely are N vacancies [38],[92].

Conclusion

In this chapter, defect-related peaks are observed in the temperature dependence of 1/*f* noise at ~ 0.2 eV, ~ 0.55 eV, and ~ 0.9 eV. On the basis of these measurements and density functional calculations, we have found that at small fluences, the decrease in magnitude of the ~ 0.9 eV peak and growth in magnitude of the ~ 0.2 eV peak are consistent with the dehydrogenation of an O_N-H complex in the AlGaN layer, and a post-irradiation ~ 0.55 eV peak is likely due to the reconfiguration of the O_N-H complex. At larger fluences, new defects appeared and gave rise to a rapid increase in the 0.2 eV peak. Less proton-induced degradation of peak transconductance was observed in ammonia-rich devices, and no significant changes in noise levels are observed with proton irradiation.

Chapter V

High Field Stress and Long Term Reliability of AlGaN/GaN HEMTs

Introduction

GaN based HEMTs are very attractive for high-power, high-frequency applications. They are of great interest for RF power applications due to their high voltage stability [108][109]. However, in RF power applications, devices may operate at high electric fields and large channel currents. Despite excellent device performance, their long-term reliability, especially in RF applications, needs to be addressed [110][111]. Degradation during high-field stress can result from energetic-carrier scattering in the AlGaN barrier layer and/or the GaN buffer layer. The semi-ON bias condition is typically the worst case for hot-carrier stress [1], [14]-[17]. DC operating parameters that are affected by high-field stress include the saturation drain current I_{Dsat}, the maximum transconductance g_m, and the threshold voltage V_{TH}. RF gain is also reduced.

In this chapter, we employ low-frequency 1/*f* noise measurements to investigate the nature of as-processed and stress-induced defects in AlGaN/GaN HEMTs fabricated via Ga-rich and ammonia-rich growth conditions. The devices are subjected to long-term DC electric stress at different drain biases. In addition to standard DC and RF measurements, low-frequency 1/*f* noise measurements are performed as a function of temperature [87[83][91][112][113], and density functional calculations (DFT) [44] [92] are employed to help understand the nature of the defects and resulting degradation. At high drain voltages, there is a large enhancement in low-frequency noise that is likely caused by first

the dehydrogenation of previously passivated defects, followed by the transport of charged interstitial defects and vacancies. This increase in noise is a precursor to device failure.

Experiment Settings

The DUTs were mounted and bonded in high-speed packages with RF connectors, as shown in Fig. 2-1 for maximizing the frequency response of the structure. Devices are placed in cryostat, setting at 300K, preventing potential heating during stress. The device/junction temperature is somehow higher than 300 K as the cooling pad is only touching the back of the high-speed package.

Devices were stressed at different drain biases under semi-ON operating conditions, which lead to worst-case response in these devices [16]. DC measurements were taken with an Agilent B1505 parametric analyzer. The RF performance was characterized from 100 MHz to 20 GHz using an Agilent N5245A network analyzer. Low frequency 1/*f* noise measurements were performed using the setup in Fig. 2-3, before and after irradiation, from 85 K to 450 K, referring to previous Chapter.

DC and RF Characterization on High Field Effects

Fig. 5-1 shows the RF power gain as a function of DC stress for Ga-rich PAMBE devices from UCSB. These AlGaN/GaN HEMTs were stressed in the semi-ON condition with V_{gs} = -2 V and V_{ds} = 20, 25, and 30 V for 24 hours, which is a sufficiently long period that the rate of degradation is reduced significantly from its initial rate. At each step of stress, the RF gain was measured at V_{ds} = 5 V. The degradation in RF performance for a stress voltage of V_{ds} = 20 V is small, and increases with stress

voltage and time. For a stress voltage V_{ds} = 30 V, the gain falls to less than unity, indicating that the "critical" bias-stress voltage above which the device is no longer useful in RF applications [17] lies between ~25 V and ~30 V for these devices.

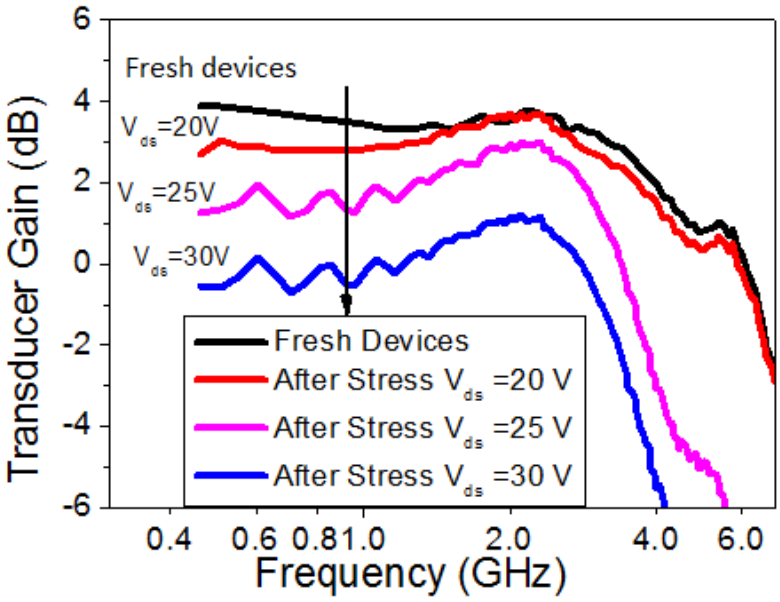

Fig. 5-1 Small signal transducer gain as a function of frequency, measured at V_{ds} = 5V with the gate voltage biased to achieve the best performance. The Ga-rich PAMBE devices from UCSB were subjected to DC stress at V_{gs} = -2V and V_{ds} = 20 V, 25 V, and 30 V for 24 hours. After 30 V stress, the device gain is less than unity. (after [83])

Fig. 5-2 shows the threshold voltage and transconductance as functions of time for different drain voltages applied during stress to the Ga-rich UCSB devices. The devices were stressed at a constant gate bias of -2 V, at a series of drain biases ranging from 5 V to 35 V with a step of 5 V. The stress period for each bias is approximately 11 hours, which is sufficiently long for degradation to reach approximate saturation at lower stress biases. The drain current under stress at V_{gs} = -2 V is around 50 mA. As shown in Fig. 5-2(a), the threshold voltage is not significantly affected by 5 V stress, but then shifts negatively with increasing drain bias. The largest and fastest shifts occur at a drain bias of 10 V.

The amount of V_{th} shift is similar for other bias conditions, and the shift always reaches approximate saturation within the testing period. The negative shift in threshold voltage indicates a reduction in the number of acceptor-like traps, causing more electrons to fill the 2DEG, most likely as a result of hole trapping in the AlGaN and buffer layers [114].

The bias dependence of the peak transconductance is shown in Fig. 5-2(b). Unlike the threshold voltage, for which the rate of change is similar during each bias step, the transconductance degrades more rapidly with increasing drain bias above 20 V. At a drain bias of 35 V, the degradation does not saturate on the time scale of the experiments (11 hours). At stress levels above 20-25 V, the rate of degradation in transconductance is much greater than the rate of degradation in threshold voltage, suggesting that defects located in the gate-drain access region are strongly affecting the transconductance but only weakly affecting the threshold voltage [115][116]. The rapid degradation above 20 V is consistent with the RF degradation observed in Fig. 5-1. At higher stress voltages, the devices failed quickly and catastrophically.

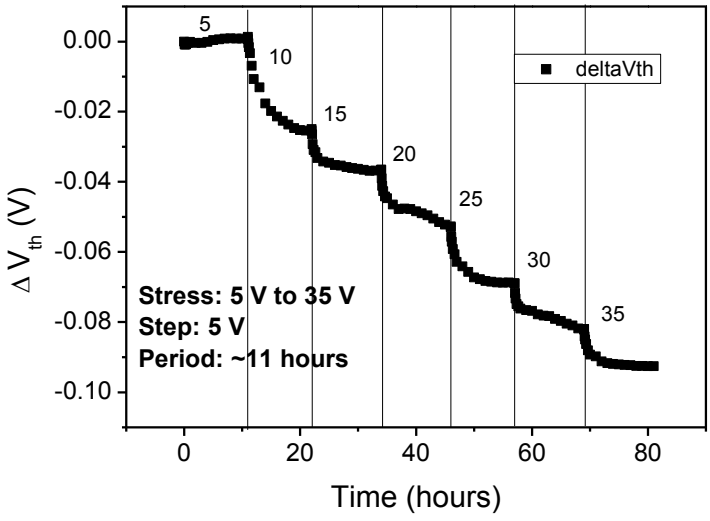

(a)

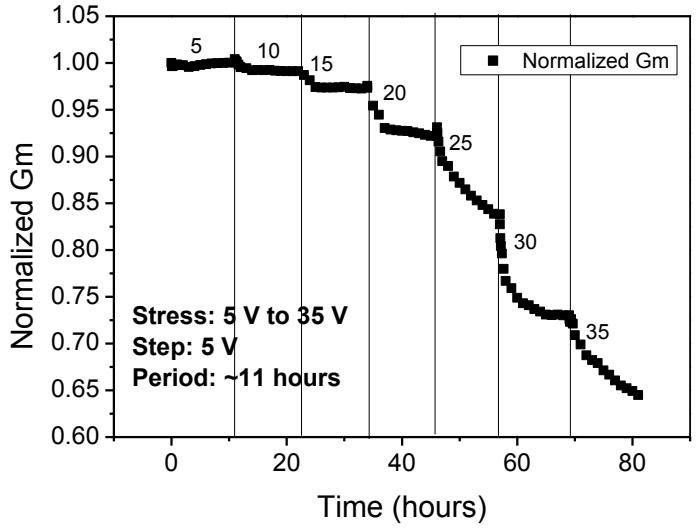

(b)

Fig. 5-2 (a) Threshold voltage shift and (b) normalized peak transconductance degradation under a series of drain biases for Ga-rich PAMBE devices from UCSB. The transconductance is normalized to the peak transconductance of a fresh device. The gate bias is -2 V during the whole process. The drain bias starts from 5 V, with a step of 5 V. For each condition, devices are stressed for around 11 hours, which is sufficiently long for degradation to reach saturation at low biases. (after [83])

NH_3-rich MBE devices from UCSB were stressed with a similar series of drain biases, ranging from V_{ds} =15 V to 35 V, with a step of 5V (Fig. 5-3). The gate bias is constant at -2 V. The threshold voltage (Fig. 5-3(a)) shifts quickly at the beginning of stress, and reaches saturation more easily at higher bias, which is consistent with observations on Ga-rich devices. The threshold voltage shift is positive. The polarity of the V_{th} shift suggests different defects are generated for the NH_3-rich devices than for the Ga-rich devices, consistent with expectations based on previous work [92]. The normalized peak transconductance drops rapidly at biases over 30 V (Fig. 5-3(b)).

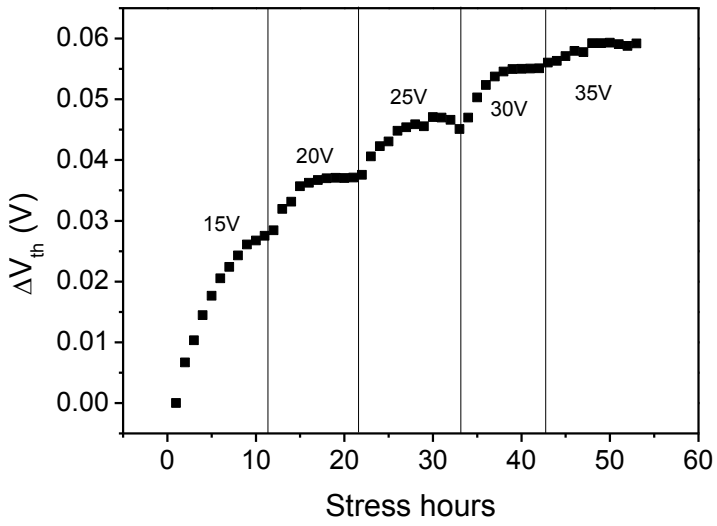

(a)

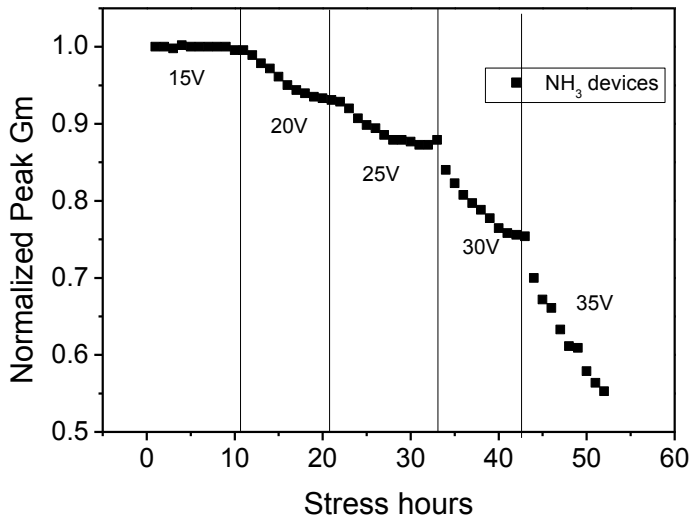

(b)

Fig. 5-3 (a) Threshold voltage shift and (b) normalized peak transconductance degradation under a series of voltage stresses on NH_3-rich MBE devices from UCSB. The transconductance is normalized to the peak transconductance of a fresh device. The gate bias is constantly at -2 V. The drain bias starts from 15 V, with a step of 5 V. For each condition, devices are stressed for around 11 hours, which is sufficiently long for degradation to reach saturation at low biases. (after [83])

Low Frequency Noise vs. Temperature

Low frequency 1/*f* noise measurements are employed to provide insight into the mechanisms of defect formation. The excess voltage noise power spectral density S_{VD} (corrected for background noise) for both type of HEMTs from UCSB is measured at constant $V_g - V_{pinch\text{-}off}$ = 2 V and V_d = 0.1 V as a function of frequency, after each period of stress discussed above. The bias voltages are chosen to ensure the noise originates primarily from the gated portion of the channel, with an approximately constant channel resistance [92]. Fig. 5-4 shows sample curves of low frequency noise of Ga-rich PAMBE devices before and after stress, showing different magnitudes and frequency-dependences at 100, 300, and 400 K.

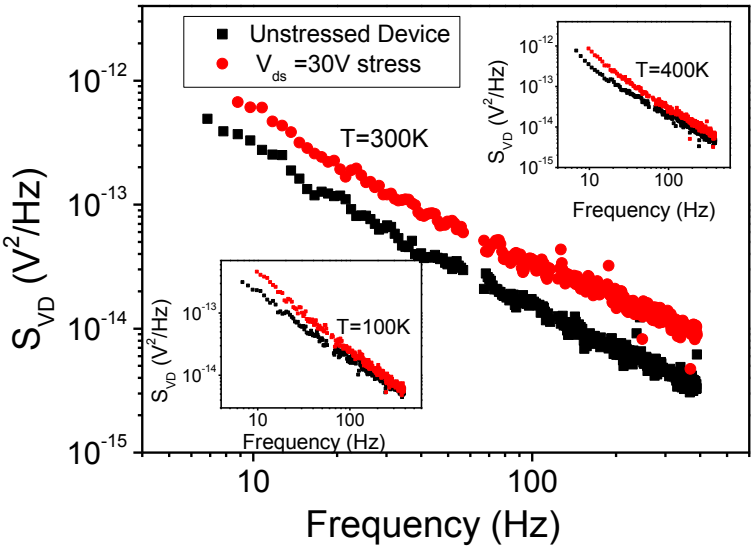

Fig. 5-4 Excess voltage noise power spectral density S_{VD} vs. frequency, at 100 K, 300 K and 400 K before and after stress for Ga-rich PAMBE devices from UCSB. The noise is measured in the linear region of device response, with V_{ds} = 0.1 V and V_{gs}-V_{th} = 2 V. (after [83])

The Dutta-Horn model check is performed for all the devices before and after stress, with sample curves shown in Fig 5-5. The experimental data follow the Dutta-Horn model calculation accurately over the entire temperature region, indicating the noise is due to random processes with thermally activated characteristic times. The accurate fitting of Dutta-Horn model allows us to estimate the shape of defect energy distributions from the low-frequency noise measurements [44].

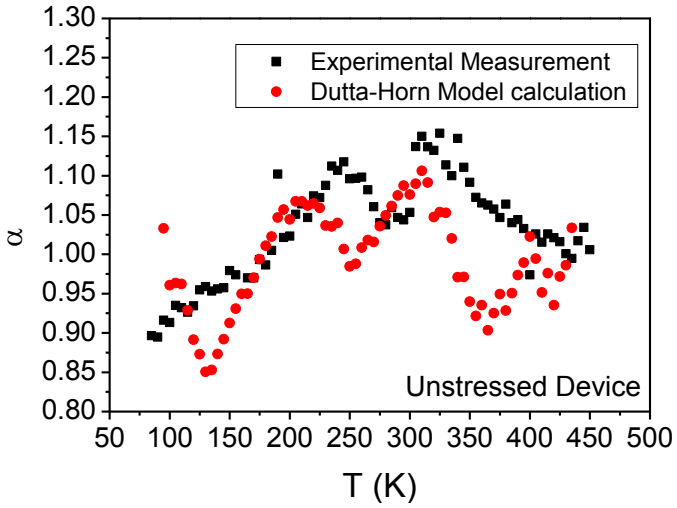

Fig. 5-5 Dutta-Horn analysis on unstressed Ga-rich PAMBE UCSB devices; similarly good correlations between measured and predicted values are observed for stressed devices (not shown). (after [83])

Fig 5-6 shows the temperature dependence of the noise of Ga-rich PAMBE devices measured at 10 Hz. The y-axis shows $(\omega/kT)*S_V$, which is proportional to the defect-energy distribution $D(E_0)$. The temperature range (bottom x-axis) then corresponds to an activation energy scale ranging from 0.2 eV to 1.04 eV (top x-axis).

Fig 5-6 clearly shows an increase in the noise with increasing stress. Before stress, the noise peaks at 80 K and 350 K. During stress, three defect peaks grow at ~ 80 K, ~ 220 K, and ~ 350 K, with the greatest increase in post-stress noise occurring for the 220 K peak. After 20 V stress, a large increase in

the 0.2 eV peak is observed, along with a small peak near 0.6 eV. A large peak at ~ 0.52 eV grows at higher stress levels. Another small peak appears at 0.8 eV. The growth of these noise peaks is associated with corresponding DC/RF degradation (Figs. 5-1, 5-2, 5-3). Peaks at ~0.5 eV to 0.6 eV are especially common in AlGaN/GaN structures [117][118], and have been recently identified with Fe_{Ga}-V_N complexes in the GaN buffer layer [119]. After 35 V stress, the noise increases significantly over the entire range of temperatures, indicating the generation of many defects with energies that are more evenly distributed throughout the band gap.

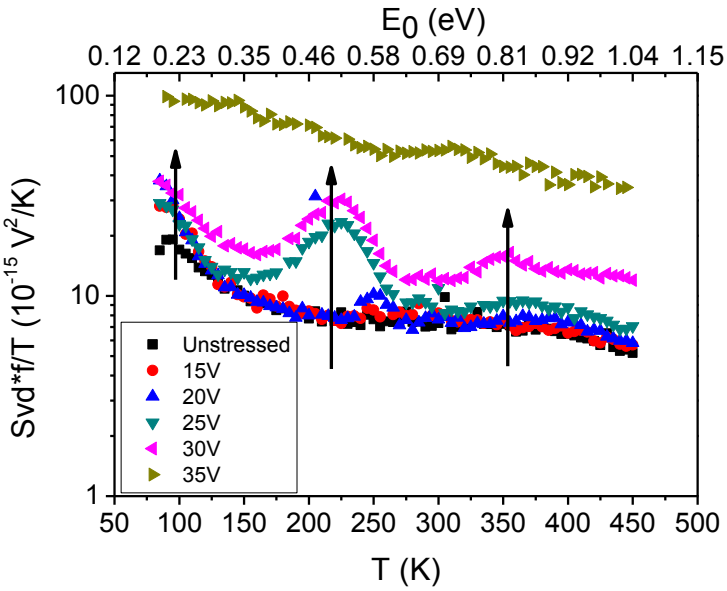

Fig. 5-6 Temperature dependent noise measurements from 85 K to 450 K, at f = 10 Hz for Ga-rich PAMBE UCSB devices. The noise is measured under the same conditions as in Fig. 5. The temperature range corresponds to an activation energy scale ranging from 0.2 eV to 1.04 eV (top x-axis). The concentration of defects increased significantly at energy levels of 0.25, 0.5 and 0.8 eV, when the device is stressed at V_d = 25-30 V. (after [83])

The temperature dependence of the low frequency noise of ammonia MBE devices is shown in Fig. 5-7. Unlike the Ga-rich devices, there are no clear noise peaks in fresh devices, and the noise levels are comparatively lower. Moreover, no significant change is observed in noise magnitude before 30 V bias

is applied, indicating improved device stability for the NH_3-rich UCSB devices, compared to the Ga-rich devices. The noise level increases rapidly when 30 V stress is applied, for the whole range of temperatures. The three peaks at ~80 K, 220 K, and ~ 350 K are also observed in NH_3-rich devices, indicating a similar defect activation mechanism after stress as for the Ga-rich devices. Limited by fabrication yielding, most DUTs cannot perform properly (e.g. short or open gate, very large off leakage) after stressed at 35 V. Very few devices showing acceptable IV characteristics show very high noise levels after stress at 35V, increased to 10 times as large as that of fresh devices, indicating significant degradation, consistent with the transconductance degradation in Fig. 5-3(b). Again, at higher drain voltages, the devices failed catastrophically.

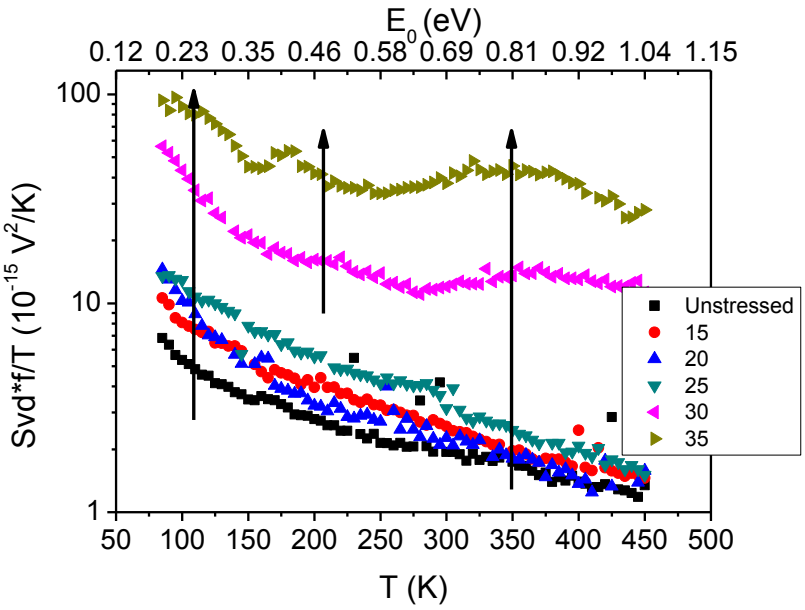

Fig. 5-7 Temperature dependent noise measurement of NH_3-rich UCSB devices, from 85 K to 450 K, at f = 10 Hz. The noise is measured under the same conditions as in Fig. 7. Compared to Ga-rich devices, the initial noise level is much lower. The concentration of defects increased at similar energy levels (0.25, 0.5 and 0.8 eV) at bias voltages of V_{gs} = -2 V and $V_d \approx$ 30-35 V. (after [83])

For comparison of the degradation of the UCSB devices with industrial devices, high-field stress was also applied to commercial GaN HEMTs from *Qorvo*. Inc. [118]. These parts were stressed in the semi-ON condition (V_{ds}=25 V and V_{gs}=-1.5 V) for 16 hours until the rate of degradation is significantly reduced (Fig. 5-8(a)). The threshold voltage shift is 0.16 V and the peak transconductance dropped by 8%. Compared to the UCSB devices whose results are shown above, these commercial parts show larger threshold voltage shifts but much less transconductance degradation. This suggests that the two types of devices, not surprisingly, contain different types of defects, leading to different responses to high-field stress. The temperature dependence of the low frequency noise of the *Qorvo* devices in Fig. 5-8(b) shows as-processed defect peaks at 0.7 eV. After semi-ON stress, the defect peaks at 0.2 eV and 0.7 eV increase, confirming that the defects in the *Qorvo* devices differ in density and energy from both the Ga-rich PAMBE and NH_3-rich MBE UCSB devices [119].

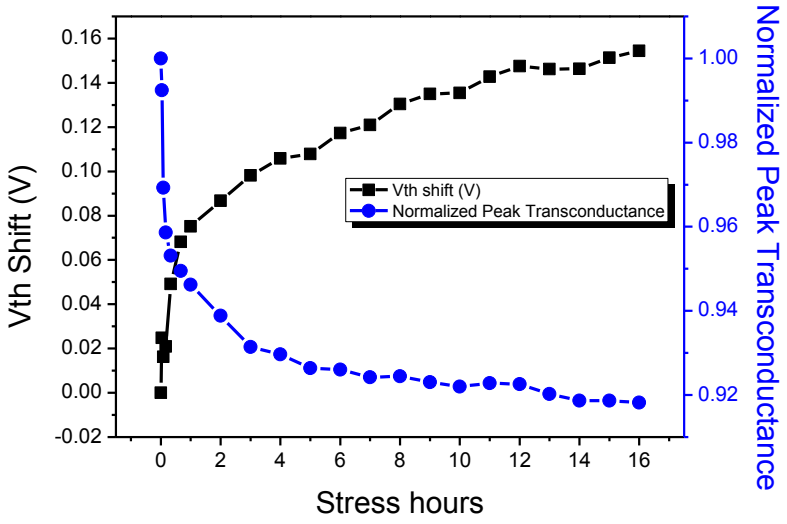

(a)

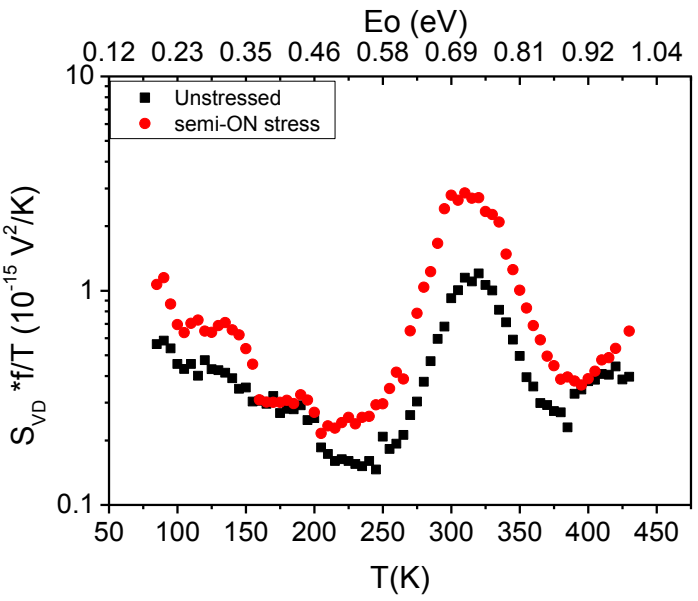

(b)

Fig. 5-8 (a) Threshold-voltage shifts and transconductance degradation and (b) temperature-dependent noise measurements on Qorvo devices after high-field stress. (After [118].) (after [83])

Defect Identification

To identify the defects responsible for the peaks in energy distribution described in Fig. 5-6 and 5-7, we employ density-functional-theory (DFT) to perform quantum-mechanical calculations of impurities and native defects. Defects are introduced during growth and often are initially passivated by hydrogen. During high-field stress, hot electrons can depassivate the defects. Along with the overall increase of the noise level, three noise peaks appear at ~0.2, ~0.5, and ~0.8 eV in the UCSB devices. The 0.2 eV peak is prominent in unstressed devices, with the ~0.5 eV and 0.8 eV peaks growing in size after high-voltage stress. Unstressed GaN HEMTs from *Qorvo* exhibit peaks at ~0.2 eV and ~0.7 eV before stress; these peaks each increase after semi-ON stress.

We attribute the growth of the ~0.2 eV peak for the two types of devices at lower stress levels to

stress-induced dehydrogenation of an O_N-H complex [91]. A substitutional oxygen impurity at a nitrogen site, $O_{N,}$ has two equilibrium positions: one for a neutral charge state and another for a positively charged state. The energy barrier of an O atom moving from one position to another is 0.2 eV. Overcoming this barrier leads to a change in charge state, which accounts for the lowest-energy peak in the noise measurements. This peak was also observed in previous proton irradiation studies of similar devices [91]. At higher stress levels, an increase in the density of N vacancy-related defects is also likely; the defects also have a charge transition level near ~ 0.2 eV [92][91].

We attribute the observed broad peak in the noise data at ~ 0.52 eV to hydrogenated divacancies and iron impurity complexes. Hydrogenated divacancies (V_{Ga}-V_N-H_x), have charge transition energy levels ~0.4-0.6 eV below the conduction-band edge, as shown in Fig. 5-9 [119][119]. The position of the Fermi level is ~ 0.4 eV below the GaN conduction band, so that the defect levels are accessible to electrons. Another defect complex contributing to this peak is Fe_{Ga}-V_N-H, which upon dehydrogenation results in Fe_{Ga}-V_N, as shown in Fig. 5-10. This complex has an electron energy level that is ~ 0.5 eV below the conduction band edge. The initial concentration of precursor defects responsible for the increase in this level in the case of Ga-rich growth (Fig. 5-6), as compared with NH_3 rich growth (Fig. 5-7), is higher due to the lower formation energy of N vacancies during Ga-rich growth than during NH_3-rich growth. This lowers the formation energy of the Fe_{Ga}-V_N-H defect complex. Complete dehydrogenation of Fe impurity complexes results in a negative threshold voltage shift [119], consistent with the Ga-rich devices of Figs. 5-2(a) and 5-6, while complete dehydrogenation of divacancy complexes causes a positive threshold-voltage shift [92][120], consistent with the NH_3-rich devices of Figs. 5-5(a) and 5-7. This suggests that densities of Fe_{Ga}-V_N impurity complexes are greater for the Ga-rich devices, but less for the NH_3-rich devices, than densities of the divacancy defects.

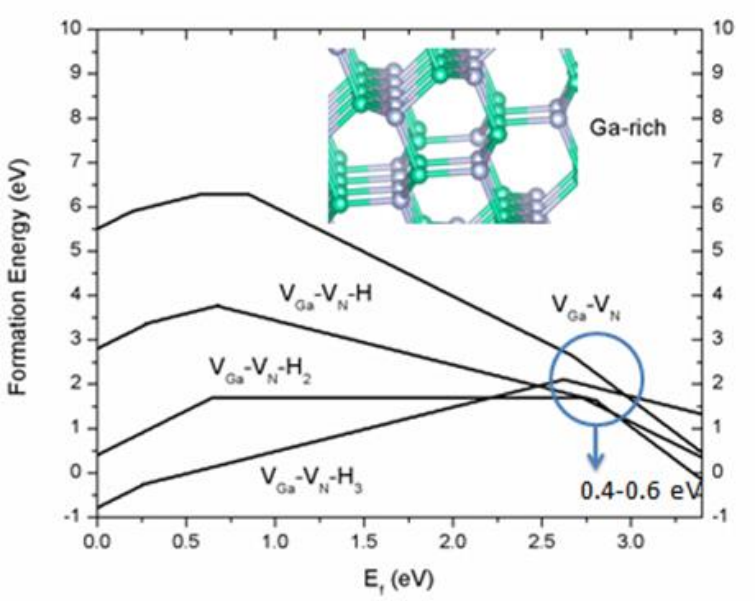

Fig. 5-9 Hydrogenated divacancy formation energies in Ga-rich GaN is plotted as a function of Fermi level. The charge transition levels are at 0.4-0.6 eV below the GaN conduction band. (After [121].)

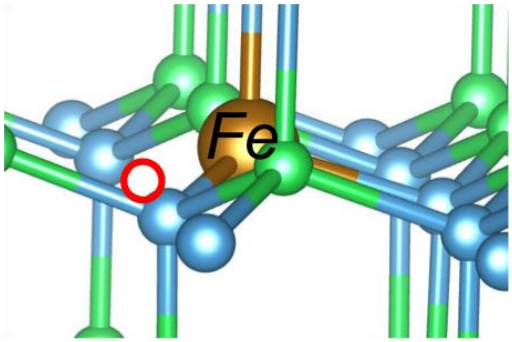

Fig. 5-10 Atomic structure of Fe-V_N defect complex in GaN. Fe is shown as a larger brown atom. The position of the missing N atom is marked by a red circle. (After [120].)

The noise data for the *Qorvo* devices in Fig. 5-8(b) exhibit significant increases in the ~0.2 eV and ~0.7 eV peaks after semi-ON stress. The threshold voltage shift, shown in Fig. 5-8(a), indicates that the response of the *Qorvo* devices is qualitatively consistent with that of ammonia-rich MBE devices from UCSB, for which the concentrations of V_{Ga} and N_{Ga} are higher due to lower formation energies, compared to the Ga-rich PAMBE devices. Thus, we attribute the increases in the 0.7 eV defect level in

the *Qorvo* devices to hydrogen removal from the hydrogenated antisite N_{Ga}-H_x, x=1~3, defects. Antisite N_{Ga}–H_3 defects, passivated by three hydrogen atoms, are shown in Fig. 5-11(a) [122]. Additional results for *Qorvo* devices exposed to a combination of high-field stress and proton irradiation are shown in [122].

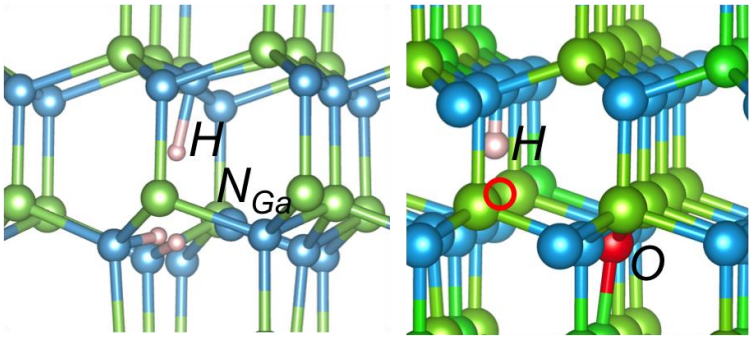

(a) (b)

Fig. 5-11 Atomic structure of hydrogenated a) nitrogen antisite N_{Ga}-H_3 and b) hydrogenated substitutional O_N-V_{Ga} complexes in GaN. (After [122].)

The increase in the broad peak at ~0.8 eV during stress for the UCSB devices is caused by two factors. One is the energy barrier of ~0.9 eV for H migration within an O_N-H complex [91]. The H atom remains within the O_N-H complex due to a relatively high barrier of ~2.0 eV for H atom removal [123]. We also note that the migration barrier of V_{Ga} is ~1 eV in the absence of an electric field [121]. This barrier is lowered in the presence of an electric field, due to the high charge states of the migrating defects, in particular, $[V_{Ga}]^{-3}$ [124], causing an increase in the concentration of V_{Ga}-O_N-H defects, shown in Fig. 13b. Since the charge transition state of the V_{Ga}-O_N-H defect is ~ 0.7 eV, the increase of its concentration increases the magnitude and broadens the observed noise peak.

The larger overall increase of the noise in the NH_3-rich UCSB devices at very high voltages is caused by a higher concentration of hydrogenated precursor defects due to higher H concentrations in

the as-processed devices. The very large increase in noise at the highest stress levels is most likely due to the nearly complete dehydrogenation of initially passivated defect sites, leading to a significant increase in interface-trap density, and a corresponding large increase in low-frequency noise magnitude at all temperatures. Following the dehydrogenation of defects, many become charged and are able to transport at high electric fields, leading to large and irreversible device degradation. The appearance of greatly enhanced low-frequency noise at the highest drain voltages (i.e., the 35 V curve in Fig. 5-6 and the 30 V and 35 V curves in Fig. 5-7) is clearly an early warning sign that the device is approaching catastrophic failure[112], [113].

Conclusions

In this chapter, the microstructures of reliability limiting defects in AlGaN/GaN HEMTs have been identified. Before stress, hydrogen-passivated Fe and O complexes contribute significantly to the noise and relability degradation in the UCSB devices, and hydrogenated antisite N_{Ga}-H_x, x=1~3, and V_{Ga}-O_N-H defects contribute to the noise and reliability degradation of *Qorvo* devices. With increasing stress, all of these complexes increasingly are dehydrogenated, leading to large increases in noise and trap density. The sequential process of (1) defect dehydrogenation, (2) defect charging, and (3) defect transport ultimately leads to failure of the device under high-field stress conditions. Reducing the densities of anti-site defects, as well as Fe and O related defects, in AlGaN/GaN HEMTs should therefore greatly improve their reliability. A significant increase in low-frequency noise is observed before device catastrophic failure, suggesting that low-frequency noise measurements could provide a useful screen for stress-induced degradation in AlGaN/GaN HEMTs.

In the next chapter, we will investigate the high field effects together with radiation exposure, obtaining potential failure mechanisms for high field space applications.

Chapter VI

Effects of Applied Bias and High Field Stress on the Radiation Response of AlGaN/GaN HEMTs

Introduction

In Chapter III and IV, proton irradiation of AlGaN/GaN HEMTs is studied similarly with all pins grounded on devices that have not been subjected to high field stress [33][38][117][126]. In Chapter V, devices are subjected to a series of high field, under which hot-carrier effects can limit the long-term reliability of GaN HEMTs, particularly for applications under high voltage/field operation [1][16][126]. However, for practical space applications, it is more likely that high field and radiation exposure can affect the devices at the same time. Thus, it is of great interest not to consider these two effects separately, but together.

In this chapter, the effects of gate bias during irradiation and the combined effects of 1.8 MeV proton irradiation and hot-carrier stress are investigated. The sensitivity of the devices to proton irradiation increases significantly when the devices are biased during irradiation and/or high-field stress is applied before the proton exposure. We have performed low-frequency $1/f$ noise measurements [81][82][113] and density functional theory (DFT) calculations [44][92] to help understand the nature of the defects in these devices. DFT calculations show that the observed irradiation and electric field response in the noise spectrum are consistent with the presence of N vacancy-related defects and hydrogenated O_N, N_{Ga}, and/or V_{Ga}-O_N complexes in the AlGaN and/or GaN layers.

Experiment Settings

The GaN HEMTs under study are fabricated by Qorvo, Inc. [127][128]. One group (A) of devices was subjected to hot carrier stress, and then irradiated with 1.8 MeV protons to a fluence of $10^{13}/cm^2$ using the Vanderbilt Pelletron. Another group (B) was irradiated to the same fluence and then electrically stressed. Previous work reported that semi-ON bias usually leads to the largest hot carrier degradation in HEMTs [1][17][98]. This is confirmed for the devices considered here in Fig. 6-1 below. Thus, the semi-ON condition (V_{ds} = 25 V and V_g = -2 V) was used for the combined irradiation/stress experiments in this work.

During irradiation, devices were biased in three different conditions that are frequently used in RF applications: 1) GND (V_{ds} = 0 V and V_g = 0 V), 2) OFF (V_{ds} = 25 V and V_g = -7 V), and 3) semi-ON (V_{ds} = 25 V and V_g = -2 V). Before and after stress/irradiation, DC measurements were obtained with an Agilent B1505 parametric analyzer. The peak transconductance is the maximum first derivative (slope) point of the I_d-V_g curves; the threshold voltage reported below is the gate-voltage axis intercept of the linear extrapolation of the I_d-V_g curve at that point [117][129]. In order to characterize the defects created during the irradiation, low frequency 1/*f* noise measurements were also performed from 85 K to 445 K. At least three devices were tested in each bias condition.

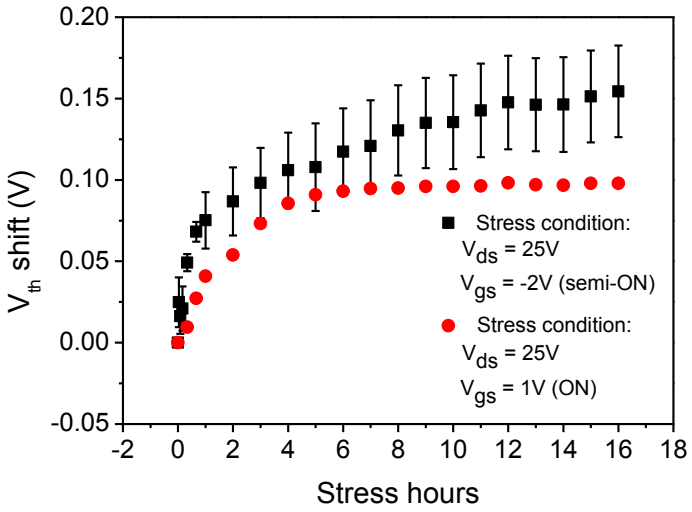

(a)

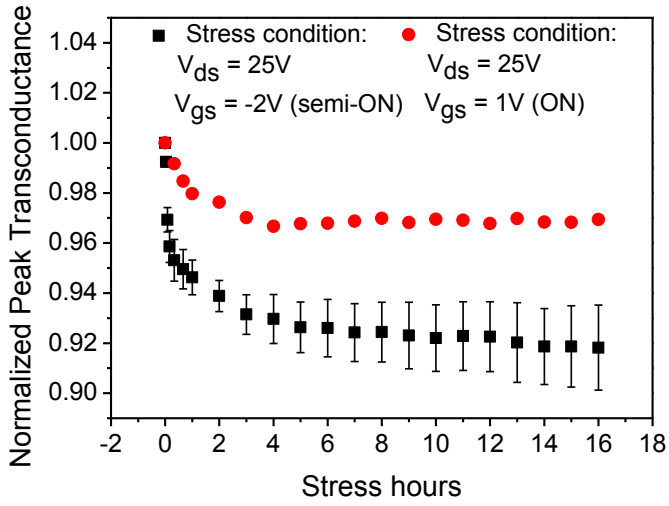

(b)

Fig. 6-1 (a) V_{TH} shift and (b) normalized peak transconductance of AlGaN/GaN HEMTs as a function of hot carrier stress time, for biases of V_{ds} = 25 V and V_g = -2 V. DC characterization was performed with V_{ds} = 5 V. ON-state stress results are also shown for comparison. (after [122])

Combined Radiation and High Field Effects

A. Hot carrier effects (unirradiated devices)

The hot carrier response of the devices stressed in the semi-ON condition is shown in Fig. 6-1.

The degradation increases monotonically, with a maximum positive threshold voltage shift of 0.15

V and a peak transconductance reduction of 8%. Error bars represent the standard deviations of the responses of 5 identical devices. In the semi-ON condition [1], hot electrons can dehydrogenate point defects via single scattering events or by multiple vibrational excitations [126]. Some electrons in the channel can also gain sufficient energy from the high field to be injected into the AlGaN layer and generate new traps in the buffer layer [114]. The dehydrogenation of previously passivated defects and the generation of traps during high-field stress cause threshold voltage shifts, mobility degradation, and increased low-frequency noise [1],[17][44] [92],[98][91], [114],[127]-[129].

B. Radiation response (unstressed devices)

The threshold voltage shift and peak transconductance reduction are plotted as functions of proton fluence (Fig. 6-2). A fluence of 10^{13} protons/cm^2 was reached after 0.83 h at a constant flux (top x-axis). Results for hot carrier stress applied for equivalent time periods are also shown for comparison. The threshold voltage shifts are strongly bias dependent, and positive under all conditions. This indicates that both proton irradiation and high-field stress create deep acceptor-like traps, which are negatively-charged when occupied [38][91].

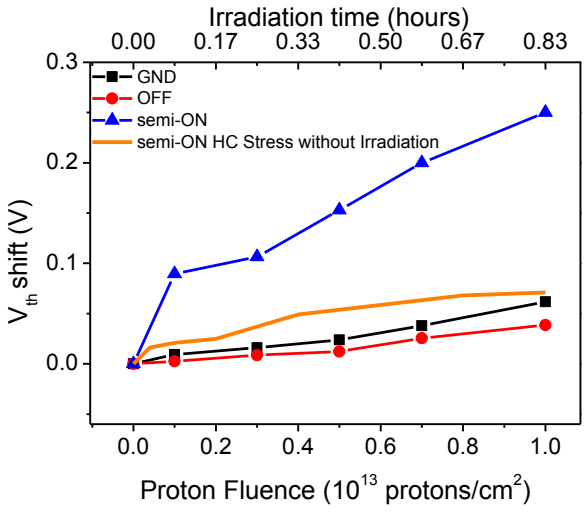

(a)

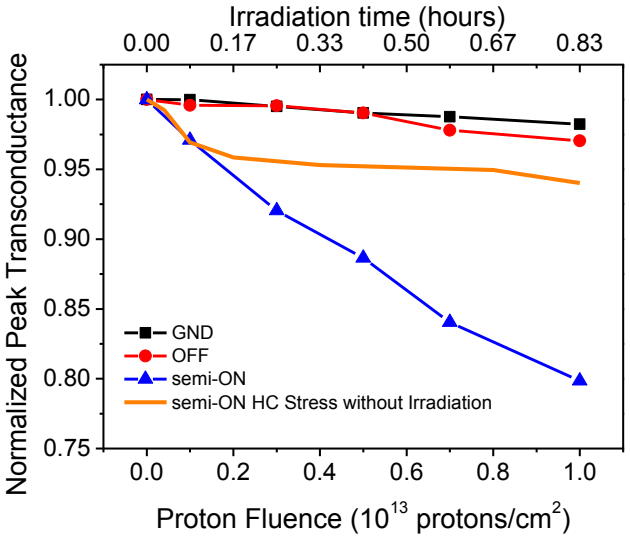

(b)

Fig. 6-2 (a) V_{TH} shift and (b) normalized peak transconductance for AlGaN/GaN HEMTs as a function of proton fluence, for V_{ds} = 25 V and V_g = -2 V. V_{ds} = 5 V during measurement. The hot carrier stress data (no irradiation) are from Fig. 6-1. (after [122])

When irradiated under GND and OFF biases, the shift in threshold voltage is less than 0.05 V and the peak transconductance drops by 5%. In contrast, devices degrade strongly when irradiated in the semi-ON condition, which is clearly the worst-case bias condition for these devices. Hot carrier stress without irradiation leads to much smaller threshold voltage shifts (less than ~ 0.05 V for these experimental conditions) and transconductance degradation (6%) than simultaneous irradiation and stress, for which the threshold voltage shift is 0.25 V and the transconductance degradation is 20%.

C. Combined high-field stress and proton irradiation

Fig. 6-3 shows a comparison of all results from devices in Groups A (irradiation after high-field stress) and B (high-field stress after irradiation). Group A devices were first subjected to semi-ON stress for 16 h (left panel in Fig. 6-3) and then irradiated to a fluence of 10^{13} protons/cm^2 in 50 min (middle panel in Fig. 6-3). Group B devices were first irradiated to a fluence of 10^{13} protons/cm^2 in

50 min (middle panel in Fig. 6-3) and then stressed for 16 h without irradiation (right panel in Fig. 6-3). Irradiations for both groups were performed under GND, OFF, and semi-ON bias conditions.

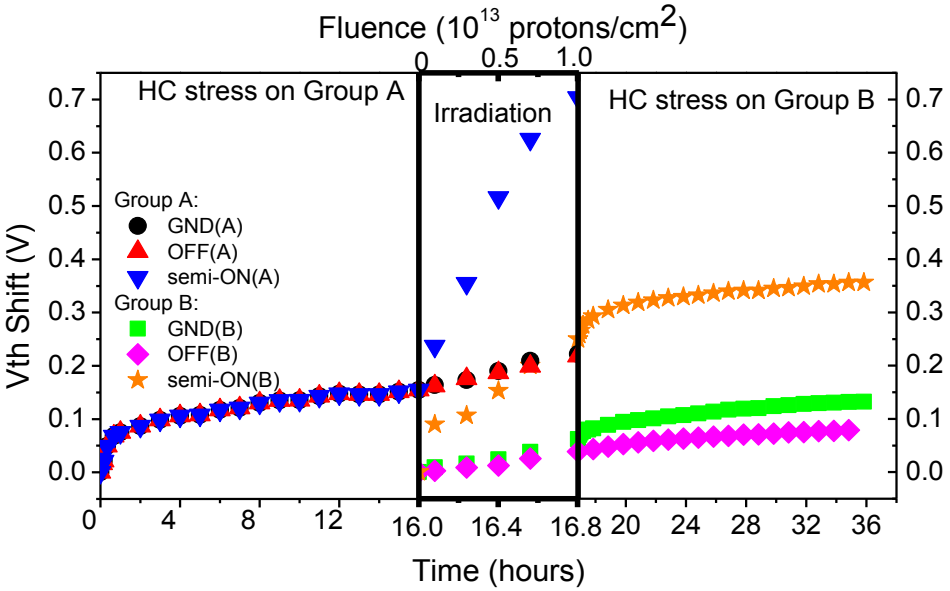

(a)

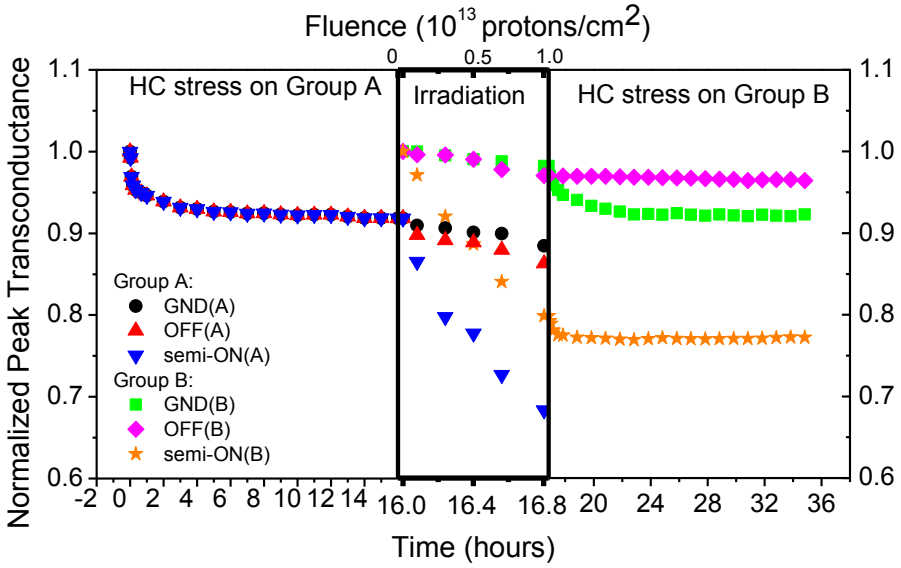

(b)

Fig. 6-3 Comparison of combined irradiation and high field stress effects. (a) V_{TH} shift and (b) normalized peak transconductance of AlGaN/GaN HEMTs as a function of time during high field stress (left and right panels) and/or proton irradiation (middle panel). The worst case set of devices (blue) are first stressed and then irradiated for biases of V_{ds} = 25 V and V_g = -2 V. DC characterizations were performed at V_{ds} = 5 V. (after [122])

For Group A devices in Fig. 6-3, the largest degradation is observed when they are first stressed for 16 h and then irradiated while maintaining gate and drain biases that correspond to the semi-ON condition. These combined high-field stress and proton exposures produce a 0.7 V shift in threshold voltage and 32% degradation in peak transconductance at the conclusion of the stressing and irradiation sequence. The V_{TH} shift during the irradiation portion of the sequence is ~ 0.5 V. For Group B devices that were not stressed before irradiation, the semi-ON bias condition is again worst case for radiation exposure, but the V_{TH} shift during irradiation in this case was only ~ 0.2 V. After the irradiation and subsequent high-field stress sequence, Group B devices showed the largest threshold voltage shift (0.35 V) and transconductance degradation (22%) when irradiated and stressed under the semi-ON bias condition. These results show that both the bias during irradiation and the application of high-field stress before radiation exposure can significantly increase the sensitivity of AlGaN/GaN HEMTs to proton-induced radiation damage. Because the non-ionizing energy loss of 1.8-MeV protons is much higher than that of the higher-energy protons that typically result in the degradation in space systems [41][43], the equivalent displacement damage doses in this study are quite high compared with most realistic space environments [96]. Moreover, both Group A and Group B devices show relatively modest degradation in peak transconductance when compared with previous work on development-stage devices [1],[2],[16][17] [37]-[38],[98]-[91],[108],[117],[126]. Thus, it is reasonable to expect these devices to function well in most space applications.

Noise Diagnosis: Biased Irradiation

To obtain insight into the defects responsible for the degradation during irradiation and/or high field stress, we measured the excess drain-voltage noise power spectral density S_V (corrected for background noise) for AlGaN/GaN HEMTs at constant $V_g - V_{TH} = 0.4$ V and $V_d = 0.03$ V as a function of frequency and temperature before and after stress/irradiation. The bias voltages are chosen to ensure that the noise originates from the gated portion of the channel, with an approximately constant channel resistance [38]. The experimental data fits the Dutta Horn model perfectly before and after stress/irradiation, with the frequency exponent ranging from 0.7~1.4 (Fig 6-4).

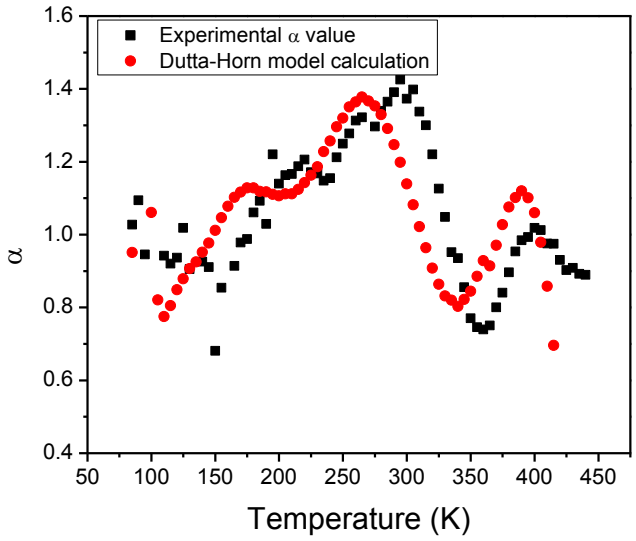

Fig. 6-4 Experimental and calculated frequency exponent of noise power spectral density as a function of temperature from 85 K to 445 K. (after [122])

Figs. 6-5 to Fig 6-7 show normalized noise magnitudes for Group A and B devices irradiated in the GND, OFF, and Semi-ON bias conditions, respectively. For each figure, (a) represents stress followed by irradiation, and (b) represents irradiation and then stress. The top x-axis represents the corresponding activation energy E_o from 0.2 eV to 1 eV, calculated from the Dutta-Horn model. The y-axis is proportional to the defect-energy distribution. For these devices before irradiation or stress, a large peak in noise magnitude at ~ 0.7 eV is observed, indicating that these particular defects are present in as-processed devices [130][131].

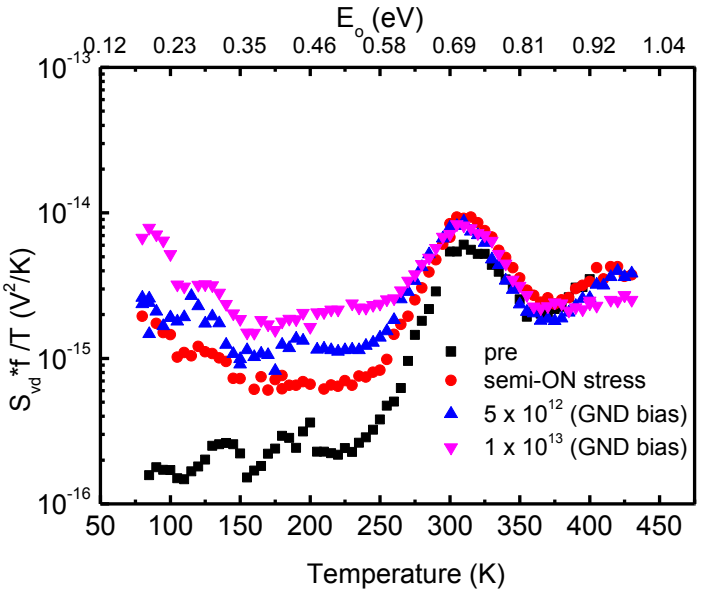

(a)

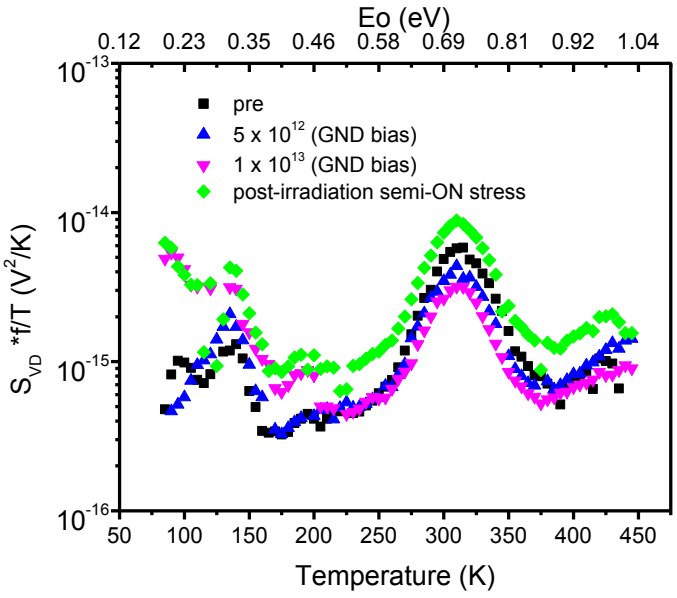

(b)

Fig. 6-5 Temperature-dependent noise measurements from 85 K to 445 K, for GND state irradiation (a) after and (b) before semi-on stress. Here $V_g - V_{threshold}$ = 0.4 V, V_d = 0.03 V at f = 10 Hz. The energy scale on the upper x-axis is derived from the Dutta-Horn model of low-frequency noise. Noise measurements were reproducible from run to run and from day to day on these devices. The statistical uncertainty in the noise measurements is approximately equal to the symbol size. Fluences are quoted in protons/cm^2. (after [122])

Fig 6-5 and Fig 6-6 show that the ~ 0.2 eV peak increases more with GND-state or OFF-state proton irradiation [92],[91] than with high-field stress. Moreover, for these bias and irradiation conditions, a relatively smaller increase is observed in the ~ 0.7 eV peak. Though the orders of irradiation and stress are reversed in Figs. 6-5(a) and (b), similar changes in noise magnitudes are observed. This result is consistent with the DC degradation for Group A and B devices irradiated under GND-state or OFF-state bias conditions in Fig. 6-3, where similar threshold voltage shifts and transconductance degradation are also observed.

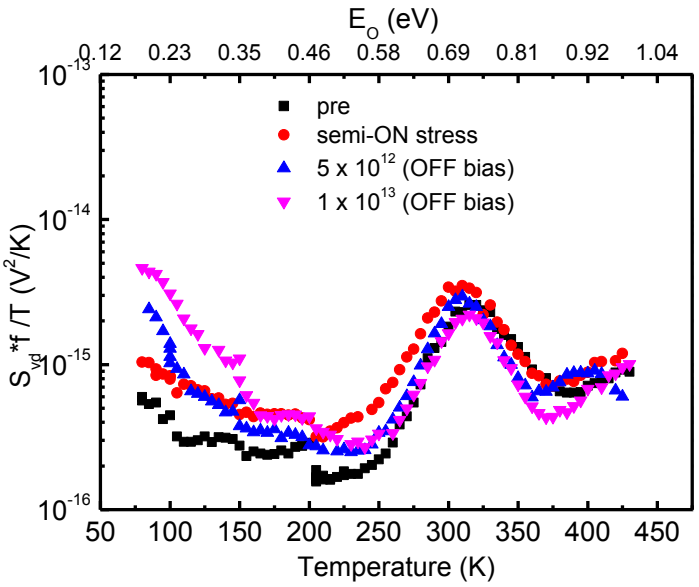

(a)

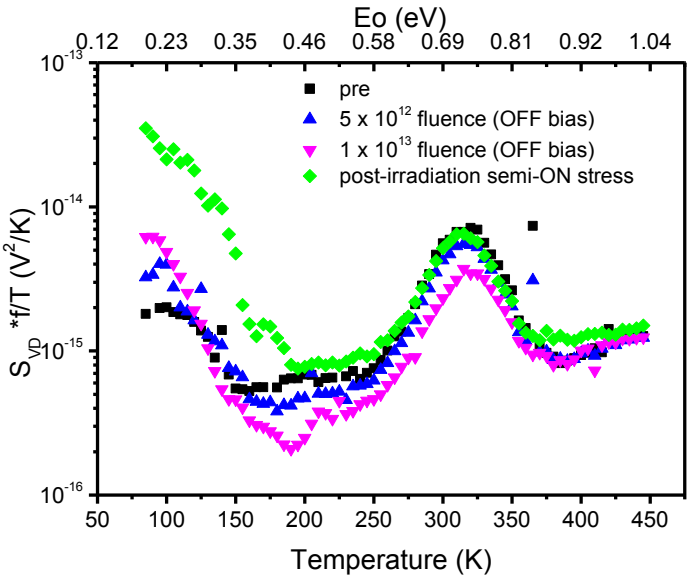

(b)

Fig. 6-6 Temperature-dependent noise measurements from 85 K to 445 K, for OFF state irradiation (a) after and (b) before semi-on stress. (after [122])

The largest increase in noise, similar to the worst-case degradation in Fig. 6-3, occurs when devices are irradiated under semi-ON bias, as shown in Fig. 6-7. For devices that were first stressed and then irradiated under semi-ON bias (Fig. 6-7(a), top curve), the noise shows a significant increase over the

entire range of energies, not only near 0.2 eV, but also near 0.7 eV. For comparison, irradiation under semi-ON bias (Fig. 6-7(b)), without prior high field stress, only leads to increases near 0.2 eV, with little increase of the ~ 0.7 eV defect peak during post-irradiation stress. Again, these results are consistent with trends in threshold voltage shifts and transconductance degradation in Fig. 6-3. This strongly suggests that the increased noise is caused by increases in densities of the defects that are limiting the performance, reliability, and radiation response of these devices. The noise for the highest fluence exposures also shows an overall increase in magnitude at all energy levels, indicating the generation of other defects with energies that are more evenly distributed throughout the band gap. But the ~ 0.2 eV and ~ 0.7 eV defects remain the dominant trapping centers in these devices, through all irradiation and stress conditions.

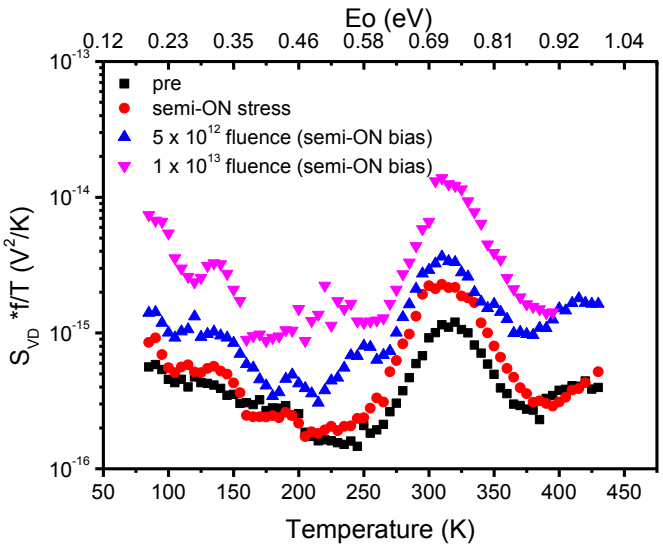

(a)

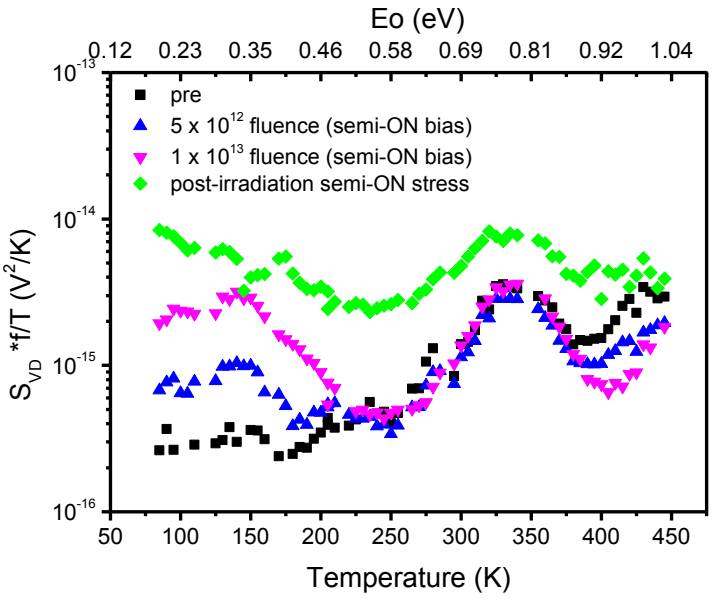

(b)

Fig. 6-7 Temperature-dependent noise measurements from 85 K to 445 K, for semi-ON state irradiation (a) after and (b) before semi-ON stress (V_{ds} = 25 V and V_g = -2 V). (after [122])

Identification of Dominating Defects

We now discuss the nature of the defects that lead to the largest effects on the charge trapping, transconductance degradation, and low-frequency noise in these devices. While other defects are clearly present at other energies, the most prominent defect levels are those at E_c-0.2 eV and E_c-0.7 eV. Defects at these energy levels were observed and denoted as *D* and A_x centers by Fang et al. in [132]. Experiments described by Arehart et al. demonstrated that the ~ 0.2 eV level in GaN decreases with increasing NH_3/Ga flux ratio during growth, but the ~ 0.7 eV level increases [131]. Recent studies of *n*-type GaN devices by Zhang et al. show that 1.8 MeV proton irradiation at fluences up to 1.1×10^{13} cm^{-2} can also lead to an increase in the ~ 0.7 eV level [130]. Based on these and other past studies of the dependencies of the trap densities on growth conditions, impurities, and/or radiation exposure

[130]-[135], the E_c-0.2 eV level has been associated with nitrogen vacancy-related defects. In recent publications [92][91] we combined density functional theory (DFT) calculations with experimental data to associate the ~ 0.2 eV level in Fig. 6 with a combination of two centers: one is a nitrogen vacancy, V_N, in GaN which has a charge state transition level at ~ 0.25 eV [44], and the other is an oxygen impurity, O_N, in AlGaN, characterized by a configurational transition with an accompanying change in charge state that occurs at ~ 0.2 eV [91]. These defects are illustrated schematically in Fig. 6-8. The contribution of the V_N related peak increases during proton irradiation to high fluences because additional nitrogen vacancies are introduced into the GaN [44],[92], ,[136]-[138], and because H atoms can be liberated from O_N-H centers[92]s. Figs. 6-5 to 6-7 strongly suggest that these increases in the ~ 0.2 eV trap level do not depend strongly on either the bias applied during proton irradiation or the presence or absence of high field stress before, during, or after proton irradiation, at least for the devices and experimental conditions of this study.

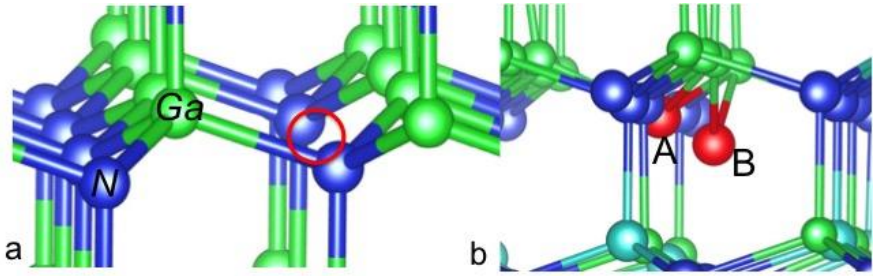

Fig. 6-8 Atomic structure of the defects related to the ~ 0.2 eV noise peak. (a) The nitrogen vacancy position is highlighted by the red circle. (b) An oxygen atom (shown in red) reconfigures from its interstitial position A to the DX center position B, with energy levels separated by ~ 0.2 eV. (after [122])

In contrast to the ~ 0.2 eV trap level which is now relatively well understood, the physical nature of the defect(s) responsible for the ~ 0.7 eV level is(are) not yet known [130]-[136]. We have

performed DFT calculations to investigate the atomic-scale structure of this defect in AlGaN/GaN HEMT devices. Calculations were performed using density-functional theory with the gradient-corrected local-density approximation as implemented in the VASP code using standard techniques [102][105]. The plane wave basis energy cutoff was set at 348 eV. The hybrid functional HSE06 was used for calculations to reproduce the correct value of the band gap, which is underestimated in the local density approximation [137].

The shift in threshold voltage is positive, indicating that the majority of generated defects act as acceptors. A broad range of native defects and impurities, such as interstitials, divacancies, carbon, iron, and their complexes with vacancies and hydrogen, were considered as candidates for this center. The only relatively common defect occurring in as-grown GaN that appears to have both the appropriate charge state and energy level is the N antisite, N_{Ga}, shown in Fig. 6-9(a). This defect has the pertinent charge transition level 0/-1 calculated to be ~ 0.65 eV below the conduction band [138], which is within 10% of the observed trap level, consistent to within calculational uncertainties. Another possible candidate is a hydrogenated oxygen impurity that is complexed with a Ga vacancy, the V_{Ga}-O_N-H, which is shown in Fig. 6-9(b). The charge states are consistent with the observed positive threshold voltage shift and this defect has the charge transition level of ~ 0.7 eV. Of these two defects, the N_{Ga} appears to be the most likely candidate in as-processed GaN, owing to its simplicity.

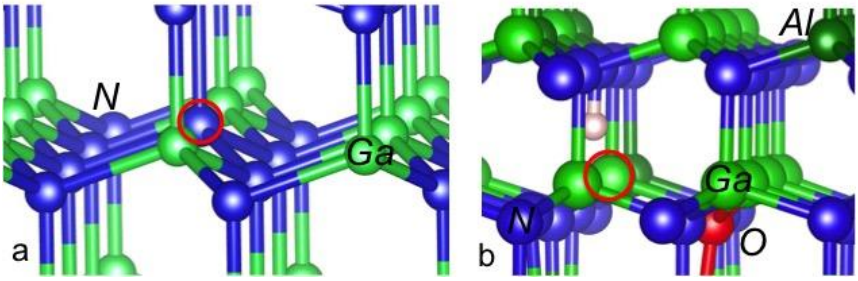

Fig. 6-9 Atomic structure of the defects potentially related to the previously unidentified ~ 0.7 eV peak in GaN: (a) A nitrogen anti-site N_{Ga}, is highlighted by the red circle. (b) A hydrogenated O_N complexed with a gallium vacancy $H\text{-}O_N\text{-}V_{Ga}$ in GaN is shown, where the circle shows the position of the missing Ga atom, and O is shown in red. (after [122])

The question remains: Why would the ~ 0.7 eV defect, if associated with N_{Ga}, increase during proton irradiation and/or high field stress? There are at least two possibilities. First, consistent with the behavior of O_N in AlGaN [91], many substitutional impurity defects in GaN and AlGaN are initially hydrogenated. Proton irradiation and/or high-field stress can remove H atoms, thereby activating defects and/or changing energy levels [91]. The dehydrogenation process is enhanced during high-field stress [120]. Hence, the application of bias during proton irradiation may well increase the concentrations of activated N_{Ga} defects. Second, during high-field stress, it is known that N interstitials and Ga vacancies can become highly mobile in GaN and AlGaN [120]. Thus, it is quite possible that some existing or N interstitials newly created by proton irradiation may transport under bias and fill pre-existing Ga vacancy sites, thereby again increasing the active N_{Ga} density. This behavior would be consistent with the lack of significant growth in the ~ 0.7 eV trap level in Figs. 6-5 and 6-6, but significant growth in Fig. 6-7. However, more work is required to confirm these atomic scale mechanisms.

Association of at least a portion of the ~ 0.2 eV trap level with an oxygen DX center in AlGaN and the ~ 0.7 eV level with an N anti-site defect in GaN suggests that two of the dominant defects in AlGaN/GaN HEMTs are analogous to common defects in GaAs. The O_N defect in AlGaN is similar in nature to the DX center in AlGaAs [139], and the NGa is analogous to the ubiquitous EL2 defect in GaAs, which is an arsenic anti-site defect [140]. While defect concentrations and energy levels are expected and observed to be different in the GaN and GaAs systems, the expected abundances and natures of the defects identified in this and previous work reinforce the plausibility of the defect identification.

Radiation Hardness Assurance

The hardness assurance implications of these results are straightforward and obvious. Characterization and qualification of AlGaN/GaN HEMTs for space applications simply must include biased irradiations as part of the testing matrix. Further, the results of Fig. 6-3 also strongly suggest that, at least during initial characterization of new technologies for space system use, combined reliability and radiation effects must be considered when attempting to assess and assure the performance, reliability, and radiation tolerance of space-based electronic systems.

Conclusion

In this chapter, we have investigated the combined effects of proton irradiation and hot carrier stress on GaN HEMTs. Devices irradiated in the semi-ON condition show greater threshold voltage

shifts and transconductance degradation than devices subjected to high field stress alone, or devices irradiated under grounded or OFF bias conditions. The worst case for combined effects is to stress the devices in the semi-ON condition and then irradiate the devices under the same bias conditions. Low frequency noise measurements identify prominent traps at ~ 0.2 eV and ~ 0.7 eV in these devices. Density functional theory calculations in this and previous work suggest that the ~ 0.2 eV peak is due to N vacancy-related defects in GaN and O_N defects in AlGaN. Our work, in conjunction with previous experimental and theoretical studies, strongly suggests that the previously unidentified ~ 0.7 trap level in GaN is associated with a N_{Ga} defect. Finally, while these particular devices are expected to perform well in a typical space environment, these results demonstrate the importance of incorporating biased irradiations in AlGaN/GaN radiation hardness assurance testing, and of evaluating combined irradiation and high-stress field stress effects for AlGaN/GaN devices that are intended for use in space.

Chapter VII

Summary and Conclusions

In this work, we have performed high field stress with or without radiation exposure on AlGaN/GaN HEMTs. Degradations via DC and RF measurements are characterized thoroughly after 1.8 MeV proton/high field stress. We employed low frequency *1/f* noise as a diagnostic tool to understand the nature of the defects that dominate the degradation. Density function theory calculations show the formation energy for the defect might be responsible for the degradation. The techniques used in identification of defects are not limited to GaN-based systems, and can be used in most semiconductor materials.

When subjected to 1.8 MeV protons, a positive shift in pinch-off voltage is typically observed, with degradation in peak transconductance due to the generation of acceptor-like traps. Small signal RF gains degrade more significantly compared to DC parameters. Device variations are observed due to processing-dependent defects, which lead to more fast traps in ammonia MBE devices than Ga-rich PAMBE devices, which result in worse AC performance.

The *1/f* noise changes after irradiation at different temperatures, indicating possible changes in the defect distribution. The experimental noise data fit the Dutta-Horn model well, which enables us to translate the noise change to thermal transition between two charge states of the defect. Before irradiation, the device originally shows two peaks at 0.2 eV and 0.9 eV. After irradiation, the 0.9 eV peak decreased while the 0.2 eV peak increased. DFT calculations shows that this change is related to H atoms removed from an O_N-H defect, and a new peak at 0.5 eV was found as an intermediate

configuration of the defect.

When the devices are stressed at high electric field, hot carriers are generated. Unlike protons, hot electrons with much smaller energy do not generate defects but interact with pre-existing defects, like dehydrogenation of defects. The noise spectra before and after stress show similar features as that of proton irradiation, confirming that protons dehydrogenate O_N-H defects during the irradiation. Before stress, hydrogen-passivated Fe and O complexes contribute significantly to the noise and relability degradation in the UCSB devices, and hydrogenated antisite N_{Ga}-H_x, x=1~3, and V_{Ga}-O_N-H defects contribute to the noise and reliability degradation of *Qorvo* devices. With increasing stress, all of these complexes increasingly are dehydrogenated, leading to large increases in noise and trap density. The sequential process of (1) defect dehydrogenation, (2) defect charging, and (3) defect transport ultimately leads to failure of the device under high-field stress conditions.

Biased irradiation experiments are also performed to examine the reliability of devices for space applications. Semi-ON bias before/during irradiation greatly enhanced the level of degradation. Characterization and qualification of AlGaN/GaN HEMTs for space applications simply must include biased irradiations as part of the testing matrix. Further, at least during initial characterization of new technologies for space system use, combined reliability and radiation effects must be considered when attempting to assess and assure the performance, reliability, and radiation tolerance of space-based electronic systems.

In summary, we have used radiation and DC stress to understand the degradations in AlGaN/GaN HEMTs. The low frequency 1/*f* noise and density functional theory calculations helped to identify the defects that limit the performance of the devices.

REFERENCES

[1] G. Meneghesso, G. Verzellesi, F. Danesin, F. Ramapazzo, F. Zanon, A. Tazzoli, M. Meneghini, and E. Zanoni, "Reliability of GaN high-electron-mobility transistors: State of the art and perspectives," *IEEE Trans. Device Materials Rel.*, vol, 8, pp. 332-343, 2008.

[2] H. Kim, V. Tilak, B.M. Green, J.A. Smart, W.J. Schaff, J.R. Shealy andL.F. Eastmanet al., "Reliability evaluation of high power AlGaN/GaN HEMTs on SiC substrate," *Phys. Stat. Sol. A*, vol. 188, no. 1, pp. 203–206, Nov. 2001.

[3] U. Mishra, P. Parikh, and Y. Wu, "AlGaN/GaN HEMTs-an overview of device operation and applications," *Proceedings of the IEEE*, vol. 90, no. 6, pp.1022-1031, Jun 2002.

[4] M. A. Khan, A. Bhattarai, J. N. Kuznia, and D. T. Olson, "High electron mobility transistor based on a GaN-$Al_xGa_{1-x}N$ heterojunction," *Applied Physics Letters*, vol. 63, no. 9, pp. 1214-1215, 1993.

[5] J. Kolník, I. H. Oğuzman, K. F. Brennan, R. Wang, and P. P. Ruden, "Monte Carlo calculation of electron initiated impact ionization in bulk zinc-blende and wurtzite GaN," *Journal of Applied Physics*, vol. 81, no. 2, pp. 726-733, 1997.

[6] G. Meneghesso, E. Zanoni and M. Meneghini, "Reliability and high field related issues in GaN-HEMT devices – Part I," *2014 IEEE workshop on, Wide Bandgap Power Devices and Applications (WiPDA)*, Oct. 2014.

[7] O. Ambacher and J. Majewski, "Pyroelectric properties of Al (In) GaN/GaN hetero-and quantum well structures," *J. Phys.: Condens. Matter*, vol. 14, pp. 3399-3434, 2002.

[8] F. Bernardini and V. Fiorentini, "Nonlinear macroscopic polarization in III-V nitride alloys," *Physical Review B*, vol. 64, no. 8, p. 085207, Aug. 2001.

[9] Palacios, T., "Beyond the AlGaN/GaN HEMT: new concepts for high-speed transistors," *Phys. Status Solidi A*, vol. 206, pp. 1145–1148, 2009.

[10] M. Micovic, A. Kurdoghlian, P. Janke, D. W. S. Wong, J. S. Moon, L. McCray, and C. Nguyen, "AlGaN/GaN heterojunction field effect transistors grown by nitrogen plasma assisted molecular beam epitaxy", *IEEE Trans. Electron Dev.*, vol. 48, no. 3, pp. 591-596, 2001.

[11] G. Koblmüller, F. Wu, T. Mates, J. S. Speck, S. Fernández-Garrido and E. Calleja, "High electron mobility GaN grown under N-rich conditions by plasma-assisted molecular beam epitaxy", *Appl. Phys. Lett.* vol. 91, no. 22, pp. 221905.

[12] G. Koblmüller, R. Chu, F. Wu, U. Mishra and J. Speck, "Dislocation reduction in AlGaN/GaN Heterostructures on 4H-SiC by molecular beam epitaxy in the thermal decomposition regime," *Appl. Phys. Express* **1** 061103.

[13] A. Corrion, F. Wu and J. Speck, "Growth regimes during homoepitaxial growth of GaN by ammonia molecular beam epitaxy," *J. Appl. Phys.* 112, 054903, 2012.

[14] H. Kim, R. M. Thompson, V. Tilak, T. R. Prunty, J. R. Shealy, and L. F. Eastman, "Effects of SiN passivation and high-electric field on AlGaN-GaN HFET degradation," *IEEE Electron Device Lett.*, vol. 24, no. 7, pp. 421-423, July 2003.

[15] G. Meneghesso, F. Rampazzo, P. Kordos, G. Verzellesi, and E. Zanoni, "Current collapse and high-electric field reliability of unpassivated GaN/AlGaN/GaN HEMTs," *IEEE Trans. Electron Devices*, vol. 53, no. 12, pp. 2932-2941, Dec. 2006.

[16]J. Joh and J. A. del Alamo, "Mechanisms for electrical degradation of GaN high-electron mobility transistors," *IEDM Tech Dig. 2006*, pp. 148-151.

[17]J. Joh and J. A. del Alamo, "Critical voltage for electrical degradation of GaN high-electron mobility transistors," *IEEE Electron Device Lett.*, vol. 29, no. 4, pp. 287-289, Apr. 2008.

[18]G. Simin, A. Koudymov, A. Tarakji, X. Hu, J. Yang, M. A. Khan, M. S. Shur, and R. Gaska, "Induced strain mechanism of current collapse in AlGaN/GaN heterostructure field-effect transistors," *Appl. Phys. Lett.*, vol 79, no. 16, pp. 2651-2653, 2001.

[19]R. Vetury, N. Q. Zhang, S. Keller, and U. K. Mishra, "The impact of surface states on the DC and RF characteristics of AlGaN/GaN HFETs," *IEEE Trans. Electron Devices*, vol. 48, pp. 560-566, Mar. 2001.

[20]J. L Jimenez and U. Chowdhury, "X-band GaN FET reliability," *IEEE Int. Reliability Phys. Symp. Dig.*, 2008, pp. 429-435.

[21]J. W. Milligan, S. Sheppard, W. Pribble, Y.-F. Wu, St. G. Muller, and J. W. Palmour, "SiC and GaN wide bandgap device technology overview," *IEEE Radar Conf. Dig.*, 2007, pp. 960-964.

[22]S. Lee, R. Vetury, J. D. Brown, S. R. Gibb, W. Z. Cai, J. Sun, D. S. Green, and J. Shealy, "Reliability assessment of AlGaN/GaN HEMT technology on SiC for 48 V applications," *IEEE Int. Reliability Phys. Symp. Dig.*, 2008, pp. 446-449.

[23]S. Singhal, A.W. Hanson, A. Chaudhari, P. Rajagopal, T. Li, J. W. Johnson, W. Nagy, R. Therrien, C. Park, A. P. Edwards, E. L. Piner, K. J. Linthicum, and I. C. Kizilyalli, "Qualification and reliability of a GaN process platform," *Int. Conf. Compound Semiconductor MANTECH Tech. Dig.*, 2007, pp. 83-86.

[24]C. W. Wang, B. S. Soong, J. Y. Chen, C. L. Chen, and Y. K. Su, "Effects of gamma-ray irradiation on the microstructural and luminescent properties of radio-frequency magnetron-sputtered GaN thin films," *Journal of Applied Physics*, vol. 88, no. 11, p. 6355-6358, 2000.

[25]V. Emtsev and V. Davydov, "Point defects in gamma-irradiated n-GaN," *Semicond Sci Tech*, vol. 15, pp. 73–78, 2000.

[26]G. A. Umana-Membreno, J. M. Dell, T. P. Hessler, B. D. Nener, G. Parish, L. Faraone, and U. K. Mishra, "^{60}Co gamma-irradiation-induced defects in n-GaN," *Applied Physics Letters*, vol. 80, no. 23, p. 4354-4356, 2002.

[27]B. Luo, J. W. Johnson, F. Ren, K. K. Allums, C. R. Abernathy, S. J. Pearton, A. M. Dabiran, A. M. Wowchack, C. J. Polley, P. P. Chow, D. Schoenfeld, and A. G. Baca, "Influence of Co-60 -rays on DC performance of AlGaN/GaN high electron mobility transistors," *Appl. Phys. Lett.*, vol. 80, pp. 604–606, 2002.

[28]G. A. Umana-Membreno, J. M. Dell, G. Parish, B. D. Nener, L. Faraone, and U. K. Mishra, "Co-60 gamma irradiation effects on n-GaN Schottky diodes," *IEEE Trans. Electron Dev.*, vol. 50, no. 12, pp. 2326–2334, Dec. 2003.

[29]O. Aktas, A. Kuliev, V. Kumar, R. Schwindt, S. Toshkov, D. Costescu, J. Stubbins, and I. Adesida, "Co-60 gamma radiation effects on DC, RF, and pulsed I-V characteristics of AlGaN/GaN HEMTs," *Solid State Electronics*, vol. 48, Issue. 3 pp: 471-475, 2004.

[30]S. A. Vitusevich, N. Klein, A. E. Belyaev, S. V. Danylyuk, M. V. Petrychuk, R. V. Konakova, A. M. Kurakin, A. E. Rengevich, A. Y. Avksentyev, B. A. Danilchenko, V. Tilak, J. Smart, A. Vertiatchikh, and L. F. Eastman, "Effects of γ-irradiation on AlGaN/GaN-based HEMTs," *Physics Status Solidi (a)*, vol. 195, no. 1, pp. 101–105, Jan. 2003.

[31]X. Hu, B. K. Choi, H. J. Barnaby, D. M. Fleetwood, R. D. Schrimpf, S. C. Lee, S. Shojah-Ardalan,

R. Wilkins, U. K. Mishra, and R. Dettmer, “The energy dependence of proton-induced degradation in AlGaN/GaN high electron mobility transistors,” *IEEE Trans. Nucl. Sci.* vol. 51, no. 2, pp. 293-297, April 2004.

[32] J. Nord, K. Nordlund, and J. Keinonen, “Molecular dynamics study of damage accumulation in GaN during ion beam irradiation,” *Physical Review B*, vol. 68, no. 18, p. 184104, Nov. 2003.

[33] B. D. White, M. Bataiev, S. H. Goss, X. Hu, A. Karmarkar, D. M. Fleetwood, R. D. Schrimpf, W. J. Schaff, and L. J. Brillson, “Electrical, spectral, and chemical properties of structures as a function of proton fluence,” *IEEE Trans. Nucl. Sci.*, vol. 50, no. 6, pp. 1934–1941, 2003.

[34] B. Luo, J. W. Johnson, F. Ren, K. K. Allums, C. R. Abernathy, S. J. Pearton, R. Dwivedi, T. N. Fogarty, R. Wilkins, A. M. Dabiran, A. M. Wowchack, C. J. Polley, P. P. Chow, and A. G. Baca, “dc and rf performance of proton-irradiated AlGaN/GaN high electron mobility transistors,” *Applied Physics Letters*, vol. 79, no. 14, p. 2196-2198, 2001.

[35] B. D. White, M. Bataiev, L. J. Brillson, B. K. Choi, D. M. Fleetwood, R. D. Schrimpf, S. T. Panelides, R. W. Dettmer, W. J. Schaff, J. G. Champlain, and U. K. Mishra, “Characterization of 1.8 MeV proton irradiated AlGaN/GaN field-effect transistor structures by nanoscale depth-resolved luminescence spectroscopy,” *IEEE Trans. Nucl. Sci.*,vol. 49, no. 6, pp. 2695–2701, Dec. 2002.

[36] X. Hu, A. Karmarkar, B. Jun, D. M. Fleetwood, R. D. Schrimpf, R. D. Geil, R. A. Weller, B. D. White, M. Bataiev, L. J. Brillson, and U. K. Mishra, “Proton-irradiation effects on AlGaN/AlN/GaN high electron mobility transistors,” *IEEE Trans. Nucl. Sci.*, vol. 50, no. 6, pp. 1791–1796, 2003.

[37] A. Kalavagunta, A. Touboul, L. Shen, R. D. Schrimpf, R. A. Reed, D. M. Fleetwood, R. K. Jain, and U. K. Mishra, “Electrostatic mechanisms responsible for device degradation in proton irradiated AlGaN/AlN/GaN HEMTs,” *IEEE Trans. Nucl. Sci.*, vol. 55, no. 4, pp. 2106–2112, Aug. 2008.

[38] T. Roy, E. X. Zhang, Y. S. Puzyrev, D. M. Fleetwood, R. D. Schrimpf, B. K. Choi, A B. Hmelo, and S. T. Pantelides, “Process dependence of proton-induced degradation in GaN HEMTs,” *IEEE Trans. Nucl. Sci.*, vol. 57, no. 6, pp. 3060–3065, 2010.

[39] H. Y. Kim, C. F. Lo, L. Liu, F. Ren, J. Kim, and S. J. Pearton, “Proton-irradiated InAlN/GaN high electron mobility transistors at 5, 10, and 15 MeV energies,” *Applied Physics Letters*, vol. 100, no. 1, p. 012107, 2012.

[40] H. Y. Kim, J. Kim, L. Liu, C. F. Lo, F. Ren, and S. J. Pearton, “Effects of proton irradiation energies on degradation of AlGaN/GaN high electron mobility transistors,” *Journal of Vacuum Science & Technology B: Microelectronics and Nanometer Structures*, vol. 30, no. 1, p. 012202, 2012.

[41] G. P. Summers, E. A. Burke, P. Shapiro, S. R. Messenger, and R. J. Walters, “Damage correlations in semiconductors exposed to gamma, electron and proton radiations,” *IEEE Trans. Nucl. Sci.*, vol. 40, no. 6, pp. 1372–1379, 1993.

[42] J. Srour, C. J. Marshall, and P. W. Marshall, “Review of displacement damage effects in silicon devices,” *IEEE Trans. Nucl. Sci.*, vol. 50, no. 3, pp. 653–670, 2003.

[43] G. Sonia, E. Richter, F. Brunner, A. Denker, R. Lossy, M. Mai, F. Lenk, J. Bundesmann, G. Pensl, J. Schmidt, U. Zeimer, L. Wang, K. Baskar, M. Weyers, J. Würfl, and G. Tränkle, “2 MeV ion irradiation effects on AlGaN/GaN HFET devices,” *Solid-State Electronics*, vol. 52, no. 7, pp. 1011–1017, Jul. 2008.

[44]Y. Puzyrev, T. Roy, E. X. Zhang, D. M. Fleetwood, R. D. Schrimpf, and S. T. Pantelides, “Radiation-induced defect evolution and electrical degradation of AlGaN/GaN High-Electron-Mobility transistors,” *IEEE Trans. Nucl. Sci.*, vol. 58, no. 6, pp. 2918–2924, 2011.

[45]J. F. Ziegler, J. P. Biersack, U. Littmark, *The Stopping and Range of Ions in Solids*, 2nd ed, New York: Pergamon Press, 1996.

[46]A. Ionascut-Nedelcescu, C. Carlone, A. Houdayer, H. J. von Bardeleben, J. L. Cantin, and S. Raymond, “Radiation hardness of gallium nitride,” *IEEE Trans. Nucl. Sci.*, vol. 49, no. 6, pp. 2733–2738, Dec. 2002.

[47]S. J. Cai, Y. S. Tang, R. Li, Y. Wei, L. Wong, Y. L. Chen, K. L. Wang, M. Chen, Y. F. Zhao, R. D. Schrimpf, J. C. Keay, and K. F. Galloway, “Annealing behavior of a proton irradiated $Al_xGa_{1-x}N$/GaN high electron mobility transistor grown by MBE,” *IEEE Trans. Electron Devices*, vol. 47, pp. 304–307, Feb. 2000.

[48]A. Johnston, “Displacement damage in Compound Semiconductors,” *Reliability and Radiation Effects in Compound Semiconductors*, Hackensack, NJ: World Scientific, 2010, ch. 10, sec. 10.4.2, pp 276.

[49]M. J. Rosker, “The present state of the art of wide-bandgap semiconductors and their future,” in *Proc. IEEE Radio Freq. Integr. Circuit Symp*., 2007, pp. 159–162.

[50]J. Würfl, V. Abrosimova, J. Hilsenbeck, E. Nebauer, W. Rieger, G.Tränkle, "Reliability considerations of III-nitride microelectronic devices," *Microelectron. Reliab.*, vol. 39, pp. 1737-1757, 1999.

[51]Menozzi, R., "Reliability of GaN-Based HEMT devices," in *Optoelectronic and Microelectronic Materials and Devices, 2008. COMMAD 2008. Conference on*, pp.44-50, July 28 2008-Aug. 1 2008

[52]Y. C. Chou, D. Leung, I. Smorchkova, M. Wojtowicz, R. Grundbacher, L. Callejo, Q. Kan, R. Lai, P. H. Liu, D. Eng, and A. Oki, “Degradation of AlGaN/GaN HEMTs under elevated temperature lifetesting,” *Microelectron. Reliab.*, vol. 44, no. 7, pp. 1033–1038, Jul. 2004.

[53]I. Daumiller, C. Kirchner, M. Kamp, K. J. Ebeling, and E. Kohn, "Evaluation of the temperature stability of AlGaN/GaN heterostructure FETs," *IEEE El. Dev. Lett.*, vol. 20, pp. 448-450, 1999.

[54]J. Würfl, J. Hilsenbeck, E. Nebauer, G. Tränkle, and H. Obloh, "Technology and thermal stability of AlGaN/GaN HFETs," *Proc. GaAs Applications Symp. (GAAS)*, pp. 430-434, 1999.

[55]J. Hilsenbeck, E. Nebauer, J. Würfl, G. Tränkle, and H. Obloh, "Aging behavious of AlGaN/GaN HFETs with advanced ohmic and Schottky contacts," *El. Lett.*, vol. 36, pp. 980-981, 2000.

[56]J. Würfl, J. Hilsenbeck, E. Nebauer, G. Tränkle, and H. Obloh, W. Österle, "Reliability of AlGaNGaN HFETs comprising refractory ohmic and Schottky contacts," *Microelectron. Reliab.*, vol. 40, pp. 1689-1693, 2000.

[57]A. Sozza, C. Dua, E. Morvan, B. Grimbert, M. A. di Forte-Poisson, S. L. Delage, and E. Zanoni, "Thermal stability of Mo-based Schottky contact for AlGaN/GaN HEMT," *El. Lett.*, vol. 41, no. 16, pp. 61-62, 2005.

[58]R. Khanna, L. Stafford, L. F. Voss, S. J. Pearton, H. T. Tang, T. Anderson, S.-C. Hung, and F. Ren, "Aging and stability of GaN high electron mobility transistors and light-emitting diodes with TiB2- and Irbased contacts," *IEEE Trans. Dev. Mat. Reliab.*, vol. 8, pp. 272-276, 2008.

[59]J. Joh and J. A. del Alamo, “Gate current degradation mechanisms of GaN high electron mobility transistors,” *in IEDM Tech. Dig.*, pp. 385–388, 2007.

[60]A. Sarua, H. Ji, M. Kuball, M. J. Uren, T. Martin, K. J. Nash, K. P. Hilton, and R. S. Balmer,

"Piezoelectric strain in AlGaN/GaN heterostructure field-effect transistors," *Appl. Phys. Lett.*, vol. 88, 103502, 2006.

[61] F. Medjdoub, J. F. Carlin, M. Gonschorek, E. Feltin, M. A. Py, D. Ducatteau, C. Gaquière, N. Grandjean, and E. Kohn, "Can InAlN/GaN be an alternative to high power high temperature AlGaN/GaN devices?" *in IEDM Tech. Dig.*, pp. 927–930, 2006.

[62] D. Kumar Sahoo, R.K. Lal, H. Kim, V. Tilak, and L. F. Eastman, "High field effects in silicon nitride passivated GaN MODFETs," *IEEE Trans. Electron Devices*, vol. 50, no. 5, pp. 1163–1170, May 2003.

[63] G. Koley, V. Tilak, L. F. Eastman, and M. G. Spencer, "Slow transients observed in AlGaN/GaN HFETs: Effects of SiNzx passivation and UV illumination," *IEEE Trans. Electron Devices*, vol. 50, no. 4, pp. 886–893, Apr. 2003.

[64] J. A. Mittereder, S. C. Binari, P. B. Klein, J. A. Roussos, D. S. Katzer, D. F. Storm, D. D. Koleske, A. E. Wickenden, and R. L. Henry, "Current collapse induced in AlGaN/GaN high-electron-mobility transistors by bias stress," *Appl. Phys. Lett.*, vol. 83, no. 8, pp. 1650–1652, 2003.

[65] T. Kunii, M. Totsuka, Y. Kamo, Y. Yamamoto, H. Takeuchi, Y. Shimada, T. Shiga, H. Minami, T. Kitano, S. Miyakuni, S. Nakatsuka, A. Inoue, T. Oku, T. Nanjo, T. Oishi, T. Ishukawa, and Y. Matsuda, "A high reliability GaN HEMT with SiN passivation by Cat-CVD," *in Proc. IEEE CSIC Symp.*, pp. 197–200, 2004.

[66] A. P. Edwards, J. A. Mittereder, S. C. Binari, D. Scott Katzer, D. F. Storm, and J. A. Roussos, "Improved reliability of AlGaN/GaN HEMTs using an NH_3 plasma treatment prior to SiN passivation," *IEEE Electron Device Lett., vol. 26, no. 4*, pp. 225–227, Apr. 2005.

[67] S. K. Jha, B. H. Leung, C. Surya, H. Schweizer, and H. Pilkhuhn, "Studies of hot-electron degradation in GaN HEMTs with varying gate recess depths," *in Proc. COMMAD, 2004*, pp. 33–36.

[68] P. Valizadeh and D. Pavlidis, "Effects of rf and DC stress on AlGaN/GaN MODFETs: A low-frequency noise-based investigation," *IEEE Trans. Device Mater. Rel.*, vol. 5, no. 3, pp. 555–563, Sep. 2005.

[69] R. Coffie, Y. Chen, I. P. Smorchkova, B. Heying, V. Gambin, W. Sutton, Y. C. Chou, W. B. Luo, M. Wojtowicz, and A. Oki, "Temperature and voltage dependent rf degradation study in AlGaN/GaN HEMTs," *in Proc. IEEE Int. Rel. Phys. Symp., 2007*, pp. 568–569.

[70] E. L. Piner, S. Singhal, P. Rajagopal, R. Therrien, J. C. Roberts, T. Li, A. W. Hanson, J. W. Johnson, I. C. Kizilyalli, and K. J. Linthicum, "Device degradation phenomena in GaN HFET technology: Status, mechanisms, and opportunities," *in IEDM Tech. Dig., 2006*, pp. 411–414.

[71] A. M. Conway, M. Chen, P. Hashimoto, P. J. Willadsen, and M. Micovic, "Accelerated rf life testing of GaN HFETs," *in Proc. IEEE Int. Rel. Phys. Symp.*, 2007, pp. 472–475.

[72] S. Singhal, J. C. Roberts, P. Rajagopal, T. Li, A. W. Hansen, R. Therrien, J. W. Johnson, I. C. Kizilyalli, and K. J. Linthicum, "GaN-on-Si failure mechanisms and reliability improvements," *in Proc. IEEE Int. Rel. Phys. Symp.*, 2006, pp. 95–98.

[73] P. Saunier, C. Lee, A. Balistreri, D. Dumka, J. Jimenez, H. Q. Tserng, M. Y. Kao, P. C. Chao, A. Souzis, I. Eliashevich, S. Guo, J. del Alamo, J. Joh, and M. Shur, "Progress in GaN performance and reliability," *in Proc. Device Res. Conf.*, 2007, pp. 35–36.

[74] Y. Inoue, S. Masuda, M. Kanamura, T. Ohki, K. Makiyama, N. Okamoto, K. Imanishi, T. Kikkawa, N. Hara, H. Shigematsu, and K. Joshin, "Degradation-mode analysis for highly reliable GaN

HEMT," *in IEEE MTT-S Int. Microw. Symp.*, 2007, pp. 639–642.

[75]T. Nakao, Y. Ohno, M. Akita, S. Kishimoto, K. Maezawa, and T. Mizutani, "Electroluminescence in AlGaN/GaN high electron mobility transistors under high bias voltage," *Jpn. J. Appl. Phys.1, Regul. Rap. Short Notes*, vol. 41, no. 4A, pp. 1990–1991, Apr. 2002.

[76]N. Shigekawa, K. Shiojima, and T. Suemitsu, "Electroluminescence characterization of AlGaN/GaN high electron mobility transistors," *Appl. Phys. Lett.*, vol. 79, no. 8, pp. 1196–1198, Aug. 2001.

[77]N. Shigekawa, K. Shiojima, and T. Suemitsu, "Optical Study of highbiased AlGaNiGaN high-electron-mobility-transistors," *J. Appl. Phys*, vol. 92, no. 1, pp. 531–535, 2002.

[78]A. van der Ziel, "Noise in solid-state devices and lasers," *Proceedings of the IEEE*, vol. 58, no. 8, pp. 1178–1206, 1970.

[79]S. Lee, K. J. Webb, and L. F. Eastman, "Intrinsic noise equivalent-circuit parameters for AlGaN/GaN HEMTs," *IEEE Trans. Microwave Theory and Techniques*, vol. 51, no. 5, pp. 1567–1577, 2003.

[80]D. M. Fleetwood, T. L. Meisenheimer, and J. H. Scofield, "*1/f* noise and radiation effects in MOS devices," *IEEE Trans. Electron Dev*, vol. 41, pp. 1953-1964, Dec. 1994.

[81]M. E. Levinshtein, S. L. Rumyantsev, R. Gaska, J. W. Yang, and M. S. Shur, "AlGaN/GaN high electron mobility field effect transistors with low 1/*f* noise," *Appl. Phys. Lett.*, vol. 73, no. 8, pp. 1089-1091, 1998.

[82]S. L. Rumyantsev, Y. Deng, E. Borovitskaya, A. Dmitriev, W. Knap, N. Pala, M. S. Shur, M. E. Levinshtein, M. A. Khan, G. Simin, J. Yang, and X. Hu, "Low-frequency noise in GaN/AlGaN heterostructure field-effect transistors at cryogenic temperatures," *J. Appl. Phys.*, vol. 92, no. 8, p. 4726-4730, 2002.

[83]J. Chen, Y. S. Puzyrev, C. X. Zhang, E. X. Zhang, M. W. McCurdy, D. M. Fleetwood, R. D. Schrimpf, S. T. Pantelides, S. W. Kaun, E. C. Kyle and J. S. Speck, "High-Field Stress, Low-Frequency Noise, and Long-term Reliability of AlGaN/GaN HEMTs", *IEEE Trans. Device Materials Rel.*, accepted, 2016.

[84]P. Dutta and P. Horn, "Low-frequency fluctuations in solids: 1/*f* noise," *Rev. Mod. Phys.*, vol. 53, pp. 497-516, 1981.

[85]E. X. Zhang, D. M. Fleetwood, N. D. Pate, R. A. Reed, A. F. Witulski, and R. D. Schrimpf, "Time-domain reflectometry measurements of total-ionizing-dose degradation of nMOSFETs," *IEEE Trans. Nucl. Sci.*, vol. 60, no. 6, pp.4470-4475, Dec. 2013.

[86]H. Tang, S. Rolfe, and M. Beaulieu, "Plasma-assisted MBE Growth of GaN on GaN/sapphire templates Grown in situ by Ammonia-MBE," *State-of-the-Art Program on Compound Semiconductors XLI and Nitride and Wide Bandgap Semiconductors for Sensors, Photonics and Electronics V: Proceedings of the International Symposia*, pp. 215-224, 2004.

[87]S. Rajan, P. Waltereit, C. Poblenz, S. J. Heikman, D. S. Green, S. James, and U. K. Mishra, "Power performance of AlGaN/GaN HEMTs grown on SiC by plasma-assisted MBE," *IEEE Electron Dev. Lett.*, vol. 25, no. 5, pp. 247-249, May 2004.

[88]S. Jagannathan, T. D. Loveless, E. X. Zhang, D. M. Fleetwood, R. D. Schrimpf, T. D. Haeffner, J. S. Kauppila, N. Mahatme, B. L. Bhuva, M. L. Alles, W. T. Holman, A. F. Witulski, and L. W. Massengill, "Sensitivity of high-frequency RF circuits to total ionizing dose degradation," *IEEE Trans. Nucl. Sci.*, vol. 60, no. 6, pp. 4498-4504, Dec. 2013.

[89]H. Matsuzaki, T. Maruyama, T. Koasugi, H. Takahashi, M. Tokumitsu, and T. Enoki, "Lateral

scale down of InGaAs/InAs composite-channel HEMTs with tungsten-based tiered ohmic structure for 2-S/mm g_m and 500-GHz f_T ," *IEEE Trans. Electron Devices*, vol. 54, no. 3, pp. 378–384, Mar. 2007.

[90]R. D. Harris, L. Z. Scheick, J. P. Hoffman, T. Thrivikraman, M. Jenabi, Y. Gim, and T. Miyahira, "Radiation characterization of commercial GaN devices," *2011 IEEE Radiation Effects Data Workshop*, pp. 1–5, Jul. 2010.

[91]J. Chen, Y. S. Puzyrev, C. X. Zhang, E. X. Zhang, M. W. McCurdy, D. M. Fleetwood, R. D. Schrimpf, S. T. Pantelides, S. W. Kaun, E. C. Kyle, and J. S. Speck, "Proton-induced dehydrogenation of defects in AlGaN/GaN HEMTs," *IEEE Trans. Nucl. Sci.*, vol. 60, no. 6, pp. 4080-4086, Dec. 2013.

[92]T. Roy, E. X. Zhang, Y. S. Puzyrev, X. Shen, D. M. Fleetwood, R. D. Schrimpf, G. Koblmueller, R. Chu, C. Poblenz, N. Fichtenbaum, C. S. Suh, U. K. Mishra, J. S. Speck, and S. T. Pantelides, "Temperature-dependence and microscopic origin of low frequency 1/*f* noise in GaN/AlGaN high electron mobility transistors," *Appl. Phys. Lett.*, vol. 99, no. 20, p. 203501, 2011.

[93]Y. Pei, C. Poblemz, A. L. Corrion, R. Chu, L. Shen, J. S. Speck, and U. K. Mishra, "X- and Ka-band power performance of AlGaN/GaN HEMTs grown by ammonia-MBE," *Electronics Letters*, vol. 44, no. 9, pp. 598-598, Apr. 2008.

[94]D. A. Frickey, "Conversions between S, Z, Y, H, ABCD, and T parameters which are valid for complex source and load impedances," *IEEE Trans. Microw. Theory Tech.*, vol. 42, no. 2, pp.205-211, Feb. 1994.

[95]S. J. Mason, "Power gain in feedback amplifiers," *IRE Trans. Circ. Theory*, vol. CT-1, pp. 20-25, 1954.

[96]M. A. Xapsos, P. M. O'Neill, and T. P. O'Brien, "Near-Earth space radiation models," *IEEE Trans. Nucl. Sci.*, vol. 60, no. 3, pp. 1691-1705, Jun. 2014.

[97]O. Mitrofanov and M. Manfra, "Mechanisms of gate lag in GaN/AlGaN/GaN high electron mobility transistors," *Superlattices and Microstructures*, Vol. 34, No. 1-2, pp. 33-53, July 2003.

[98]J. A. del Alamo and J. Joh, "GaN HEMT reliability," *Microelectron. Reliab.*, vol. 49, no. 9-11, pp. 1200-1206, Sep. – Nov. 2009.

[99]S. M. Sze, *Physics of Semiconductor Devices*. New York: Wiley, 1981, pp. 342–343.

[100]S. Naseh, M. J. Deen, and O. Marinov, "Effects of hot-carrier stress on the RF performance of 0.18 μm technology NMOSFETs and circuits," in *Proc. IEEE 40nd Annu. Int. Reliability Physics Symp.*, Dallas, TX, Apr. 2002, pp. 98–104.

[101]D. M. Fleetwood, H. D. Xiong, S. Member, Z. Lu, C. J. Nicklaw, J. A. Felix, R. D. Schrimpf, and S. T. Pantelides, "Unified model of hole trapping, 1/*f* noise, and thermally stimulated current in MOS devices," vol. 49, no. 6, pp. 2674–2683, 2002.

[102]G. Kresse and J. Furthmüller, "Efficient iterative schemes for ab initio total-energy calculations using a plane-wave basis set," *Phys. Rev. B*, vol. 54, pp. 11169-11186, 1996.

[103]J. P. Perdew, K. Burke, and M. Ernzerhof, "Generalized gradient approximation made simple," *Phys. Rev. Lett.*, vol. 77, pp. 3865-3868, 1996.

[104]P. E. Blöchl, O. Jepsen, and O. K. Andersen, "Improved tetrahedron method for Brillouin-zone integrations," *Phys. Rev. B*, vol. 49, pp. 16223-16233, 1994.

[105]G. Kresse and D. Joubert, "From ultrasoft pseudopotentials to the projector augmented-wave method," *Phys. Rev. B*, vol. 59, pp. 1758-1775, 1999.

[106]G. Henkelman, B. P. Uberuaga, and H. Jonsson, "A climbing image nudged elastic band method

for finding saddle points and minimum energy paths," *J. Chem. Phys.*, vol. 113, no. 22, pp. 9901-9904, Dec. 2000.

[107]S. N. Rashkeev, D. M. Fleetwood, R. D. Schrimpf, and S. T. Pantelides, "Proton-induced defect generation at the Si-SiO_2 interface," *IEEE Trans. Nucl. Sci*., vol. 48, no. 6, pp. 2086-2092, Dec. 2001.

[108]T. Palacios, A. Chakraborty, S. Rajan, C. Poblenz, S. Keller, S. P. DenBaars, J. S. Speck, and U. K. Mishra, "High-power AlGaN/GaN HEMTs for Ka-band applications," *IEEE Electron Device Lett..*, vol. 26, no. 11, pp. 781–783, Nov. 2005.

[109]U. K. Mishra, L. Shen, T. E. Kazior and Y. F. Wu, "GaN-based RF power devices and amplifiers," *Proc. IEEE*, vol. 96, pp. 287-305, Feb. 2008.

[110]J. Joh and J. A. del Alamo "RF power degradation of GaN high electron mobility transistors", *IEDM Tech. Dig.*, pp. 20.2.1 -20.2.4, 2010.

[111]A. Chini, V. Di Lecce, F. Fantini, G. Meneghesso, and E. Zanoni "Analysis of GaN HEMT failure mechanisms during DC and large-signal RF operation," *IEEE Trans. Electron Devices*, vol. 59, no. 5, pp. 1385-1392, May 2012.

[112]D. M. Fleetwood, "1/*f* noise and defects in microelectronic materials and devices," *IEEE Trans. Nucl. Sci.*, 62, no. 4, pp. 1462-1486, Aug. 2015.

[113]L. K. J. Vandamme, "Noise as a diagnostic tool for quality and reliability of electronic devices," *IEEE Trans. Electron Dev.*, vol. 41, no. 11, pp. 2176–2187, Nov, 1994.

[114]M. Meneghini, A. Stocco, M. Bertin, D. Marcon, A. Chini, G. Meneghesso, and E. Zanoni, "Time-dependent degradation of AlGaN/GaN high electron mobility transistors under reverse bias," *Appl. Phys. Lett*, vol. 100, p. 033505, 2012.

[115]I. Hwang, J. Kim, S. Chong, H.-K. Choi, S.-K. Hwang, J. Oh, J. K. Shin and U.-I. Chung, "Impact of channel hot electrons on current collapse in AlGaN/GaN HEMTs," *IEEE Electron Device Lett.*, vol. 34, no. 12, pp. 1494-1496, Oct. 2013.

[116]N. Braga, R. Mickevicius, R. Gaska, X. Hu, M. S. Shur, M. A. Khan and J. Yang, "Simulation of hot electron and quantum effects in AlGaN/GaN heterostructure field effect transistors," *J. Appl. Phys.*, vol. 95, pp. 6409-6414, May. 2004.

[117]J. Chen, E. X. Zhang, C. X. Zhang, M. W. McCurdy, D. M. Fleetwood, R. D. Schrimpf, S. W. Kaun, E. C. Kyle and J. S. Speck, "RF performance of proton-irradiated AlGaN/GaN HEMTs," *IEEE Trans. Nucl. Sci*., vol. 61, no. 6, pp. 2959-2964, Dec. 2014.

[118]A. R. Arehart, A. Sasikumar, S. Rajan, G. D. Via, B. Poling, B. Winningham, E. R. Heller, D. Brown, Y. Pei, F. Recht, U. K. Mishra, and S. A. Ringel," Direct observation of 0.57 eV trap-related RF output power reduction in AlGaN/GaN high electron mobility transistors", *Solid-State Electronics*, vol. 80, pp 19–22, 2013.

[119]D. W. Cardwell, A. Sasikumar, A. Arehart, S. W. Kaun, J. Lu, S. Keller, J. S. Speck, U. K. Mishra, S. A. Ringel, and J. P. Pelz, "Spatially-resolved spectroscopic measurements of E_c - 0.57 eV traps in AlGaN/GaN high electron mobility transistors," *Applied Physics Letters*, vol. 102, no. 19, p. 193509, May 2013.

[120]Y. Puzyrev, T. Roy, M. Beck, R. D. Schrimpf, D. M. Fleetwood, and S. T. Pantelides, "Dehydrogenation of defects and hot-electron degradation in GaN high-electron-mobility transistors", *J. Appl. Phys.* Vol. 109, p.034501, 2011.

[121]K. H. Warnick, Y. Puzyrev, T. Roy, D. M. Fleetwood, R. D. Schrimpf, and S. T. Pantelides, "Room-temperature diffusive phenomena in semiconductors: The case of AlGaN," *Phys. Rev.*

B., vol. 84, p. 214109, 2011.

[122]J. Chen, Y. S. Puzyrev, R. Jiang, E. X. Zhang, M. W. McCurdy, D. M. Fleetwood, R. D. Schrimpf, S. T. Pantelides, A. R. Arehart, S. A. Ringel, P. Saunier and C. Lee, "Effects of Applied Bias and High Field Stress on the Radiation Response of GaN/AlGaN HEMTs," I*EEE Trans. Nucl. Sci.*, vol. 62, no. 6, pp. 2423-2430, Dec. 2015.

[123]Y. Puzyrev, S. Mukherjee, J. Chen, T. Roy, M. Silvestri, R. D. Schrimpf, D. M. Fleetwood, J. Singh, J. M. Hinckley, A. Paccagnella, and S. T. Pantelides, "Gate bias dependence of defect-mediated hot-carrier degradation in GaN HEMTs," *IEEE Trans. Electron Devices*, vol. 61, no. 5, pp. 1316-1320, 2014.

[124]Y. S. Puzyrev, R. D. Schrimpf, D. M. Fleetwood, and S. T. Pantelides, "Role of Fe complexes in the degradation of GaN/AlGaN high-electron-mobility transistors," *Appl. Phys. Lett*., vol. 106, no. 053505, 2015.

[125]L. Liu, C. F. Lo, Y. Xi, Y. Wang, F. Ren, S. J. Pearton, H. Y. Kim, J. Kim, R. C. Fitch, D. E. Walker Jr., K. D. Chabak, J. K. Gillespie, S. E. Tetlak, G. D. Via, A. Crespo and I. I. Kravchenko, "Dependence on proton energy of degradation of AlGaN/GaN high electron mobility transistors," *J. Vac. Sci. Technol. B*, 31(2), article no. 022201, 2013.

[126]T. Roy, Y. S. Puzyrev, B. R. Tuttle, D. M. Fleetwood, R. D. Schrimpf, D. F. Brown, U. K. Mishra and S. T. Pantelides, "Electrical-stress-induced degradation in AlGaN/GaN high electron mobility transistors grown under gallium-rich, nitrogen-rich, and ammonia-rich conditions," *Appl. Phys. Lett.*, vol. 96, article no. 133503, 2010.

[127]C. Della-Morrow, C. Lee, K. Salzman, R. Coffie, V. Li, G. Drandova, T. Nagle, D. Morgan, P. Horng, S. Hillyard and J. Ruan, "Achieve manufacturing readiness level 8 of high-power, high effeciency 0.25 μm GaN on SiC HEMT Process," CS MANTECH Conf., May 13th - 16th, New Orleans, LA, USA, 2013.

[128]G. I. Drandova, J. L. Jimenez, P. T. Goeller, and A. P. Ferreira, "TriQuint's 2nd generation TQGaN25 technology reliability assessment," *Proc. JEDEC Workshop on Reliability of Compound Semiconductors*, pp. 95-97, 2013.

[129]A. Ortiz-Conde, F. J. Garcia Sanchez, J. J. Liou, A. Cerdeira, M. Estrada, and Y. Yue, "A review of recent MOSFET threshold voltage extraction methods," *Solid-State Electron.*, vol. 47, no. 4, pp. 677–683, 2003.

[130]Z. Zhang, A. R. Arehart, E. Cinkilic, J. Chen, E. X. Zhang, D. M. Fleetwood, R. D. Schrimpf, B. McSkimming, J. S. Speck and S. A. Ringel, "Impact of proton irradiation on deep level states in *n*-GaN," *Appl. Phys. Lett.*, vol. 103, article no. 042102, 2013.

[131]A. Arehart, A. Corrion, C. Poblenz, J. S. Speck, U. K. Mishra and S. A. Ringel, "Deep level optical and thermal spectroscopy of traps in n-GaN grown by ammonia molecular beam epitaxy," *Appl. Phys. Lett.*, vol. 93, article no. 112101, 2008.

[132]Z. Q. Fang, D.C. Look, J. Jasinski, M. Benamara, Z. Liliental-Weber, and R.J. Molnar, "Evolution of deep centers in GaN grown by hydride vapor phase epitaxy," *Appl. Phys. Lett*., vol. 78, pp. 332-334, 2001.

[133]A. Armstrong, A.R. Arehart, D. Green, U.K. Mishra, J.S. Speck and S.A. Ringel, "Impact of deep levels on the electrical conductivity and luminescence of GaN co-doped with carbon and silicon," *J. Appl. Phys.*, vol. 98, article no. 053704, 2005.

[134]Z. Zhang, C. A. Hurni, A. R. Arehart, J. Yang, R. C. Myers, J. S. Speck, and S. A. Ringel, "Deep traps in nonpolar m-plane GaN grown by ammonia-based molecular beam epitaxy," *Appl. Phys.*

Lett., vol. 100, article no. 052114, 2012.

[135]A.Y. Polyakov, N. B. Smirnov, A. V. Govorkov, A. V. Markov, N. G. Kolin, D. I. Merkurisov, V. M. Boiko, K. D. Shcherbatchev, V. T. Bublik, M. I. Voronova, S. J. Pearton, A. Dabiran, and A. V. Osinsky, "Neutron irradiation effects in p-GaN," *J. Vac. Sci. Technol. B* , vol. 24, pp. 2256-2261, 2006.

[136]Z. Zhang, A. R. Arehart, E. C. H. Kyle, J. Chen, E. X. Zhang, D. M. Fleetwood, R. D. Schrimpf, J. S. Speck, and S. A. Ringel, "Proton irradiation effects on deep level states in Mg-doped *p*-type GaN grown by ammonia-based molecular beam epitaxy," *Appl. Phys. Lett.*, vol. 106, article no. 022104, Jan. 2015.

[137]C. Freysoldt, B. Grabowski, T. Hickel, J. Neugebauer, G. Kresse, A. Janotti, *et al.*, "First-principles calculations for point defects in solids," *Rev. Mod. Phys.*, vol. 86, pp. 253-305, Mar. 2014.

[138]C. G. de Walle and J. Neugebauer, "First-principles calculations for defects and impurities: Applications to III-nitrides," *J. Appl. Phys*., vol. 95, pp. 3851-3879, 2004.

[139]D. J. Chadi and K. J. Chang, "Theory of the atomic and electronic structure of DX centers in GaAs and $Al_xGa_{1-x}As$ alloys," *Phys. Rev. Lett.*, vol. 61, no. 7, pp. 873-876, Aug. 1988.

[140]J. Dabrowski and M. Scheffler, "Theoretical evidence for an optically inducible structural transition of the isolated As anti-site in GaAs: Identification and explanation of the EL2?" *Phys. Rev. Lett.*, vol. 60, no. 21, pp. 2183-2186, May 1988.